THERMAL PERFORMANCE ASSESSMENT OF HISTORICAL TURKISH BATHS

A THESIS SUBMITTED TO
THE GRADUATE SCHOOL OF NATURAL AND APPLIED SCIENCES
OF
MIDDLE EAST TECHNICAL UNIVERSITY

BY

PINAR (KIRMIZIDAĞ) ÇİÇEK

IN PARTIAL FULFILLMENT OF THE REQUIREMENTS
FOR
THE DEGREE OF MASTER OF SCIENCE
IN
BUILDING SCIENCE
IN
ARCHITECTURE

SEPTEMBER 2009

Approval of the thesis:

THERMAL PERFORMANCE ASSESSMENT OF HISTORICAL TURKISH BATHS

submitted by **PINAR (KIRMIZIDAĞ) ÇİÇEK** in partial fulfillment of the requirements for the degree of **Master of Science in Architecture Department, Middle East Technical University** by,

Prof. Dr. Canan Özgen _____
Dean, Graduate School of **Natural and Applied Sciences**

Assoc. Prof. Dr. Güven Arif Sargın _____
Head of Department, **Architecture**

Asst. Prof. Dr. Ayşe Tavukçuoğlu _____
Supervisor, **Architecture Dept., METU**

Examining Committee Members:

Prof. Dr. Şahinde Demirci _____
Chemistry Dept., METU

Asst. Prof. Dr. Ayşe Tavukçuoğlu _____
Supervisor, Architecture Dept., METU

Part-Time Instr., Assoc. Prof. Dr. Arda Düzgüneş _____
Architecture Dept., METU

Prof. Dr. Emine N.Caner Saltık _____
Architecture Dept., METU

Mechanical Engineer, Part-Time Instr. Levent Tosun _____
Architecture Dept., METU

Date: September, 11th 2009

I hereby declare that all information in this document has been obtained and presented in accordance with academic rules and ethical conduct. I also declare that, as required by these rules and conduct, I have fully cited and referenced all material and results that are not original to this work.

Name, Last Name: Pınar (Kırmızıdağ) Çiçek

Signature :

ABSTRACT

THERMAL PERFORMANCE ASSESSMENT OF HISTORICAL TURKISH BATHS

Çiçek, Pınar (Kırmızıdağ)
M.Sc., Department of Architecture, in Building Science
Supervisor: Asst. Prof. Dr. Ayşe Tavukçuoğlu

September 2009, 137 pages

Comprehensive studies are needed to discover materials and construction technologies contributing to the thermal performance of historical buildings and to keep them in working order over time. Examined in this study were the thermal performance characteristics of Şengül Hamamı, a 15th Century Ottoman bath, to discover original thermo-physical properties of historic materials and to assess thermal failures in present situation by taking into consideration recent incompatible repair work.

The analyses were done by using non-destructive investigation methods, such as microclimatic monitoring, quantitative infrared thermography (QIRT), heat and water vapour transfer calculations, supported by laboratory analyses on thermo-physical properties of historic materials. The results were evaluated in terms of thermal properties of historic materials establishing the historic dome section, microclimatic characteristics of Şengül Hamamı, its original thermal characteristics, and thermal failures occurred in time due to wrong repairs. An *in-situ* assessment method was also developed for the identification of thermal and moisture failures at real boundary conditions by joint interpretation of QIRT and heat transfer calculation results.

The study showed that historic dome structure of Şengül Hamamı was originally configured to provide sufficient thermal insulation characteristics owing to good thermal properties of its materials. That success was attributed to conscious use of low-density,

high-porosity historic materials having low thermal conductance and high vapour permeability characteristics. It was seen that the thermal performance of historic structure was severely destroyed by recent repairs using concrete and cement-based materials, which were incompatible with historic fabric of the structure due to their different thermo-physical properties.

Keywords: Quantitative Infrared Thermography, Heat Transfer Analyses, Water Vapour Transfer Analyses, Historical Turkish Baths (Hamam), Thermal Failures.

ÖZ

TARİHİ TÜRK HAMAMLARININ ISIL PERFORMANSLARININ İNCELENMESİ

Çiçek, Pınar (Kırmızıdağ)
Yüksek Lisans, Mimarlık Bölümü, Yapı Bilimleri
Tez Yöneticisi: Yrd. Doç. Dr. Ayşe Tavukçuoğlu

Eylül 2009, 137 sayfa

Tarihi Türk hamamlarının ısıl performanslarına etki eden malzeme ve yapım teknolojilerini keşfetmek ve bu işlevlerinin uzun yıllar boyu devamını sağlamak için kapsamlı araştırmalar gerekmektedir. Bu çalışma kapsamında, 15. yüzyıl Osmanlı dönemi yapısı olan Şengül Hamamı'nın (Ankara) ısıl performans özellikleri ve onarımlar sonucu ortaya çıkan ısıl sorunları incelenmiştir.

Çalışmalar mikroklimatik incelemeler, kızılötesi ısıl görüntüleme ve ısı transfer analizlerinin birlikte kullanımı ve su buharı transfer analizleri gibi tahribatsız yöntemler kullanılarak yapılmış ve laboratuar analizleri ile desteklenmiştir. Sonuçlar, "tarihi Türk hamamlarında kullanılan tarihi malzemelerin ısıl ve fiziksel özellikleri", "yapının özgün mikroklima özellikleri", "tarihi yapının ısıl yalıtım özellikleri ve günümüzdeki durumu ile karşılaştırılması", "yanlış onarımlar sonucu meydana gelen ısıl sorunlar" ve "yapıların gerçekte taşıdığı ısıl sorunların teşhisinde kızılötesi ısıl görüntüleme ve ısı transfer hesaplarının birlikte kullanılması" açılarından değerlendirilmiştir.

Şengül Hamamı'na ait tarihi üst örtüsünün özgününde iyi tasarlanmış ısı yalıtım özelliklerine sahip olduğu ve tarihi malzemelerin düşük ısı iletkenliği ve yüksek su buharı geçirimliliği gibi iyi ısıl özellikler taşıdığı anlaşılmıştır. Bu başarıda tarihi yapı malzemelerinin bilinçli kullanımı önemli rol oynamaktadır. Tarihi malzemelerinkine göre yüksek ısıl iletkenlik ve düşük su buharı geçirimliliğine sahip olan beton ve çimento

sıvaları, ısı yalıtımı açısından tarihi Türk hamamlarının onarımlarında kullanılmamalıdır. Bu malzemeler ile yapılan onarımlar sonucunda tarihi hamam yapıları, özgününde sahip oldukları iyi tasarlanmış ısıl performans özeliklerini tamamen kaybetmişlerdir.

Anahtar Kelimeler: Nicel Kızılötesi Isıl Görüntüleme, Isı Transfer Analizleri, Su Buharı Transfer Analizleri, Tarihi Türk Hamam Yapıları, Isıl Sorunlar.

To My Little Daughter

ACKNOWLEDGMENTS

I gratefully thank my supervisor, Asist. Prof. Dr. Ayşe Tavukçuoğlu for the scientific guidance, remarkable contributions and constant encouragement she has provided throughout the study.

I wish to express my appreciation and thanks to Prof. Dr. Emine N. Caner-Saltık, the director of the Turkish team within the EU Project, "*Hammam-517704: Aspects and Multidisciplinary Methods for the Mediterranean Region*", *EU, FP6, INCO, Specific Targeted Project, 2006-2008,* for her guidance and recommendations throughout the progress of the study from beginning to end. I would also like to thank the staff of the Materials Conservation Laboratory for their support during the experimental stage of the study.

Special thanks are to other attending jury members, Assoc. Prof. Dr. Arda Düzgüneş, Prof. Dr. Şahinde Demirci and Part-time Instr. Levent Tosun for their criticism and advice in the evaluation of the study. I am grateful to Mr. Ermanno Grinzato for his precious contributions to the study with his deep knowledge and experience on IRT.

I am also grateful to The Scientific and Technological Research Council of Turkey (TUBITAK) for their grant of a scholarship for the duration of my graduate studies.

I would also like to thank the General Directorate of Pious Foundations (Vakıflar Genel Müdürlüğü) for providing measured drawings of Şengül Hamamı.

I am forever indebted to my dear parents, Güllü and Hasan Kırmızıdağ, my sister and brother, Çiğdem and Çağlayan for the great sacrifices, endless love and continuous support they have never ceased to give me throughout my life.

Finally, my special thanks and love to my husband, Reis Çiçek for his great encouragement, support and understanding and to our little daughter, Lüle Çiçek. This thesis is dedicated to her.

TABLE OF CONTENTS

ABSTRACT iv
ÖZ vi
ACKNOWLEDGEMENTS ix
TABLE OF CONTENTS x
LIST OF TABLES xiii
LIST OF FIGURES xv
LIST OF ABBREVIATIONS xxi
LIST OF UNITS xxiii

CHAPTERS

1. INTRODUCTION 1
   1.1 Argument 1
   1.2 Objectives 3
   1.3 Procedure 4
   1.4 Disposition 5
2. LITERATURE SURVEY 6
   2.1 Historical Turkish Baths in the Ottoman Period 6
      2.1.1 Architectural characteristics 7
      2.1.2 Heating system 10
   2.2 Parameters Affecting the Thermal Performance of Building Materials 14
      2.2.1 Thermo-physical properties 14
      2.2.2 Water vapour permeability properties 18
      2.2.3 Moisture content of materials 20
      2.2.4 Thermal failures 22
   2.3 Heat Transfer Mechanisms of Building Components 25
   2.4 Physical Properties of Historic Masonry Materials 29
   2.5 Quantitative Infrared Thermography (QIRT) 36

3. MATERIAL AND METHOD 40
3.1 Material: Şengül Hamamı 40
3.1.1 The heating system of Şengül Hamamı 41
3.1.2 Roof and wall sections of Şengül Hamamı: *ORIGINAL* and *AS-IS* cases 45
3.2 Laboratory Analyses 48
3.2.1 Determination of basic physical properties 50
3.2.2 Determination of thermal properties 51
3.3 *In-Situ* Analyses 56
3.3.1 Microclimatic monitoring 57
3.3.2 Infrared thermography 57
3.4 Heat Transfer Analyses 58
3.4.1 Determination of the total thermal resistance and transmittance values 58
3.4.2 Heat transfer calculations 60
3.5 Water Vapour Transfer Analyses 61
3.5.1 Analyses of water vapour transmission/flow 62
3.5.2 Analyses of partial vapour pressure distribution 62
4. RESULTS 65
4.1 Basic Thermo-Physical Properties of Historic Materials 65
4.2 Microclimatic Analyses 69
4.3 Quantitative Infrared Thermography Analyses 74
4.4 Heat Transfer Analyses 78
4.4.1 Total thermal resistance and transmittance values of the dome sections 78
4.4.2 Heat transfer analyses through the dome section 81
4.5 Water Vapour Transfer Analyses 87
4.5.1 Continuity of water vapour permeability through the dome section 87
4.5.2 Partial vapour pressure distribution through the dome section 90

5. DISCUSSION AND CONCLUSIONS 94
5.1 Thermal Properties of Materials Used in Historical Turkish Baths 94
5.2 Microclimatic Characteristics of the Structure 96
5.3 Thermal Characteristics of the Historic Structure and Its Comparison with the Present Situation 97
5.4 Thermal Failures due to Improper Recent Repairs 99
5.5 Joint Use of QIRT and Heat Transfer Calculations for the Thermal Failure Assessment of Real Situations 102
5.6 Conclusions 104
REFERENCES 107
APPENDICES
A. TECHNICAL SPECIFICATIONS OF THE INSTRUMENTS USED IN THE STUDY 116
A.1 AGEMA 550 Camera - Radiometric Handheld Infrared Camera 116
A.2 FLIR ThermaCAM E65 Infrared Camera 118
A.3 HOBO WarePRO Temperature/Relative Humidity/Light/External Data Loggers 121
B. SATURATED WATER VAPOUR PRESSURE AT A GIVEN TEMPERATURE 122
C. THERMO-PHYSICAL PROPERTIES OF HISTORIC MATERIALS IN METRIC UNITS 124
D. RESULTS OF PARTIAL VAPOUR PRESSURE DISTRIBUTION ANALYSES OF THE DOME SECTION OF WOMEN'S HOT SPACE FOR ALL MONTHS 125

LIST OF TABLES

TABLES

Table 2.1 Acceptable U values given in TS 825 for quality construction of buildings situated in the 3rd region of Turkey. 18

Table 2.2 Classification of water vapour permeability properties of materials in terms of S_D values. 20

Table 2.3 Inside surface resistances, R_{si}, in $m^2K\ W^{-1}$. 28

Table 2.4 External surface resistances, R_{se}, in $m^2K\ W^{-1}$ for various exposures and surfaces. 28

Table 2.5 The bulk density and porosity values of historic materials, which were used in the various analyses in the context of this thesis, the historical bath buildings they belong to and the literature from which the values were cited. 35

Table 2.6 Resistance to water vapour permeation values, μ, of historic brick, brick mortar and exterior plasters with the buildings they belong to and the literature from which the values were cited. 35

Table 2.7 Resistance to water vapour permeation values, μ, of contemporary building materials and the literature from which the values were cited. 36

Table 2.8 The bulk density and thermal conductivity values of light construction materials produced for thermal insulation purposes and the literature from which the values were cited. 36

Table 3.1 Names and types of the samples of historic brick, stone, brick and stone mortar, interior and exterior plasters together with the historical buildings and cities they belong to. 49

Table 4.1 Thermo-physical properties of historic brick (HB), brick mortar (HBM), exterior plasters (HEP) and interior plasters (HIP) in SI units forming the brick dome masonry. 66

Table 4.2 The thermal resistance values, R, of all layers forming the *ORIGINAL* and *AS-IS* roof/dome sections of Şengül Hamamı. 79

Table 4.3 The equivalent air layer thickness of water vapour diffusion values, S_D, for layers forming the dome sections of Şengül Hamamı in the *ORIGINAL* and *AS-IS* cases calculated with their resistance to water vapour permeation values, μ, and real thicknesses. 89

Table B.1 Saturated water vapour pressures in Pa for the temperatures between 0°C and -30°C 122

Table B.2 Saturated water vapour pressures in Pa for the temperatures between 0°C and 40°C 123

Table C.1 The thermo-physical properties of historic brick (HB), brick mortar (HBM), exterior plasters (HEP) and interior plasters (HIP) in metric units forming the brick dome masonry. 124

LIST OF FIGURES

FIGURES

Figure 2.1 A schematic drawing that shows the organization of the spaces in an historical Turkish bath. 8

Figure 2.2 A schematic drawing that shows the heating system of historical Turkish baths. 11

Figure 2.3 Plan showing the hypocaust under the bathing spaces of Haseki Hürrem Sultan Hamamı in the Sultanahmet district, İstanbul. 12

Figure 2.4 Drawings showing the construction of the "raised floor" of historical baths. 12

Figure 2.5 Views of terracotta draft chimneys (*tüteklik*) rising inside the wall up to the roof in Yıldırım Beyazıt Hamamı, in Mudurnu, Bolu. 12

Figure 2.6 Sections showing the elements of the heating system for Çukur Hamam; furnace, *cehennemlik* and draft chimneys. 13

Figure 3.1 Plan of Şengül Hamamı showing sections for the women's and men's parts and service spaces. 41

Figure 3.2 Views of the furnace in Şengül Hamamı. 42

Figure 3.3 Section showing the heating system of Şengül Hamamı. 43

Figure 3.4 Roof plan showing the distribution of draft chimneys, *D*, in Şengül Hamamı. 43

Figure 3.5 Representative drawing showing the diffusion of hot gases coming out of the furnace in the hypocaust of Şengül Hamamı and its orientation towards the outlets of draft chimneys. 44

Figure 3.6 View of two draft chimneys; one out of use (on the left) and one with a damper mechanism to open and close the top (on the right) on the roof of Şengül Hamamı. 44

Figure 3.7 Section showing the location of furnace underneath the hot water storage room. 45

Figure 3.8 Views of Şengül Hamam's roof covered by an 8 cm-thick mesh-reinforced concrete layer. 45

Figure 3.9 Geometric descriptions of dome models showing the order and thickness of the layers for the "*ORIGINAL case*" representing the historic dome structure of Şengül Hamamı (at left) and for the "*AS-IS case*" including the recent repairs with cement-based materials (at right). 47

Figure 3.10 Geometric descriptions of wall models showing the order and thickness of the layers for the "*ORIGINAL case*" representing the historic wall structure of Şengül Hamamı (at left) and for the "*AS-IS case*" including the recent repairs with cement-based materials (at right). 47

Figure 3.11 Samples of historic brick, stone, brick and stone mortar, interior and exterior plasters collected from the historical baths belonging to the same period with Şengül Hamamı. 48

Figure 3.12 Views (at left) and schematic drawing (at right) of the calorimeters that were used in the experiments for the determination of specific heat capacity values of historic samples. 53

Figure 3.13 Photographs showing the experimental setup for the determination of specific heat capacity values of historic samples. 54

Figure 3.14 Plan showing the distribution of data loggers in different parts of Şengül Hamamı. 57

Figure 3.15 Partial and equilibrium water vapour pressure distribution in a wall where (a) there is no risk of condensation and where(b) condensation occurs. 64

Figure 4.1 Bulk density (ρ) and porosity ($\varnothing$) of historic and cement-based repair materials. 67

Figure 4.2 Thermal conductivities of historic and cement-based repair materials. 68

Figure 4.3 The monthly means of ambient temperatures, showing the gradual increase in temperature between the spaces, starting from the outside air to the entrance hall, then to the undressing room, and to the warm and hot bathing spaces of the women's part. 70

Figure 4.4 The monthly means of ambient temperature and relative humidity in the women's and men's hot spaces and at outside during a year. 70

Figure 4.5 The daily means of ambient temperature and relative humidity at women's and men's hot spaces in January and August; showing the interior ambient temperature differences of 2.9°C ±0.7°C and 2.7°C ±0.6°C measured between the months of August and January at the women's (a) and men's (b) hot spaces, respectively, while the humidity conditions were remained the same. 71

Figure 4.6 The curves of air temperature close to the exterior dome surface and outside air temperature for a period of three-and-a-half hours in February at night, showing that the air temperature close to the dome surfaces was warmer than the outdoor temperature with a temperature difference of 3.1°C ± 0.5°C. 72

Figure 4.7 The daily temperature and relative humidity fluctuations at the women's and men's hot spaces for a period of one week in January and August; showing the daily ambient temperature fluctuations in the range of 0.72°C±0.12°C and 0.57°C±0.16°C in the women's hot space (a) and in the range of 0.56°C±0.20°C and 0.23°C±0.09°C in the men's hot space (b) in January and August, respectively. 73

Figure 4.8 The IR images of the selected regions; F1 (at top) and F2 (at bottom) were taken at night in July at the boundary conditions of 26^{o}C and 30% RH while the interiors' conditions being around 38^{o}C and 95%RH. 74

Figure 4.9 The IR image taken from the north side of the dome of the women's hot space at outdoor ambient air conditions of 10.7°C and 40%RH in November; and its differential IR image (at bottom right), that is the temperature difference between the last and first IR images in the sequence, showing the heat loss from the concrete-clad dome surfaces with ΔT=+0.2°C in 322s during the cooling period at night. 75

Figure 4.10 A partial view from the west wall of the men's undressing room and its IR image showing that surface temperatures of the wall were warmer than the ambient temperature of 2.8°C in February, at night, with a temperature difference of 6.5°C. 75

Figure 4.11 A partial view from the west wall of men's hot space on the axis of chimney and its IR image showing that surface temperatures of the wall were warmer than the ambient temperature of 2.8°C in February, at night, with a temperature difference of 12.5°C. 76

Figure 4.12 A partial view from the north side of the women's undressing room and its IR image taken at the boundary conditions of 26°C and 30% RH at night in July, showing significant heat loss at the lower parts of the chimney and circular dome-lights. 77

Figure 4.13 The IR and differential IR images taken from the dome of the men's hot space at the boundary conditions of 12.7°C and 40%RH in November, showing the significant heat loss at the circular dome-lights and at the bottom edge of the chimney stack, reaching ΔT = 3.2°C and ΔT = 6.3°C in 420s, respectively, during the cooling period of night in November. 77

Figure 4.14 The curves showing the temperature gradients through layers forming the domes of the women's warm and hot spaces in January (at top) and in August (at bottom), calculated according to the thermal conductivity values and thicknesses of each layer at the steady state conditions for the *AS-IS case* (at left); and for the *ORIGINAL case* (at right) with and without earth cover. 80

Figure 4.15 Visible light photographs taken from the dome of the women's warm space and the IR images of selected regions: the exterior views (at top) and the interior views (at bottom). Here, the temperature scales are in the range of -0.8 ºC - +7.8ºC and +7.1 ºC - +25.1 ºC. 81

Figure 4.16 Visible light photographs taken from the dome of the women's hot space and the IR images of selected regions: the exterior views (at top) and the interior views (at bottom). Here, the temperature scales are in the range of -8.2ºC - +10.2ºC and +9.4 ºC - +33.4ºC. 82

Figure 4.17 The thermal models of the domes of the women's warm (at top) and hot (at bottom) spaces representing the real interior and exterior surface temperatures of dome sections. 82

Figure 4.18 Sections through the domes of the women's warm (at left) and hot (at right) spaces, showing temperature gradients through each component calculated according to the thermal conductance and thickness of each layer (lines in black); and heat flow curves produced according to the real surface temperatures measured at inside and outside surfaces of the dome structures. 83

Figure 4.19 Real surface temperatures of some regions selected from the exterior dome surfaces of the women's warm (at top) and hot (at bottom) spaces, taken during the cooling period of night for 300s in February, showing their relationship with the outside air and warm boundary air temperatures. 84

Figure 4.20 Real surface temperatures of some regions selected from the interior dome surfaces of women's warm (at top) and hot (at bottom) spaces, taken during the constant interior ambient temperatures during the cooling period of night for 300 s in February. 85

Figure 4.21 μ values of historic and cement-based repair materials with their S_D values calculated by their layer thickness, showing that the mesh-reinforced concrete layer had the highest μ value and the cement-based plaster layers had higher μ values than those of historic brick, brick mortar and plasters. 89

Figure4.22 Total S_D values of the dome sections of Şengül Hamamı in the *ORIGINAL* (at left) and *AS-IS* (at right) cases. 90

Figure 4.23 Partial (*pi* and *pe*) and equilibrium (*ps*) water vapour pressure distributions of the dome sections of Şengül Hamamı for the *ORIGINAL* (at top) and *AS-IS* (at bottom) cases; according to the mean values of January – exterior conditions of 1.5°C and 76.3% RH and interior conditions of 34.5°C and 95.3% RH; showing that in both cases the dome section was totally under the risk of interstitial condensation, being extremely wet in the AS-IS case. 92

Figure 4.24 Partial (*pi* and *pe*) and equilibrium (*ps*) water vapour pressure distributions of the dome sections of Şengül Hamamı for the *ORIGINAL* (at top) and *AS-IS* (at bottom) cases; according to the mean values of August – exterior conditions of 27.8°C and 30.5% RH and interior conditions of 37.4°C and 94.1% RH; showing that the dome section was completely dry in the *ORIGINAL* case while it was under the risk of interstitial condensation in the *AS-IS* case. 93

Figure D.1 The partial vapour pressure distribution analyses of the dome section of women's hot space in *ORIGINAL* (at top) and *AS-IS* (at bottom) cases for the monthly-mean temperature and RH values of January (in middle), together with those for above (at left) and below (at right) the range of monthly means. 126

Figure D.2 The partial vapour pressure distribution analyses of the dome section of women's hot space in *ORIGINAL* (at top) and *AS-IS* (at bottom) cases for the monthly-mean temperature and RH values of February (in middle), together with those for above (at left) and below (at right) the range of monthly means. 127

Figure D.3 The partial vapour pressure distribution analyses of the dome section of women's hot space in *ORIGINAL* (at top) and *AS-IS* (at bottom) cases for the monthly-mean temperature and RH values of March (in middle), together with those for above (at left) and below (at right) the range of monthly means. 128

Figure D.4 The partial vapour pressure distribution analyses of the dome section of women's hot space in *ORIGINAL* (at top) and *AS-IS* (at bottom) cases for the monthly-mean temperature and RH values of April (in middle), together with those for above (at left) and below (at right) the range of monthly means. 129

Figure D.5 The partial vapour pressure distribution analyses of the dome section of women's hot space in *ORIGINAL* (at top) and *AS-IS* (at bottom) cases for the monthly-mean temperature and RH values of May (in middle), together with those for above (at left) and below (at right) the range of monthly means. 130

Figure D.6 The partial vapour pressure distribution analyses of the dome section of women's hot space in *ORIGINAL* (at top) and *AS-IS* (at bottom) cases for the monthly-mean temperature and RH values of June (in middle), together with those for above (at left) and below (at right) the range of monthly means. 131

Figure D.7 The partial vapour pressure distribution analyses of the dome section of women's hot space in *ORIGINAL* (at top) and *AS-IS* (at bottom) cases for the monthly-mean temperature and RH values of July (in middle), together with those for above (at left) and below (at right) the range of monthly means. 132

Figure D.8 The partial vapour pressure distribution analyses of the dome section of women's hot space in *ORIGINAL* (at top) and *AS-IS* (at bottom) cases for the monthly-mean temperature and RH values of August (in middle), together with those for above (at left) and below (at right) the range of monthly means. 133

Figure D.9 The partial vapour pressure distribution analyses of the dome section of women's hot space in *ORIGINAL* (at top) and *AS-IS* (at bottom) cases for the monthly-mean temperature and RH values of September (in middle), together with those for above (at left) and below (at right) the range of monthly means. 134

Figure D.10 The partial vapour pressure distribution analyses of the dome section of women's hot space in *ORIGINAL* (at top) and *AS-IS* (at bottom) cases for the monthly-mean temperature and RH values of October (in middle), together with those for above (at left) and below (at right) the range of monthly means. 135

Figure D.11 The partial vapour pressure distribution analyses of the dome section of women's hot space in *ORIGINAL* (at top) and *AS-IS* (at bottom) cases for the monthly-mean temperature and RH values of November (in middle), together with those for above (at left) and below (at right) the range of monthly means. 136

Figure D.12 The partial vapour pressure distribution analyses of the dome section of women's hot space in *ORIGINAL* (at top) and *AS-IS* (at bottom) cases for the monthly-mean temperature and RH values of December (in middle),together with those for above (at left) and below (at right) the range of monthly means. 137

LIST OF ABBREVIATIONS

ABBREVIATIONS

A ..... Surface area, m^2

c ..... Specific heat, J $kg^{-1}K^{-1}$

C ..... Thermal mass, J K^{-1}

D ..... Draft chimney

e ..... Thermal effusivity, W $s^{-1/2}m^{-2}K^{-1}$

IR ..... Infrared

IRT ..... Infrared Thermography

k ..... Thermal conductivity, W $m^{-1}K^{-1}$

l ..... Thickness, m

M ..... Mass of the substance, g

M_{dry} ..... Dry weight, g

M_{sat} ..... Saturated weight, g

M_{arc} ..... Weight of the sample in water, g

p ..... Partial vapour pressure, Pa

ps ..... Equilibrium water vapour pressure at a given temperature, Pa

q ..... Heat, J or cal

Q ..... Heat flow, W m^{-2}

QIRT ..... Quantitative Infrared Thermography

R ..... Thermal resistance, $m^2K\ W^{-1}$

R_{si} ..... Thermal resistance of interior surface, $m^2K\ W^{-1}$

R_{se} ..... Thermal resistance of exterior surface, $m^2K\ W^{-1}$

R_a ..... Thermal resistance of air space, $m^2K\ W^{-1}$

R_T ..... Total thermal resistance, $m^2K\ W^{-1}$

S_D ..... Equivalent air layer thickness of water vapor diffusion, m

T ..... Temperature, ˚C

T_i ..... Interior air temperature, °C

T_e ..... Exterior air temperature, °C

U ..... Thermal transmittance, W $m^{-2}K^{-1}$

VHC ..... Volumetric Heat Capacity, in J $m^{-3}K^{-1}$

α ..... Thermal diffusivity, $m^2 s^{-1}$

μ ..... Water vapor diffusion resistance

φ ..... Relative humidity, %

ΔT ..... Temperature difference, °C

ρ ..... Bulk density, $kg\ m^{-3}$

$\varnothing$ ..... Porosity, %

LIST OF UNITS

UNITS

cal	Calorie
cal $g^{-1}°C^{-1}$	Calorie per gram degree Celsius
cal $s^{-1}cm^{-1}°C^{-1}$	Calorie per second centimeter degree Celsius
cal $cm^{-1}°C^{-1}$	Calorie per centimeter degree Celsius
°C	Degree Celsius
g	Gram
g cm^{-3}	Gram per cubic centimetres
J	Joule
J $kg^{-1}K^{-1}$	Joule per kilogram Kelvin
J $m^{-3}K^{-1}$	Joule per cubic meter Kelvin
J K^{-1}	Joule per Kelvin
kg	Kilogram
kg m^{-3}	Kilograms per cubic meter
m	Meter
m^2	Square meter
m^2 s^{-1}	Square meter per seconds
m^2K W^{-1}	Square meter Kelvin per Watt
Pa	Pascal
s	Seconds
W $s^{-1/2}m^{-2}K^{-1}$	Watt per square root second square meter Kelvin
W $m^{-1}K^{-1}$	Watt per meter Kelvin
W $m^{-1}°C^{-1}$	Watt per meter Celsius
W m^{-2}	Watt per square meter
W $m^{-2}K^{-1}$	Watt per square meter Kelvin
%	Percent

CHAPTER 1

INTRODUCTION

In this chapter, the argument for and the aim of the study on which this thesis was based are presented under the respective sections. It continues with a section titled “Procedure” where the basic steps of the study are outlined and ends with one titled “Disposition” which gives a preview of what is embodied in the rest of the study.

1.1 Argument

Historical Turkish baths are the valuable documents reflecting the builders’ knowledge of the past in terms of historical building, materials and functional technologies. Those structures present those technologies acting in a harmony which establish a durable structure functioning like a machine with all its heating, water supply and drainage, lighting and ventilation systems. Their indoor climate is particularly different than the other historic structures. They involve three different microclimates under the same roof that deserves to discover the technological features contributing to that particular thermal performance. In that regard, it is interesting to investigate the thermal insulation characteristics of historic building materials and building components of those structures. That knowledge on those historical technologies is essential for the maintenance and conservation of historical Turkish baths in order to keep them in working order with their authentic features overtime.

This study focused on the assessment of the thermal performance characteristics of historical Turkish baths with an emphasis on the thermo-physical properties of the historic materials, any thermal failures in their present situation due to recent indifferent repairs. The literature showed a singular lack of pertinent knowledge on the thermal properties of building components used in the subject buildings, such as coefficients of total thermal resistance, R_T, and thermal transmittance, U. The number of studies on the basic thermo-physical features of historic materials and microclimatic conditions particular for bath structures were found to

be rather limited in terms of both scope and quantity. Comprehensive studies seemed to be sorely needed in this regard.

The present study was conducted on an Ottoman bath, a "*hamam*" dating from the 15th Century, Şengül Hamamı, located in the city of Ankara, Turkey. This structure is a typical double bath, consisting of two separate parts: one for men and one for women. It still represents the continuing experience of hamam culture in Anatolia by keeping its original architecture and building technologies. Hence it was selected as a case study to examine its thermal performance characteristics in terms of microclimatic parameters of its structure, thermal properties of its historic masonry and failures that occurred in its lifetime that could be attributed to recent repairs. For this purpose, two configurations were produced, namely the "*ORIGINAL case*" and the "*AS-IS case*". The former represented the historic structure of Şengül Hamamı while the later represented the present structure with the recent repairs with cement-based materials. The *ORIGINAL case* was defined according to the historical baths belonging to the same period with Şengül Hamamı and still including the historic/original materials and construction techniques.

It was considered most desirable to conduct this investigation by non-destructive methods, since these allow the necessary analyses to be made without any physical intervention to it. The infrared thermography is one of those methods which make it possible to detect the problems areas in a structure, such as thermal failures, moist areas and materials defects. That method is also promising for the in-situ assessment of such failures (Disli, Tavukcuoglu, Tosun and Grinzato, 2008a; Disli, Tavukcuoglu and Tosun 2008b; Grinzato, Bison and Marinetti, 2002a; Grinzato, Bressan, Marinetti, Bison and Bonacina, 2002b; Tavukçuoğlu, Duzgunes, Demirci and Caner-Saltık, 2005; Tavukcuoğlu, Düzgüneş, Demirci and Caner-Saltık, 2007; Kandemir-Yucel, Tavukcuoglu, Caner-Saltik, 2007; Titman, 2001). However there was a necessity to improve the quantitative analyses of infrared data for the thermal insulation assessment of the overall historic wall/dome section and the enhance in-situ methods for acquiring accurate infrared data in that regard. To this end, it was decided to use quantitative IR thermography (QIRT) together with microclimatic monitoring, heat and water vapour transfer calculations. Laboratory analyses were done to determine the thermo-physical properties of the historic materials, such as historic brick and brick mortar, lime-based interior and exterior plasters forming the overall historic dome structure. The QIRT analyses and heat transfer calculations were, therefore, used together in order to assess the

thermal failures of the building envelope, such as heat loss, thermal bridges, air leakages and condensation and entrapped moisture under natural in-use situations, on quantitative basis.

1.2 Objectives

This study was conducted to discover the original thermal performance characteristics of historical Turkish baths, especially with an emphasis on thermal insulation properties of historical materials contributing to their performance. That knowledge was essential to better understand the building and material technologies of historical Turkish baths establishing their particular thermal features and to keep these inherent technological features for the future by means of well-planned maintenance/conservation programs. The present thermal performance of the historical Turkish baths was also examined in relation to the use of improper repair materials.

In the light of these concerns, the specific objectives of the study were:

1. To discover the original thermal characteristics of historical baths in terms of thermo-physical properties of historic materials and thermal insulation and water vapour permeability features of building components.

2. To define the microclimatic characteristics particular to historical baths having three different microclimate under the same shelter.

3. To evaluate the potentials of QIRT for the *in-situ* assessment of thermal failures in historical structures, such as heat loss, thermal bridges, air and moisture leakages and condensation.

4. To improve the quantitative analyses of surface temperature data together with heat transfer calculations in steady state conditions, especially to examine the present/real situation of historical buildings.

Şengül Hamamı, which is a typical historical Turkish bath, was examined to achieve the knowledge based on these objectives.

1.3 Procedure

This study was conducted in four basic phases. In the first, a comprehensive literature survey was done on historical Turkish baths of the Ottoman period, in terms of their architectural characteristics and heating systems. Parameters affecting the thermal performance of building materials and heat transfer mechanisms of building components were also described in this phase. In addition, the physical properties of historic masonry materials were summarized here. Information on the Quantitative Infrared Thermography (QIRT) method was also given as a non-destructive method as used extensively in this study. This survey was done to provide preliminary information needed for initiation of the study.

In the second phase, a 15th Century Ottoman bath, Şengül Hamamı, located in Ankara, Turkey was described together with its heating system and roof and wall sections for its *ORIGINAL* and *AS-IS* cases. The measured drawings of this structure were taken from General Directorate of Pious Foundations. A set of investigation methods used for the evaluation of thermal performance characteristics of Şengül Hamamı was also defined in this section. The study consisted of laboratory analyses, *in-situ* analyses including microclimatic monitoring and infrared thermography, heat transfer analyses and water vapour transfer analyses.

In the third phase, the data obtained from the various investigation methods and the joint interpretation of QIRT and heat transfer calculations were evaluated and this part was described in the following chapter “Materials and Methods”.

In the final, the results of the study were evaluated and discussed in terms of the thermal properties of historic materials used in historical Turkish baths; the microclimatic characteristics of the structure; the thermal characteristics of the historic structure and its comparison with the present situation; the thermal failures due to improper recent repairs and the joint use of QIRT and heat transfer calculations for the thermal failure assessment of real situations. In the light of findings, the author gave some recommendations for future studies.

1.4 Disposition

The study is presented in five chapters, of which this introduction is the first. In the second is given a summary of the literature basically on the historical Turkish baths in Ottoman period. It continues with an overview of the parameters affecting the thermal performance of building materials, the heat transfer mechanisms of building components and the physical properties of historic masonry materials. Quantitative Infrared Thermography (QIRT) is also described in this chapter.

In the third chapter is given a description of the material, Şengül Hamamı, together with that of its heating system and the roof/wall sections of its *ORIGINAL* and *AS-IS* cases. Also described in this chapter are the investigation methods used in the study.

The fourth chapter is where the results obtained from the various analyses and the joint interpretation of QIRT and heat transfer calculations are presented in the form of tables, figures, drawings and charts. In the fifth and last chapter are presented a discussion on the results and a conclusion regarding the study as a whole. Some suggestions for the improvement of the thermal performance of historical baths and suitable maintenance and conservation programs as well as those for future studies are also given here.

CHAPTER 2

LITERATURE SURVEY

In this chapter, the literature survey of the study is presented. First of all, historical Turkish baths of the Ottoman period were described in terms of their architectural characteristics and heating systems. Then, parameters affecting the thermal performance of building materials and heat transfer mechanisms of building components were described. In addition, the physical properties of historic masonry materials were summarized here. Lastly, information on the Quantitative Infrared Thermography (QIRT) was given as a non-destructive method as used extensively in this study.

2.1 Historical Turkish Baths in the Ottoman Period

The term "Turkish bath" is a widely-used one that identifies the baths developed in the land of Anatolia under the rules of Islam. According to Işık (1995), historical Turkish baths include and refer to the typical characteristics of the Anatolian-Islamic baths developed especially throughout the Ottoman period. Caner-Saltık (2008) notes that these baths reflect the continuous experience of bathing culture in Anatolia and that they therefore have a significant value since they represent the architectural and technological knowledge of our past starting from the Hittite period. In Anatolia, the first examples of the use of a separate space for bathing and cleaning purposes were found in Boğazköy (Darga, 1985).

Işık (1995) also states that the bath and bathing are as old as the earliest civilizations and the separate structures for bathing could be found in the architecture of almost every civilization. In Antique times bathing was not only a bodily function for the purpose of cleaning; it was also enriched with social meanings and attainment. Başaran and Ilken (1997) say that the ancient Greeks were the first people to give importance to baths, but it was in the Roman world that bathing became an inseparable part of daily life. Işık (1995) also states that Anatolia was introduced to Roman bathing culture during the Byzantine period. When the Turks arrived in Anatolia, they encountered the small public baths of Byzantine cities. It was

stated in the study of Temizsoy, Esen, Sahlan, Tunç and Telatar (2003) that a unique synthesis was achieved with the combination of the cleaning tradition of Islam and the existing cultural, architectural and technological heritage of baths in Anatolia. As a result, the new 'Turkish Bath', or so-called '*hamam'*, tradition had been created.

Işık (1995) further explains that the hamam tradition in Anatolia reached a peak in the 16th Century parallel to the growth of the Ottoman Empire. The hamam became an indispensable part of urban architecture under the administration of the vakıf organization, within the reach of the public. The historical Turkish baths in Anatolia could be classified into two groups as private and public (Çakmak, 2002; Önge, 1995; Taşcıoğlu, 1998; Işık, 1995). According to Önge (1995), while the former group referred to the baths of palaces, military barracks or caravanserais to serve a small group of people; the latter group was open to public serving for the people living in a village, a district or a part of a city.

The public baths, which can also be called as *halk hamamı* or *çarşı hamamı*, were either constructed as *single baths* or mostly as *double baths* (Çakmak, 2002; Taşcıoğlu, 1998; Önge, 1995). According to Taşçıoğlu (1998), single baths were either for men or for women. It was called as "*kuşluk hamamı*" when used by both men and women by arranging different days and hours. On the other hand, double or *çifte* baths were twin buildings - one reserved for men and the other for women - placed back to back with separate managements and supplied by the same service system. According to Önge (1995), the men's part was slightly larger than the women's part. Entrance to the men's part was from the main street, while that of women's was from a side street for privacy. In addition, there were also thermal baths (*kaplıca*) in Anatolia constructed over natural hot water reservoirs (Çakmak, 2002; Önge, 1995, Önge, 1988). Although they may also be called as hamam, they were generally used for curative purposes rather than bathing.

2.1.1 Architectural characteristics

A three-sectioned plan was used in the construction of historical Turkish baths of the Ottoman period (Temizsoy, *et al.,* 2003). The main sections of Ottoman baths were changing section, bathing section and service section; which are explained below. The plan of a typical historical Turkish bath is given in Figure 2.1.

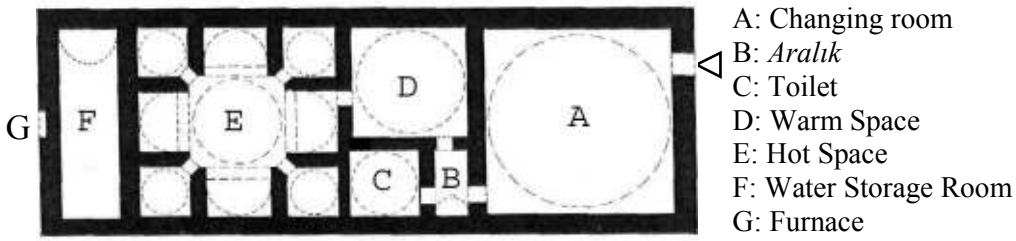

Figure 2.1 A schematic drawing that shows the organization of the spaces in an historical Turkish bath (*Source: Çakmak, 2002: 12*).

Changing section, which is called as Apodyterium in Roman baths is used for changing clothes, waiting and resting near the entrance and sometimes it includes the entrance (Başaran, 1995). It is generally the largest section of the bath. Temizsoy *et al.* (2003) states that the main entrance to the bath is directly from this section or from an additional entrance space for privacy and control of the interior climatic conditions. This section generally had high massive walls, the high ceiling of which was covered with a timber pitched roof or a dome with a lantern window (*fener*) at the center for illumination (Temizsoy, *et al.,* 2003). In addition, Işık (1995) says that in this section there were wooden cubicles either on raised balconies or on two-storey wooden galleries for clients to change their clothes inside. The characteristic features of this section were a coffee-house serving coffee to clients for relaxation after bathing and a small pool (*şadırvan*) with its water jet (*fiskiye*) in the middle for enjoying the sound of running water.

Bathing section is composed of two main parts: warm space (*ılıklık*) and hot space (*sıcaklık*); which are called Tepidarium and Caldarium in Roman baths, respectively (Önge, 1995). According to Aru (1949), the warm space (*ılıklık*) is a resting and refreshing area between the changing room and hot space where the body temperature can adapt it to the difference in heat before entering the bathing area. As Temizsoy *et al.* (2003) note, *ılıklık* is usually in the shape of a corridor covered with either dome or vaults. The toilets, herb or shaving room are separately connected to this area. The second part of the bathing section is the hot space (*sıcaklık*), which is the hottest part of the bath in which bathing activity takes place (Taşcıoğlu, 1998 and Temizsoy *et al.,* 2003). Önge (1995) describes the hot space as being composed of a central area surrounded by axially placed iwans (*eyvan*) and rooms at the corners (*halvet*) used as small private bathing cells. There is a marble slab (*göbektaşı*) in the center of the main space, which is usually called the heart of the bath, being its hottest

surface (Temizsoy *et al.*, 2003). Taşcıoğlu (1998) adds that there are marble banks (*seki*) 20 cm from the floor in the bathing areas and *halvets*, where the marble basins (*kurna*) for bathing are placed. The illumination of the central space, iwans and halvets is done by overhead skylights on the domes, semi-domes or vaults.

In the early examples of Turkish baths in Anatolia, there was an additional space between the changing and bathing sections, called as "*aralık*", which was composed of toilets and depilatory cells (Önge, 1995; Işık, 1995; Aru, 1949; Temizsoy *et al.,* 2003; Taşcıoğlu, 1998). According to Önge (1995) it was one of the most important architectural elements of early baths in Anatolia with a function of preventing the leakage of the hot air and steam from the bathing sections and so providing the control of heat transfer between cold and hot rooms. As Aru (1949) stated, in later examples it was replaced by a shaft over the door separating the changing and bathing sections to perform the same purpose and thus the toilets and depilatory cells become part of the bathing section.

The **service section** of historical Turkish baths is described by Dişli (2008) as being composed of hot and cold water storage rooms, firewood storage room and furnace together with the hypocaust *(cehennemlik)*. The hot and cold water storage rooms are where bathing water is stored. The hot water storage rooms are placed over the furnace and lie along one side of the hot space (*sıcaklık*). Both Temizsoy *et al.* (2003) and Önge (1995) state that the hot water storage room has a small window called an "*observation window*" as a connection to the hot space. Önge (1995) further explains the main purpose of this window as to control the amount of water in these rooms, to benefit from the steam generated there, to be able to do necessary repairs and to add water when necessary.

Firewood storage room is another part of this section where the wood necessary for heating the bath is stored (Önge, 1995). Both Temizsoy, *et al.* (2003) and Taşçıoğlu (1998) state that next to this area is placed furnace, which is the center that heats the water in the hot water storage room and the interiors of the bathing spaces. There is a concave copper boiler over the fireplace for heating water in the hot water storage room by the fire in the furnace. The hypocaust (*cehennemlik*) and draft chimneys (*tüteklik*) are the elements of heating system and parts of the service section.

2.1.2 Heating system

The comprehensive studies related with the heating system of historical baths are conducted by Aru (1949), Önge (1995), Yegül (1992) and Yegül (2006). According to Yegül (1992, 2006), the order and organization of spaces in historical baths is directly affected by the development of the heating systems. In the plan organization of these buildings, it is possible to see the clear separation of served and serving spaces and effective concentration on the heating elements. As Önge (1995) states that the historical baths were designed in such a way to increase the efficiency of the heating system. Temizsoy *et al.,* (2003) also support this idea by saying that the main design principle behind of the water supply and heating systems of *hamam*s is to get optimum use of water and heat sources, which is closely interrelated to the architectural and technological features of *hamam*s.

According to Yegül (1992, 2006), heating technology of historical Turkish baths followed their Roman and Byzantine prototypes with a fully developed hypocaust system (sub-floor heating system), which was defined as a "system in which the floor of the room was supported on short pillars and the space provided under it was filled with hot gases from a furnace which is stoked from outside." (Yegül, 1992: 357). The definition of the heating system of historical Turkish baths was given in the study of Önge (1995). According to her, in historical Turkish baths the same system was used for heating both the water in the hot water storage room and the interiors of the bathing spaces (Figure 2.2). The wood and/or coal stored in the firewood storage room is burned in the furnace by means of an arched opening in the form of a fireplace for lighting the fire. The water in the hot water storage room is heated by fire in the furnace via the copper boiler placed just over the fireplace, in the middle (Temizsoy, *et al,*. 2003; Taşçıoğlu, 1998; Önge, 1995).

Önge (1995) further explains that the interiors of the bathing section are generally heated by the circulation and dispersion of flame and smoke that result from the burning up of firewood inside the furnace. This circulation and dispersion take place inside the hypocaust (*cehennemlik*), which is the subterranean area of the bath composed of the interconnecting spaces underneath the floors of bathing sections (Figure 2.3). In the study of Temizsoy, *et al.* (2003) the hypocaust was defined as a space composed of a "raised floor" supported by short, closely spaced pillars of square or round bricks or stone pieces (Figure 2.4). The raised floor is constructed of two layers; a layer of slate stone slabs topped by a layer of mortar as

bedding for a marble slabs, for the hot air not to come into contact with the marble panels. The thickness of the floor also changes from one space to another according to the need of heating.

Önge (1995) goes on to explain that in order to maintain the circulation of hot gases the hypocaust (*cehennemlik*) has links to the outlets of draft chimneys (*tüteklik*), specifically built within the wall sections of the structure. These draft chimneys are constructed as a hole inside the massive rubble stonewalls with terracotta vertical pipes (*künk*) inside (Temizsoy, *et al.,* 2003) (Figure 2.5). The flow and orientation of the hot smoke under the floor as well as its pressure are controlled by the opening and closing the tops of these chimneys. According to Temizsoy, *et al.* (2003), *tüteklik* on the exterior walls, besides heating, provide control of heat loss or transfer while ones on the interior walls keep hot water circulates at a certain temperature inside the bath. The same author continues to state that hot steam, coming out of the observation window and rising from the *kurna*s during the bathing, also contributes to the heating of the interiors of the historical baths. An elevated marble platform, *"göbektaşı",* was located at the center of the hot space, which is the hottest surface of the bath. The undressing room is heated by means of a stove located at its center.

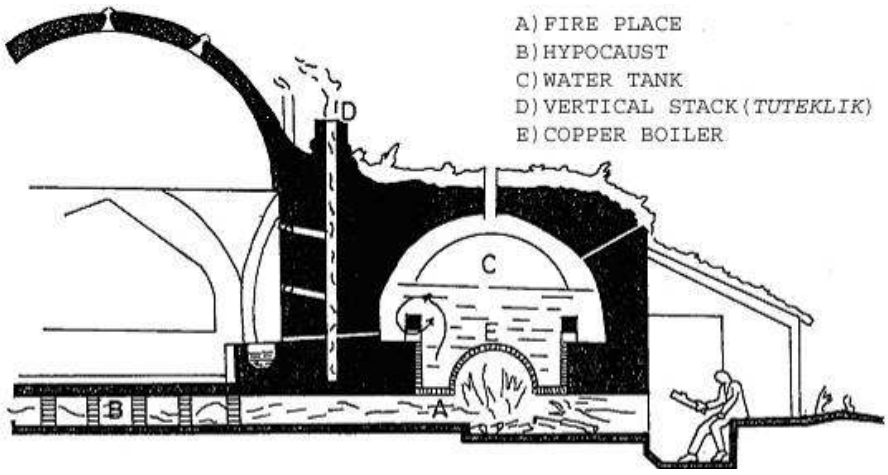

Figure 2.2 A schematic drawing that shows the heating system of historical Turkish baths (*Source: Aru, 1943: 37*)

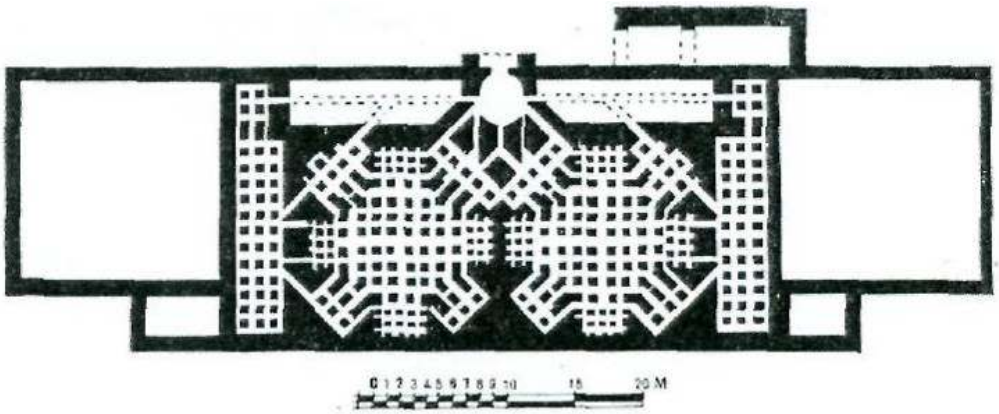

Figure 2.3 Plan showing the hypocaust under the bathing spaces of Haseki Hürrem Sultan Hamamı in the Sultanahmet district, Istanbul (*Source: Islam Encyclopedia, 1964, v.1:176*).

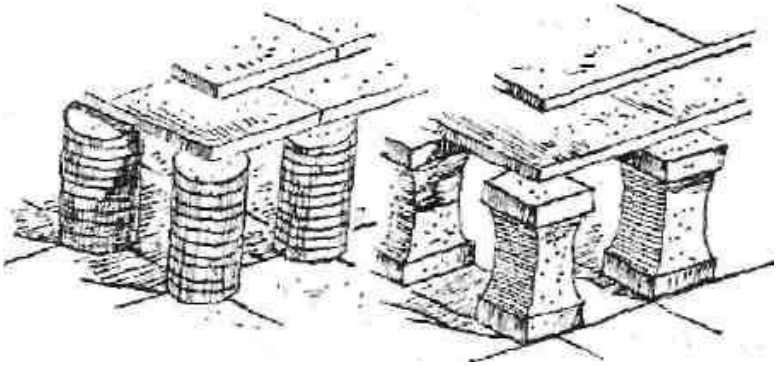

Figure 2.4 Drawings showing the construction of the "raised floor" of historical baths (*Source: Aru, 1949: 15*).

Figure 2.5 Views of terracotta draft chimneys (*tüteklik*) rising inside the wall up to the roof in Yıldırım Beyazıt Hamamı in Mudurnu, Bolu (*Source: Archives of Gülşen Dişli*).

There are many studies making the visual description of the heating system of historical Turkish baths; however the studies on the efficiency and capacity of the heating system of such buildings are limited (Temizsoy, *et al.,* 2003; Başaran, 1995; Başaran and İlken, 1998). In the study of Temizsoy, *et al.* (2003), a 14th Century Principalities period bath, Çukur Hamam, in Manisa was examined in terms of design principles, architectural elements and their construction techniques with special references to water supply, surface-water discharge and heating systems. In this paper, as most important elements of heating system, such as furnace and the hypocaust (*cehennemlik*) were inaccessible, a description of the heating system was made based on information in the sources and the parts of this system were indicated in drawings (Figure 2.6). The heating system of this bath was defined by means of vertical and horizontal flow of smoke under floor and within walls, multi-use of heating source for both heating water and spaces and architectural elements of the system.

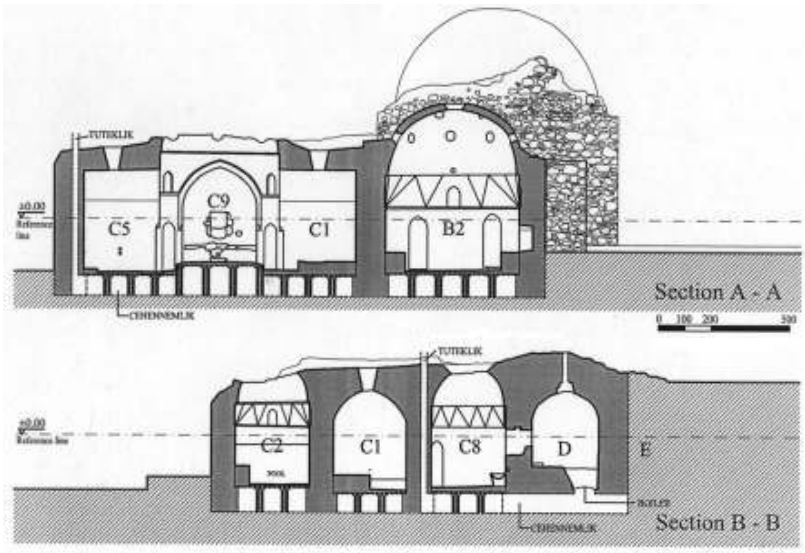

Figure 2.6 Sections showing the elements of the heating system for Çukur Hamam; furnace, *cehennemlik* and draft chimneys (*Source: Temizsoy, et al., 2003*)

Basaran and İlken (1998) and Başaran (1995) also made studies on the heating system of the historical baths. They made the thermal analyses of the heating system of Small Bath in Ancient Phaselis. In their studies, a computer program based on the finite difference method was prepared in order to calculate the temperature distributions on the surfaces, heat transfer to/from the bath and the change of chimney's gas temperature. At the end of these studies, it was found out that the amount of heat transfer from hypocaust to bath is less than heat loss

from bath to outside, making it impossible to provide necessary inside temperature conditions in winter unless the amount of energy is increased. However, it was also stated that when the heat gains from evaporation, gas radiation, sun radiation and people in the bath were added to the calculations, the difference between the heat gain and heat loss would decrease. Başaran (1995) added that the convection coefficients in the hypocaust determined according to mass flow rate was found to be small, causing a decrease in the amount of heat transfer and in the temperature of chimney's gas.

Basaran and İlken (1998) and Başaran (1995) also found out that there were not very big differences in the surface temperatures of floor areas between caldarium and tepidarium since the floor thicknesses were similar to each other. These temperature values increased toward the wall, with the effect of heating through the wall. In addition to this, they claimed that positive effect of supports on heat transfer was observed on the floor surfaces, increasing the surface temperatures where present.

2.2 Parameters Affecting the Thermal Performance of Building Materials

2.2.1 Thermo-physical properties

The following definitions are basic thermo-physical properties of building materials, presented here to describe the ways they affect the thermal performance of building materials. These concepts also characterize how the heat flow develops through a building component.

Bulk density, "ρ" of a material represents the ratio of the mass to the bulk volume of that particular material, expressed in g cm^{-3} (RILEM, 1980; Teutonino, 1986). There is a direct relationship between the density of a building material and its thermal performance; that is they are inversely proportional (Hoffmann & Niesel, 1996; Cook, 1978; Langlais, Silberstein and Sandberg, 1994).

Porosity, "$\varnothing$", of a material is the ratio of the pore volume to the bulk volume of that particular material and expressed by the percentage of volume (RILEM, 1980; Teutonico,

1986). There is a direct relationship between the porosity of a building material and its thermal performance; that is they are directly proportional (Hoffmann & Niesel, 1996; Akkuzugil, 1997; Tye, 1994).

Bulk density and porosity affect the thermal performance of building materials as they have a direct effect on thermal conductivity, thermal capacity and thermal resistance (Hoffmann & Niesel, 1996; Langlais, *et al.,* 1994; Tye, 1994; Straaten, 1967; Akkuzugil, 1997). According to Straaten (1967), thermal conductivity varies appreciably with bulk density, which is very much a function of porosity. Generally, the less dense a material the more air is contained between the pores or particles, and the lower its thermal conductivity. The difference in thermal conductivity of materials with the same bulk density is mostly due to structural differences including the size, distribution and interconnection of pores or voids. It increases strongly with rising medium pore diameter; which means that when the pores get bigger, they conduct more heat (Akkuzugil, 1997; Hoffmann and Niesel, 1996; Tye, 1994).

Craome and Sherratt (1972) also add that materials of high bulk density generally have a greater thermal capacity than those of a low bulk density. For them, buildings made of dense materials or materials of high thermal capacity warm and cool more slowly than buildings constructed with lightweight or low thermal capacity materials such as light frames or cladding. In addition, the thermal resistance of materials increases when the bulk density of the materials decreases (Tye, 1994).

Specific heat capacity, "*c*", of a material defines the heat energy required to raise the temperature of the material by one degree per unit of weight and is expressed in J $kg^{-1}K^{-1}$ (TS 4048, 1984). The specific heat capacity is constant for any substance, at least while in a particular phase. It can also be described as "a measure of how much heat a material can absorb per unit weight" (Goulart, 2004).

Volumetric heat capacity, "*VHC*" of a material is a measure of heat capacity of that particular material per unit volume. It describes the ability of a given volume of a material to store internal energy while undergoing a given temperature change, but without undergoing a phase change. It is different from specific heat capacity in that the VHC depends on the volume of the material, while the specific heat is based on the mass of the material. It is

equal to the specific heat capacity (c) times the bulk density (ρ) and expressed in J $m^{-3}K^{-1}$. (Goulart, 2004; http://www.beodom.com)

Thermal mass or **heat capacity,** "*C*" is the capacity of a body to store heat. Thermal mass provides "inertia" against temperature fluctuations, so it is effective in improving building comfort in any place that experiences daily temperature fluctuations – both in winter as well as in summer. It is equal to the product of the mass (m) of the body and the specific heat capacity (c) of the material and expressed in J $°C^{-1}$ or J K^{-1}. Ideal materials for thermal mass are those having high bulk density and specific heat capacity properties (http://en.wikipedia.org).

Thermal conductivity, "*k*", of a material is the amount of heat flow through unit area of a homogeneous material at unit thickness when one unit temperature difference exists between two surfaces of it (Hall, v.1, 1994; Strother and Turner, 1990; Akkuzugil, 1997; Cook, 1978). It can be described as the property of a material that measures the effectiveness of a material to conduct heat and expressed in W $m^{-1}K^{-1}$ (Kumaran, 2001; Cook, 1978). The smaller the thermal conductivity value of a material, the better the material is regarding thermal insulation (http://www. beodom.com). Thermal conductivity is an intensive physical property of a material; influenced by several factors including moisture content, temperature, bulk density and porosity of the materials. It does not depend on the thickness and size of the material (Straaten, 1967; Akkuzugil, 1997; Langlais, *et al.*, 1994; http://www.beodom.com).

Thermal effusivity, "*e*", represents the capacity of a material to absorb and release heat and characterizes how easily heat can be absorbed at the surface of a material. The thermal effusivity of a homogeneous material is defined as the square root of the product of thermal conductivity, bulk density and specific heat and expressed as W $s^{-1/2}m^{-2}K^{-1}$. So, it tends to be higher when both thermal conductivity and specific heat storage capacity are high (Goulart, 2004; http://www.beodom.com). Thermal effusivity determines how easily heat can be exchanged at the surface of a material. Materials with high thermal effusivity (such as metals) are not good to store heat because heat dissipates outside very quickly as soon as temperature drops. On the contrary, materials with high thermal inertia and low thermal effusivity, such as clay or stone can hold heat much longer (http://www.beodom.com).

Thermal diffusivity, "α", of a material indicates how easy a material undergoes temperature change and determines how rapidly heat flows within it. Thermal diffusivity is a physical property of a material which determines the time rate of temperature change at any point within a body (Goulart, 2004; Strother & Turner, 1990; Kumaran, 2001; http://www.beodom.com). Thermal diffusivity is equal to thermal conductivity divided by the product of specific heat capacity and bulk density and expressed in $m^2 s^{-1}$ (Goulart, 2004; Strother & Turner, 1990; Kumaran, 2001). While thermal conductivity (k) determines how much heat will flow in a material, thermal diffusivity (α) determines how rapidly heat will flow within it. For materials with similar k, heat will flow faster in those with less heat storage capacity (http://www.beodom.com). According to Cook (1978), materials with higher thermal diffusivity values can be more effective for cyclic heat storage (twenty-four hours for instance) at greater depth than materials with lower values.

Thermal resistance, "R", of a material is described as the ability of that particular material to restrict the flow of heat. Thermal resistance is defined as a property of a particular material measured by the ratio of the differences between the average temperatures of two surfaces to the bulk density of the heat flow rate through them under a steady-state condition (Kumaran 2001; Akkuzugil, 1997; Hall, v.1, 1994). It is simply the thickness (l) of the material divided by the thermal conductivity (k) of that material and expressed in $m^2K\ W^{-1}$. The greater the R value, the smaller the heat flow rate for a given temperature difference or the better the material insulates. A higher thermal resistance can be obtained by increasing the thickness of the layer (Hens, 2007; http://www.beodom.com).

Total thermal resistance, R_T, and total thermal transmittance, U, are the thermo-physical properties of building sections affecting the thermal performance of building components. **Total thermal resistance**, "R_T", represents the sum of all thermal resistances for each layer of the building section, including the surface thermal resistance of both sides of the section. Its unit is $m^2K\ W^{-1}$ (TS 825, 1998; Strother and Turner, 1990; BRE, 1969; Hens, 2007; Goulart, 2004). When evaluating a thermal resistance of a wall, all layers of the section have to be taken into account as well as the heat transfer coefficients of the interior and exterior wall surfaces as the exchange of heat between the wall and the ambient air occurs via convection and radiation (Cook, 1978; TS 825, 1998; Goulart, 2004; Strother and Turner, 1990; BRE, 1969; http://www.beodom.com). The higher the total thermal resistance, the lower the steady-state heat flow rate and the better the wall insulates (Hens, 2007).

Total thermal transmittance, "*U*" represents the amount of heat transferred through a building section, between the indoor and outdoor climate, for a unit of surface and temperature. It is expressed in W $m^{-2}K^{-1}$. Thermal transmittance is simply equal to the inverse of the total thermal resistance ($1/R_T$) and it determines the rate of heat flow through a given building component (Goulart, 2004; Hens, 2007; Cook, 1978; Hall, v.1, 1994; Strother and Turner, 1990; http://www.beodom.com). *U* value rates the energy efficiency of the combined materials in a building component or section. The smaller the *U* value, the better the solution is in term of thermal insulation and energy saving.

Total thermal resistance (R_T) and total thermal transmittance (U) are used to rate and compare building solutions. They are also used in various construction norms around the world to set the acceptable standards for new constructions. Turkish Standards give the acceptable values required for the energy efficient buildings for the four climatic regions in Turkey (TS 825, 1998). Table 2.1 shown below represents the acceptable *U* values given in this standard for quality construction of the buildings situated in Ankara, which is in the 3rd region of Turkey (TS 825, 1998).

Table 2.1 Acceptable *U* values given in TS 825 for quality construction of buildings situated in the 3rd region of Turkey (Source: TS 825, 1998:17).

Building Component	***U* (W $m^{-2}K^{-1}$)**
Walls	0.50
Ceilings	0.30
Floors	0.45

2.2.2 Water vapour permeability properties

Building materials can basically be categorized for two essential roles: to minimize direct ingress of water into or within a building (*barrier*) and to control water vapor movement within and through the building envelope (*retarder*) (Tye, 1994). This can be better explained with the "water vapour permeability" of a material, which can also be described as its "breathing" property. A water vapour permeable material lets the passage of water vapour through its body easily.

Hughes (1986) explains the importance of water vapour permeable building envelopes by comparing the construction techniques of contemporary and old buildings. According to this author, contrary to modern buildings which rely on a system of barriers to prevent moisture penetrating the walls, the old buildings constructed before the mid 19th Century generally rely on a "breathing" fabric. While the concept behind the construction of old buildings was to enable the moisture entering the wall to evaporate, modern buildings rely on keeping water out by a system of barriers. Any failure at these impermeable layers, such as tiny cracks, may cause moisture penetration into and entrapping in the wall section, resulting in considerable moisture problems in buildings.

It was also mentioned in BRE (1969) that, if the outer side of an exterior wall is water vapour permeable, condensation will not be troublesome as the moisture can evaporate to the outside air gradually. On the other hand, if the outer surface is impermeable to water vapour, the condensed moisture will tend to accumulate in the wall and ultimately saturate the material. The situation is most severe when the humidity of the indoor air is high. As the outer surface doesn't permit wall to evaporate, any moisture within the wall section will tend to accumulate in the wall and accelerate the problems sourced from moisture. So it is important for the finish coats of building components to be water vapour permeable in order to let the passage of the water vapour in the building section, while resisting to the rain water penetration like a watertight material (Tye, 1994; Örs, 2006).

As the moisture content and water vapour pressure of inside an occupied building is usually higher than outside, the water vapour tends to move towards outside by diffusion (İzocam, 2004; BRE, 1992 and 1969; Strother and Turner, 1990; Örs, 2006). Water vapour permeability characteristics of each layer are significant parameters on the water vapour flow in a building section, which should be continuous to prevent condensation within the section or between its layers. It means that, all the layers forming a building component should be vapour permeable in order to prevent any accumulation of moisture in the section and let it transmit to the exposed surface.

There are some parameters used to define the water vapour permeability properties of materials; such as equivalent air layer thickness of water vapour diffusion (S_D) and water vapour diffusion resistance index (μ), which will be used in this study. **Equivalent air layer thickness of water vapour diffusion**, "S_D", is defined as the thickness of the motionless air

in meters (*m*) which has the same vapour resistance on the material with a certain thickness, "*l*" (TS prEN ISO 7783-2, 1999; TS 7847, 1990; DIN 52615, 1987; Örs, 2006). Akkuzugil (1997) defines it as the same amount of water vapour passes through both a known thickness of the material and the S_D thick air at a given time. The numerical data for S_D values and the classification for permeability properties given in Turkish standards (TS prEN ISO 7783-2, 1999) were given in Table 2.2 in order to summarize the ranges for low, medium and high water vapour permeable materials.

Table 2.2 Classification of water vapour permeability properties of materials in terms of S_D values (*Source: TS prEN ISO 7783-2, 1999*)

Permeability	$\boldsymbol{S_D}$ **(m)**
Low Permeable	$S_D > 1.4$ m
Medium Permeable	$0.14 \text{ m} < S_D < 1.4$ m
High Permeable	$S_D < 0.14$ m

Water vapour diffusion resistance index, "μ" indicates the resistance of a material to the water vapour transmission. It is a unitless parameter, which is used to compare the materials regardless of their thicknesses (TS 7847, 1990; DIN 52615, 1987). In a building section, it is possible to calculate the S_D values of all layers by multiplying μ value of materials with the application thickness. When applied in thin layers, a material having high μ value may have considerably low S_D value. It means that achieving more permeable layers is possible with a conscious application of layer thickness (Esen, *et al.*, 2004; Akyazı, 1998; Akkuzugil, 1997; Caner, 2003; Örs, 2006).

2.2.3 Moisture content of materials

Moisture is a significant parameter that affects the thermal performance of building materials. It can also cause physical, mechanical, chemical and biological decay, which may indirectly influence the thermal performance of insulating materials (Tye, 1994). According to Tye, depending upon the bulk density and porosity of a material, the presence of any moisture can have a significant impact on the overall thermal performance of a material,

increasing the thermal conductivity and the specific heat by its presence. This in turn affects the thermal diffusivity due to a direct increase in bulk density. In addition, if moisture condenses and accumulates in or on a material within the structure and cannot be removed, then it provides a direct conductive "thermal bridge" thus contributing further to heat losses (or gains) within the envelope.

Strother and Turner (1990) explain the basic principle of mass thermal insulation as large number of very small air or gas spaces in its volume, where air convection currents are unable to form. If the insulation becomes wet, either due to being subjected to liquid water or by condensation of water vapour, the air spaces are all or partially filled with liquid water. These authors give the conductivity of water at 21°C as 0.62 $Wm^{-1}K^{-1}$, being 28 times greater than that of still air, the conductivity of which is very low, namely 0.022 $Wm^{-1}K^{-1}$ at the same temperature. According to Langleis, *et al.* (1994), since water and ice have a much higher thermal conductivity than air or other gases in the pores of materials, a moist material has a higher thermal conductivity than a dry material. Strother and Turner (1990) adds that regardless of the thermal conductivity of light weight insulation materials, as they gather water, their conductivity begins to approach the conductivity of that percentage of water in their volume.

According to Tye (1994), although most of the moisture effects are more critical for highly porous insulation and wood materials, its effects on all materials, especially masonry types which have a large range of porosity, is also important since overall performance has to be evaluated by considering the total system and all contributions. Strother and Turner (1990) claim that thermal conductivity and thermal resistance values of all materials are given in a dry-state. Therefore, any small amount of liquid moisture in the material greatly affects the thermal conductivity and hence the heat conducting properties of materials. Straaren (1967) gives the percentage increase in thermal conductivity above the absolute dry state of bricks as 20% for internal walls, 45% for external walls in temperate climates and 65% for external walls in extremely wet climates. The corresponding values for concrete were given to be 40%, 70% and 100%, respectively. For Akkuzugil (1997), as moisture in any form; such as, water vapour adsorption, condensation or even accidental water infiltration affects thermal performance, in the case of existence of any moisture in a material, it is better to remove it as soon as possible.

2.2.4 Thermal failures

Thermal bridges, condensation (surface and interstitial condensation), air and moisture leakages are among the thermal failures seen commonly in building envelopes. The definitions of these failures and their effects on the thermal performance of building materials and sections are described below.

Thermal bridge is an area of the building fabric having a higher thermal transmission than other parts of the fabric (Hall, v.1, v.3, 1994). For Hens (2007) and Straaren (1967), it refers to a spot on the envelope where heat transfer develops in two or three dimensions, with a higher rate of conductive heat flow compared with that of the wall. Here, the word envelope indicates the entirety of floors, facades, windows and roofs, which separate the inside from the outside, from grade and from all adjoining unheated volumes. According to Moss (2007), the thermal bridge areas causes the inside surface temperature to be at a lower value than the rest of the inner surface, resulting in not only increased heat flow but also problems of pattern staining and condensation (Straaren, 1967; Moss, 2007). According to Straaren (1967), they are formed by materials with little resistance to heat flow passing through an otherwise well-insulated element. For Hens (2007), the thermal bridges may be of geometric or structural; that is the consequence of the three dimensional character of a building or the consequence of the structural decisions.

Condensation, either on the surface or within the section of a building component, is another essential failure affecting the thermal performance of building materials and envelopes by changing the moisture content of them. According to Strother and Turner (1990), the amount of water vapour that air can contain is limited and when this limit is reached the air is said to be saturated. The relative amount of water vapour that is contained in air at a given temperature to the maximum amount of water vapour which could be held by the air at that same temperature is known as relative humidity, *RH*, which is expressed in percentage (%)(Strother and Turner, 1990; İzocam, 2004; BRE, 1969; Straaten, 1967). In the case of saturation RH reaches to 100%, and any additional moisture or water vapour which might be put into the air would liquefy and be deposited as condensation (Strother and Turner, 1990; BRE, 1969).

Condensation of water vapour can be either on the surface of a building component, which is called surface condensation or within the structural elements, which is called interstitial or concealed condensation (Hall, v.3, 1994; BRE, 1969; BRE, 1992). Sweating is also a form of surface condensation, occurring as a dew formation when moisture vapour condenses on a cool surface of a building component (Strother and Turner, 1990). According to BRE (1992), interstitial condensation has less immediate impact on the occupants than the surface condensation however it can cause much more serious problems in long term, causing decay in vulnerable materials, degrading thermal performance and affecting the structural integrity of the building. In addition, condensed moisture in materials increases their thermal conductivity coefficient which is especially considered for thermal insulation materials (Langlais, *et al.*, 1994; Strother and Turner, 1990; BRE, 1969; Örs, 2006; Akkuzugil, 1997).

In the study of Akkuzugil (1997) it was stated that moisture movement differs with seasonal variations. In case that internal air temperature and vapour pressure is higher than those of outside, pressure difference causes the heat and water vapour to migrate through the building components in an effort to restore the balance (BRE, 1969). The condensation potential increases with high indoor humidity conditions when outdoor temperatures are low. So, the low outdoor temperature and high indoor humidity conditions are critical variables in winter, since indoor moisture tends to move towards the drier outdoors and may condense on the siding. In any case, the condensed water changes both the thermal and vapour transmission properties of porous materials (BRE, 1969).

Air transfer and leakage through building materials and components are important failures affecting the thermal performance of building materials and envelopes. Air carries heat (enthalpy) and water vapour. According to Hens (2007), air transfer may have both positive and negative effects on materials and building components. The passage of dry air increases the drying potential of a construction and discharges water vapour before it may condense. On the other hand, air outflow affects the thermal and moisture performance of materials, as the continuous flow around the thermal insulation increases heat loss or gain. The same author goes on to explain that the presence of still air in a material or a building component does not bring about many difficulties. The effects become more negative if the air is migrating in and through the section. In fact, moving air entrains water vapour into the parts where it may condense, causing an increased moisture presence. At the same time, air displacement adds enthalpy transport to heat conduction.

Hens (2007) further explains that air leakage through materials, building components and buildings occurs in two cases, one of which is when wind, stack forces and fans create air pressure differences over the various elements, between different rooms and between a building and its environment. It may also occur when the construction elements are air permeable. Air permeability may be a desired characteristic; in the case of ventilation grids are used. However, it is typically an unwanted consequence of using air permeable materials, of fissures and cracks in and between parts and of the joints in layers.

Moisture transfer and leakage through the building envelope can also cause serious problems including reduction in thermal resistance of materials, mold growth, and deterioration of the structural integrity of the building components (Fang, Athienitis and Fazio, 2009). Moisture is one of the major problems in buildings mainly sourced from rain penetration, rising damp, condensation and leakages in the piping system of the building (Strother and Turner, 1990; Hens 2007). If moisture sources are not taken away from the building or excessive humidity in the building component does not come out of its section by moisture transportation, it causes several problems which end up with the deterioration of the materials (Caner, 2003; Tye, 1994; Strother and Turner, 1990; Hens, 2007; Fang, *et al.,* 2009, Akkuzugil, 1997). Hens (2007) defines it as one of the major causes of early degradation and damages and states that up to the 70% of all construction problems are directly or indirectly related to moisture. According to the same author, moisture transport is a combination of water vapour and liquid displacement, included the movement of dissolved substances. The mechanisms responsible for this transfer are equivalent diffusion, air transport, capillary suction, gravity and external pressures.

According to Fang, *et al.* (2009), the moisture transfer in a building component is coupled with the heat transfer, depending on the temperature distribution in it. Meanwhile, the heat transfer in a building component is affected by the moisture distribution. Moisture transfer and accumulation in building envelopes can cause increase in thermal conductivity of materials and larger heat flows as a result of latent heat transfer (Hens 2007). Strother and Turner (1990) state that in order to control heat energy and accomplish thermal efficiency in building components, it is essential to control moisture. According to Santos and Mendes (2008), in the construction area detailed heat, air and moisture analysis are needed in order to increase the accuracy of heat and moisture transfer calculation between outdoor and indoor environments for better prediction of thermal loads, indoor thermal comfort and air quality

indices and mold growth risk. For the thermal performance evaluation of building envelopes, the presence of moisture implies an additional latent heat transport that may cause great differences on the indoor air temperature and humidity values.

2.3 Heat Transfer Mechanism of Building Components

Heat, "*q*", is the energy that is transferred from one region to another when there is a temperature difference between the regions (Strother and Turner, 1990; Straaren, 1967). It is a form of energy and a measurable quantity, which is expressed in Joule or Calorie. When a temperature difference exists, heat (energy) will flow from regions of higher temperature to regions of lower temperature.

Heat flow, "*Q*", indicates the heat loss from the unit area of a building section at a unit time. It is expressed in W m^{-2} (Izocam, 2004; TS 825, 1998; Strother and Turner, 1990; BRE, 1969; Örs, 2006). According to Strother and Turner (1990), a steady flow of energy through any medium of transmission is directly proportional to the force causing the flow and inversely proportional to the resistance to that force. This simple relationship is the basis upon which most insulation calculations are built. Thus, it is possible to say that heat is a form of energy flow and temperature difference provides the driving force for this flow.

Heat Flow Rate is a constant directly proportional to the thermal conductivity, *k*, of the material and the temperature differences, ΔT, between two surfaces, and inversely proportionate to the thickness of the wall, *l* (Hens, 2007). According to Hens, for given *l* and ΔT values, a lower *k* value decreases the heat flow rate, resulting in lower heat loss or gain. This is the reason why materials with a low thermal conductivity are called thermal insulation materials. According to Hall (v.1, 1994), the rate of heat transfer through a material may be affected by the amount of moisture in the material, the variations in the composition of the material and jointing of the component parts. In heat flow calculations, however, it is assumed that a steady-state condition exists which would result if the material is homogeneous; for example it has the same composition throughout and the material is also dry.

Steady-state condition is defined by Hens (2007) as the condition in which the temperatures and heat flow rates are independent of time. In this respect, constant boundary conditions, time independent material properties and constant energy dissipation are needed. All these, but especially the constant boundary conditions distort reality. Straaten (1967) explains that steady state heat transfer is only approximated in practice because of the fact that outdoor climate never remains constant over long periods. Nevertheless, unilateral heat transfer theory can be applied with sufficient accuracy when temperature differences between indoor and outdoor air is large with respect to the short-term fluctuations in outdoor air temperature. This is more or less the case in bath buildings, which have almost stable indoor climate, being heated continuously.

There are three mechanisms in which heat transfer or flow from the hotter to the cooler parts of a body or by virtue of an existing temperature difference between two or more objects or substances can take place; conduction, convection and radiation (Hall, v.1, 1994; Strother and Turner, 1990; Straaren, 1967; Hens, 2007; Moss, 2007). The building envelope should be constructed to control the different components of heat transmittance (Akkuzugil, 1997; Langlais, *et al.,* 1994)

Conduction refers to the transfer of heat between solids at different temperature in contact with each other and between points at different temperature within the same solid. According to Strother and Turner (1990), the heat transfer by conduction in building components is a function of the thermal conductivity of the body, the temperature difference across the body and cross-sectional area of the body. Conduction always occurs from points at a high temperature to points at lower temperature and its rate increases with higher temperature differences (Hens, 2007; Strother and Turner, 1990; Hall, v.1, 1994). Hall (v.1, 1994) also adds that conduction is greater in solids than in gases. Still air conducts heat very slowly and an unventilated cavity provides a good insulator, which is the reason for the good heat-insulating characteristics of still air pockets in insulating materials.

Convection stands for the displacement of molecule groups by others at a different temperature. Straaren (1967) defines convection as the mechanism whereby heat energy is transferred by mixing one portion of a fluid with another. Therefore, it always involves motion or material flow. Strother and Turner (1990) explains that when the liquids or gasses come in contact with a body of higher temperature, their temperature increases with the

energy transmitted to them by conduction and radiation. So the bulk density of them also increases causing a movement of the liquids or gasses. This hotter and denser masses move away from the higher temperature body and lower temperature masses move in. Thus, the process of heating the close molecules by conduction and radiation and their subsequent movement away from the higher temperature body continues.

Convection can be distinguished as forced, natural and mixed one depending on whether or not the movement is caused by an external force, by a difference in fluid bulk density and the action of gravity or both (Straaren, 1967; Hens, 2007; Moss, 2007; Strother and Turner, 1990). In practice, forced convection generally plays a far more important role than natural convection. When the thermal convection is applied to the thermal insulation of a building, it means that the building must be airtight. This is necessary to prevent hot air from escaping outside and being replaced by cold air from outside. Air tightness is not easy to achieve in construction. And because hot air rises, thermal insulation of the roof or ceiling is extremely important to prevent heat loss (http://www.beodom.com*)*.

Radiation is the exchange of energy in the form of electromagnetic waves between two or more bodies at different temperatures separated by space or a medium that is transparent or non-absorbing to the heat waves (Straaren, 1967; Strother and Turner, 1990; Hall, v.1, 1994). According to Hens (2007), it refers to heat transfer caused by the emission and absorption of electromagnetic waves. Moss (2007) states that all surfaces which are above absolute zero (-273.15 °C or 0.0 K) are emitting radiant heat or absorbing, reflecting and transmitting heat radiation depending upon whether they are emitting surfaces or receiving surfaces and upon whether the material is opaque or transparent. For Hens (2007), heat transfer through radiation does not need a medium. On the contrary, it is least hindered in vacuum and fallows physical lows which diverge strongly from conduction and convection. According to Hall (v.1, 1994), all bodies emit radiant heat and receive radiant heat back from other bodies. The higher the temperature of the body, the greater the radiant heat emitted. Matt black surface generally radiate or receive more heat than white, or bright shiny surface.

According to Moss (2007) and Straaren (1967), when heat passes through a building element it is first transmitted from ambient air to one surface of the element mainly by convection and radiation; then it is conducted through the fabric of the element and eventually transferred from the further surface to the air on the other side of the element, again by

convection and radiation. Consequently, it is not only the thermal resistances of the materials comprising the element that determines the rate of heat flow, but also the thermal resistances of both surfaces or the surface coefficients of heat transfer.

The surface thermal resistances of a building section represents the resistance to heat transfer via convection and radiation between the ambient air and the surface of that building section (TS 825, 1998; Hall, v.1, v.3, 1994, TS EN 1745, 2004; TS EN ISO 6946, 2007; Strother and Turner, 1990; BRE, 1969). According to Straaren (1967), these values are influenced by some factors such as the emissivity of the surface, its roughness, the rate of air movement over it, its temperature in relation to that of the air near it and its position. According to this author, a rise in these parameters results in increased heat loss from the surface by convection and radiation, increasing the surface coefficient. The surface coefficients are also different for vertical and horizontal surfaces, being also dependent on the direction of heat flow in the latter (Straaren, 1967 and Hall, v.3, 1994). In Tables 2.3 and 2.4 inside surface resistances, R_{si}, and external surface resistances, R_{se}, were given, respectively.

Table 2.3 Inside surface resistances, R_{si}, in $m^2K\ W^{-1}$ (*Source: Hall, v.1, 1994: 32*)

Building Components	**Heat Flow**	**Surface Resistance in $m^2K\ W^{-1}$**	
		High Emissivity	**Low Emissivity**
Walls	Horizontal	0.123	0.304
Ceilings and Floors	Upward	0.106	0.218
	Downward	0.150	0.562

Table 2.4 External surface resistances, R_{se}, in m^2KW^{-1} for various exposures and surfaces (*Source: Hall, v.1, 1994: 32*)

Building Components	**Emissivity of Surface**	**Surface Resistance for stated exposure in $m^2K\ W^{-1}$**		
		Sheltered	**Normal (Standard)**	**Severe**
Wall	High	0.08	0.055	0.03
	Low	0.11	0.067	0.03
Roof	High	0.07	0.045	0.02
	Low	0.09	0.053	0.02

Sheltered: up to third-floor buildings in city centers. *Normal*: most suburban and country premises and the fourth to eighth floors, of buildings in city centers. *Severe*: buildings on the coast or exposed hill sides and above the fifth floor of buildings in suburban or country districts or above the ninth floor of buildings in city centers.

2.4 Physical Properties of Historic Masonry Materials

Survival of historical buildings through centuries has a direct relation with the success of the architectural and technological achievements of the past. That success was due to the conscious use and selection of historic materials used in the construction of these buildings. The technological achievements presented by those historic building materials that provided survival and proper functioning of historical structures are not fully investigated, yet. However, studies done on the technological characteristics of historical building materials have shown that long term durability of historical structures were closely related to the compatibility properties of these materials with which they come in contact. The definition of compatibility of a material can be done as its suitability with other building materials used together in terms of some material properties that should be similar to each other to prevent any failure of the assembly (Williams and Williams, 1994; Andolsun, 2006; Caner, 2003; Örs, 2006). There are several physical, mechanical and chemical properties affecting the durability and compatibility of materials and health of constructions. In this study, an emphasis was given on the compatibility in terms of basic physical properties of historic materials, such as bulk density, porosity and water vapour permeability properties of historic masonry materials.

In this regard, there are many researches on the physical, mechanical and compositional properties of materials used in the historical bath structures (Esen, Tunç, Telatar, Tavukcuoglu, Caner-Saltık and Demirci, 2004; Çizer, 2004; Uğurlu, 2005; Caner, Akoglu, Caner-Saltik, Demirci and Yasar, 2005; Caner-Saltik, Demirci, Güney, Akoglu and Caner, 2003a; Caner-Saltık, Tavukcuoğlu, Akoglu and Güney, 2003b; Caner-Saltik, Demirci, Akoglu, Caner and Güney, 2005a and Caner-Saltık, Tavukcuoglu, Akoglu, Guney, 2005b). Here, the basic physical properties of historic brick, brick mortar, interior plasters and roof covering plasters for those structures, were summarized in terms of their bulk density and porosity values.

The study of Esen *et al.* (2004) involved the determination of basic physical properties of building materials used in the construction of Çukur Hamam in Manisa, built in 14th Century by Saruhanoğulları Beyliği. The results of the study revealed that the basic physical properties of historic brick and its mortars used in the domes of studied bath were similar. The mean bulk density and porosity values were found to be 1.67g cm^{-3} and 34% for brick

and 1.75g cm^{-3} and 38% for brick mortar, respectively. In addition, the mean bulk density and porosity values of stone mortars were found to be 1.90g cm^{-3} and 31%, respectively. According to the same study, the mean bulk density of the interior plasters was 1.33g cm^{-3}, being in the range of 0.97g cm^{-3}-1.84g cm^{-3}. The mean porosity of them was given as 43% with a range of 29%-59%. The bulk density and porosity values of the only exterior plaster layer covering the dome surfaces of the examined bath were found to be 1.84g cm^{-3} and 29%, respectively, showing that the exterior plasters had been prepared to prevent the leakage of rain water into the structure. This study revealed that the bath buildings had a homogeneous and lightweight upper-structure with low dense and high porous historic materials such as brick, brick mortar and the plasters forming the brick masonry together.

In the study of Çizer (2004), lime mortars used in the walls and domes of some historic Ottoman baths – Hersekzade, Ulamış, Kamanlı and Düzce Hereke Baths – in Seferihisar-Urla region were analyzed in order to understand their characteristics for the purpose of conservation of these buildings. At the end of the study, it was stated that the basic physical properties of stone masonry mortars used in walls and brick masonry mortars used in domes of studied bath buildings were similar. Bulk density and porosity values of stone masonry mortars were found to be in the range of 1.50g cm^{-3}-1.84g cm^{-3} and 26.82%-41.85% by volume, respectively. Similarly, the same values for brick masonry mortars were given in the range of 1.40g cm^{-3}-1.72g cm^{-3} and 31.85%-43.46%, respectively. Furthermore, bulk density and porosity values of bricks used in the domes were in the range of 1.67g cm^{-3} -1.80g cm^{-3} and 29.45%-35.96%, respectively, showing that the mortars and bricks forming the brick dome masonry of the examined baths had similar physical properties. According to Çizer (2004), all these results indicated a lime mortar technology developed according to the use of the lime mortars in structural layout and its tradition character peculiar to the Ottoman baths in Seferihisar-Urla region.

In the study of Uğurlu (2005), characteristics of horasan and lime plasters and building bricks of three Ottoman bath buildings in Urla and Seferihisar region were investigated. According to the author, two plaster layers, horasan and lime, were applied on the interior surface, which were distinguishable by their texture and color. Lower levels up to 1.5m height from the existing floor surface were composed of one, two or three rough horasan plaster layers with a very thin finishing layer, while the upper levels were composed of a rough horasan layer with a fine lime plaster layer. She also stated that the multi-layered

horasan plaster application with less porous finishing layer provided a waterproof surface for lower levels which are subjected to water more than upper levels, and by this way prevent water entry into the structure. It was also stated that all horasan plasters used in different spaces, levels and layers had almost the same physical properties, with bulk density and porosity values in the range of 1.0g cm^{-3}-1.7g cm^{-3} and 31%-54% by volume, respectively. They were porous and low dense materials, durable to the high humid and hot atmosphere of bath buildings. Moreover, lime plasters applied on horasan plasters had bulk density and porosity values in the range of 1.3g cm^{-3}-1.8g cm^{-3} and 25%-46%, respectively. In the same study, the average bulk density and porosity values of dome bricks were found as 1.8g cm^{-3} and 31%, respectively.

The plaster layers covering the interior surfaces of a 15th Century Ottoman bath, Amasya Hizir Pasa Bath, were analyzed in the study of Caner-Saltık *et al.* (2005b). The results of this study indicated that the interior wall and dome surfaces of bathing spaces were covered by two different layers of plasters. When the samples of historic plaster layers were analyzed, it was seen that the lower levels of walls up to the height of 1.5m were composed of a layer of pink plasters having a thickness of 2.5cm and two layers of white plaster with a total thickness of 1.1cm. While, the upper levels were composed of a 1.5cm-thick layer of pink plaster and three layers of white plaster with a total thickness of 1.7cm. All the interior surfaces were covered with a very thin finishing layer called lime wash.

In the studies of Caner *et al.* (2005) and Caner-Saltık *et al.* (2003, 2005a), the technological properties of some plasters used as roof covering material in two 15th Century baths in Urla-İzmir – Hersekzade Ahmed Paşa and Yahşi Bey Baths –were examined. In these baths, the only roof covering materials were plasters applied in three layers and rainwater drainage detailing were formed with those plasters. The thicknesses of these plaster layers from exterior to interior were found to be 13cm, 16cm and 34cm, respectively. The results of these studies indicated that roof covering plasters of these two Ottoman baths were light and porous materials, with bulk density and porosity values in the range of 1.4g cm^{-3}-1.7 gcm^{-3} and 23%-48%, respectively.

There are also some researches on the water vapour permeability properties of historical building materials especially on the historical plasters which are directly in touch with water such as exterior plaster of the walls and domes and the interior plaster of the bath buildings

(Akkuzugil, 1997; Caner, 2003; Esen *et al.,* 2004; Caner *et al.,* 2005; Caner-Saltik *et al.*, 2005a, 2005b; Caner-Saltik, Tavukcuoglu, Akoglu and Guney, 2009) and of contemporary building materials used in the repair of historical buildings (TS 825, 1998; Örs, 2006; Andolsun, 2006).

In the study of Akkuzugil (1997), some historical plasters of timber-framed historical buildings in Ankara were examined in terms of their S_D, μ and permeance values. In this work, lime plasters were found to have relatively higher μ values than mud and gypsum plasters. The μ values of the historic lime, mud and gypsum plasters studied by this author were found to range from 3.04 to 18.27, 1.19 to 3.16 and 2.88 to 13.33, respectively. The S_D values of the lime coats indicated that these plasters were high-vapour-permeable materials, being in the range of 0.026m and 0.059m. At the end of the study, the author pointed out that although some of the plaster layers had higher resistance to water vapour permeation, a continuous passage of water vapour through all plaster layers was achieved by the conscious application of different thicknesses. In the same study, the μ values of historic mud-brick and its mortar were found to be in the range of 2.75- 3.23 and 1.92-2.70.

Caner (2003), who studied the physical and mechanical properties of some historic interior and exterior plasters belonging to Seljuk period, pointed out the necessity of water-vapour-permeable plaster layers in her thesis. She found the μ values of the plasters ranged from 1.79 to 9.22 and the S_D values ranged from 0.020m to 0.069m. As a conclusion, she stated that the plaster layers had good breathing properties and continuity of water vapour transfer was provided through the plaster layers without danger of condensation.

The study by Esen *et al.* (2004) also involved the determination of water vapour permeability properties of plasters used in the interiors of Çukur Hamam. This study revealed the advanced plaster technology used in this historical building. The results of the study showed that the μ values of plaster samples were in the range of 2.3-16.2, with a mean value of 7.6. In the study, this wide range of μ values were related to the water impermeability properties of plasters, that is to say that the plaster layers with high μ values were those used in the lower levels of the bathing spaces that was in direct contact with water. However, S_D values of all plaster samples were found be similar, being in the range of 0.04-0.15m with a mean of 0.08m, showing that they were high permeable layers. This meant that, the continuity of the water vapour permeability through the plaster layers was achieved by the thin application of

plaster layers with high μ values. At the end, it was concluded that the all the plasters had good breathing properties in other words; water vapor could travel easily through the plaster layers without the danger of condensation in the wall. The walls were found to be permeable to water vapor but impermeable to water.

In the study of Caner-Saltik *et al.* (2005b), the two layers of plasters – PLA.SI.M.120 and PLA.SI.W.060 – covering the interiors of a 16th Century Ottoman bath in Tire, Yalınayak Bath, were investigated in terms of water vapour permeability characteristics. The μ values of these plaster layers were defined to be 3.91 and 10.28, respectively. In the same way, μ values of the interior plaster layers – 04P2a and 04P2b – covering the interiors of a 15th Century Ottoman bath in Bergama, Tabaklar Bath, were studies in another study and found out to be 4.81 and 10.07, respectively (Caner-Saltik *et al.,* 2009).

Similarly, in the studies of Caner *et al.* (2005) and Caner-Saltık *et al.* (2005a), the water vapour permeability properties of roof covering plasters of Hersekzade Ahmed Paşa and Yahşi Bey Baths were also examined. In these baths, as roof covering materials three layers of plasters, HA-R (U), HA-R (L) and HA-A12-DBM from exterior to interior, were used in 0.013m, 0.016m and 0.034m thicknesses to form the detailing of the rainwater drainage system. According to the study, the μ values of these plaster layers were 8.041, 8.292 and 8.231 with S_D values of 0.106, 0.131 and 0.283, respectively. The results showed that these plasters had high water vapor permeability and high water impermeability properties, which was also proved by the well protected domes of the examined baths throughout the centuries. All studies have shown that in historical buildings there was a very conscious use of plaster technology according to the function of the spaces in terms of material production, selection and application.

There are also sources including the vapour permeability properties of contemporary building materials used in the repair of historical buildings (TS 825, 1998; Örs, 2006; Andolsun, 2006). TS 825 (1998) gives the μ value for the mesh reinforced concrete in the range of 70-150. The μ value for the wall structure constructed with brick and aerated concrete were also given in the range of 5-10. It is not possible to find the μ values of all the contemporary building materials in the standards. However, there are several studies done to find out the S_D and μ values of some types of contemporary materials such as aerated concrete and contemporary finish coats (Örs, 2006; Andolsun, 2006)

Örs (2006) has worked on the compatibility properties of some contemporary finish coats, cement-, synthetic- and polymer-based finish coats, together with their complementary layers used in insulated exterior walls in terms of water vapour permeability and modulus of elasticity. She found out that although water vapour diffusion resistance, μ values, of the finish coats, especially polymer-based ones, were found to be high, all of them were found to be high water vapour permeable according to their S_D values in the range of 0.036±0.04m and 0.119±0.005m, which were provided by the use of finish coats in thin layers. Cement-based undercoats, on the other hand, were found to be medium permeable layers due to their S_D values in the range of 0.215±0.021m and 0.552±0.074m.

In another study, Andolsun (2006) examined some physical, mechanical, compositional and durability properties of autoclaved aerated concrete (AAC), its neighboring plasters and jointing adhesive. She found that whether used as an infill or load-bearing material, the S_D and μ values of a 20cm-thick AAC masonry wall were 0.88m and 4.4, respectively. The experimental μ values of the base coat, undercoat, finish coat and water repellent finish coat were given as 11.5, 1.4, 11.5 and 5.8, respectively.

All these studies have revealed that the historic materials used in the construction of historical buildings had similar physical properties in terms of density, porosity and water vapour permeability making them compatible with each other. That success was due to a very conscious production, selection and application of historic materials. Without doubt, the thermo-physical properties of these materials such as thermal conductivity and specific heat should also be similar. However, the literature showed a singular lack of pertinent knowledge on this context. In this study, an emphasis was given to the thermo-physical properties of historic masonry materials together with interior and exterior plasters used in historical Turkish baths.

The basic physical properties of some historic and contemporary materials were obtained directly from the literature to be used in various calculations in the context of this study. These historic samples were chosen from those materials, such as historic brick, mortar and plasters used in the construction of historical bath buildings of the Ottoman period. The bulk density and porosity values of historic brick, brick mortar and exterior plasters were given in Table 2.5, while the resistances to water vapour permeation values, μ, of the same materials were presented in Table 2.6 with the buildings they belong to and the literature from which

the values were cited. Moreover, Table 2.7 shows the μ values of some contemporary materials used as repair materials in historic bath buildings.

Table 2.5 The bulk density and porosity values of historic materials, which were used in the various analyses in the context of this thesis, the historical bath buildings they belong to and the literature from which the values were cited.

Historic Materials	**Historic Bath Buildings**	**Historic Samples**	***ρ*** **g cm^{-3}**	***ø*** **%**	***Literature***
Historic Dome Brick	Yalinayak Bath	BRI.SO.M.07	1.30	47.55	Caner-Saltik *et al.*, 2005b
	Cukur Bath	32B	1.47	39.84	Esen *et al.*, 2004
	Hersekzade Pasa Bath	HA-A3-VB-C	1.52	38.90	Caner-Saltik *et al.*, 2003a
Historic Brick Mortar	Yahsi Bey Bath	YDM1c	1.55	38.10	Caner-Saltik *et al.*, 2003a
	Yahsi Bey Bath	YDM1d	1.52	38.30	Caner-Saltik *et al.*, 2003a
Historic Roof Covering Plasters	Hersekzade Pasa Bath	HA-R (U)	1.48	40.80	Caner *et al*., 2005; Caner-Saltik *et al.*, 2003a,2005a
	Hersekzade Pasa Bath	HA-R (L)	1.39	43.40	Caner *et al.*, 2005; Caner-Saltik *et al.*, 2003a,2005a

Table 2.6 Resistance to water vapour permeation values, μ, of historic brick, brick mortar and exterior plasters with the buildings they belong to and the literature from which the values were cited.

Historic Materials	**Historic Bath Buildings**	**Historic Samples**	***μ***	***Literature***
Historic Dome Brick	Yalinayak Bath	BRI.SO.M.07	2.92	Caner-Saltik *et al*., 2005b
	Hersekzade Pasa Bath	HA-A3-VB-B	2.826	Caner-Saltik *et al*., 2003a
	Hersekzade Pasa Bath	HA-A3-VB-C	2.593	Caner-Saltik *et al*., 2003a
Historic Brick Mortar	Cukur Bath	27BM	2.3	Esen *et al.*, 2004
Historic Interior Plasters	Yalınayak Bath	PLA.SI.W.120	3.91	Caner-Saltik *et al*., 2005b
	Yalınayak Bath	PLA.SI.M.060	10.28	Caner-Saltik *et al*., 2005b
Historic Exterior Plasters	Hersekzade Pasa Bath	HA-R (U)	8.041	Caner *et al*., 2005; Caner-Saltik *et al*., 2003a,2005a
	Hersekzade Pasa Bath	HA-R (L)	8.292	Caner *et al*., 2005; Caner-Saltik *et al*., 2003a,2005a
	Hersekzade Pasa Bath	HA-A12-DM	8.231	Caner *et al*., 2005; Caner-Saltik *et al*., 2003a,2005a

Table 2.7 Resistance to water vapour permeation values, μ, of contemporary building materials and the literature from which the values were cited.

Contemporary Building Materials	***μ***	***Literature***
Mesh Reinforced Concrete	70-150	TS 825, 1998
Cement Based Under Coat	27.6	Örs, 2006
Cement Based Finish Coat	21.5	Örs, 2006

In addition, the thermo-physical properties of some light construction materials used in contemporary buildings having good thermal insulation properties such as tuffs, mud-brick, aerated concrete and porous light brick, were given in Table 2.8. These materials were produced for thermal insulation purposes to contribute to the thermal performance of buildings in terms of energy efficiency.

Table 2.8 The bulk density and thermal conductivity values of light construction materials produced for thermal insulation purposes and the literature from which the values were cited.

Material	***ρ*** **g cm^{-3}**	***k*** W m^{-1}K^{-1}	***Literature***
Nevşehir-Göreme Tuffs		0.28-0.73	Erdoğan, 1986
Cappadocia Tuffs	1.15-1.40	0.30-0.49	Erguvanlı and Yüzer, 1977
Contemporary hollow and hand-made bricks	1.20-1.80	0.50-0.81	TS 825, 1998
Mud-brick		0.23-0.93	Houben and Guillaud, 1994
Aerated concrete	0.50-0.80	0.22-0.29	TS 825, 1998
		0.36	Kurama, Topcu, Karakurt, 2009
Concrete with cinder	1.47-1.67	0.54-0.67	Strother and Turner, 1990

2.5 Quantitative Infrared Thermography (QIRT)

Quantitative Infrared Thermography (QIRT) is a well-established, important and powerful technique for consideration when investigating any structural situation where a ready source of surface heating (or cooling) is available, or where the object under investigation supplies such conditions itself (Titman, 2001). It is a non-destructive testing (NDT) and monitoring

technique, which can give possibility to produce thermal maps of surfaces showing the temperature distribution in colors corresponding to a temperature scale. According to Titman (2001), a thermographic survey may, in general, be very rapidly completed, with minimal access requirements and can therefore be very cost-effective. There are many studies that give information on the use and development of QIRT method such as: Avdelidis and Moropoulou (2003); Titman (2001); Datcu, Ibos, Candau and Mattei (2005); Meola, Di Maio, Roberti and Carlomagno (2005) and Clark, McCann and Forde (2003).

Titman (2001) further explains that there is a wide range of applications of QIRT in many fields and it can be used to investigate a very broad range of situations where variation in surface temperature may indicate a problem in or a particular property of the material below the surface. Meola, *et al.* (2005) adds that IRT is a remote temperature mapping system which may be successfully exploited in many industrial and/or research fields, such as meteorology, environment, medicine, architecture, engineering, where the surface temperature represents a key parameter.

Clark, *et al.* (2003) explains the general principle behind the application of thermography as the increase in the temperature of most materials caused by the absorption of infrared radiation over a wide range of wavelengths. According to them, all objects with a temperature greater than absolute zero emit infrared energy. Thermal imaging is a technique for converting a thermal radiation pattern, which is invisible to the human eye, into a visual image. To achieve this, an infrared camera is used to measure and image the emitted infrared radiation from an object. Since this radiation is dependent upon the object surface temperature, it makes it possible for the camera to calculate and display this temperature. However, radiation measured by the camera does not only depend on the temperature of the object, but also its emissivity and its absorption by the atmosphere (Clark, *et al.*, 2003).

QIRT method can be used as single and sequential. In the first one the surfaces can be scanned in segments by taking single IR images together with their visible-light photographs. The sequential IR imaging, on the other hand, is carried out by taking infrared sequences of some surfaces at 5-10 seconds intervals for a period of 5-10 minutes. The differential IR images, where the decrease and/or increase in surface temperature are evaluated, can also be produced by taking the temperature differences as a function of time. According to Titman (2001), it is possible to detect surface temperature variations both qualitatively and

quantitatively. In the latter case, various parameters need to be entered into the software for accurate measurement, typically: ambient temperature, humidity, distance from target, and emissivity of the target surfaces.

According to Titman (2001), there are three types of conditions necessary for thermography to be useful. These are *heat (cold) source*, where a hotter (colder) object is embedded at depth of a material, *thermal gradient*, where steady-state conditions are necessary and *induced heating* where a hot (or cold) source is applied to a surface. In practice, there may be a combination of two or all of the above factors present. In this study, the second one – thermal gradient – is used, where a stable thermal gradient exists through an element of a structure and there is no significant variation in thermal conductivity of the materials within the element. Titman claims that the surface temperature over the warm and cool faces should be constant in this case. The fluctuations in the surface temperature indicate the variations in conductivity due to material omission or local damage within the element.

Although thermography can be used as a stand alone technique, there are also circumstances where the effectiveness of an investigation can be enhanced by the combination of thermography with other destructive and/or non-destructive methods (Titman, 2001). The joint use of IRT with other investigation methods is highly used for the examination of buildings at present (Kandemir-Yucel, *et al.*, 2007; Tavukçuoğlu, Çiçek, Grinzato, 2008; Haralambopoulos and Paparsenos, 1998; Grinzato, Bison, Marinetti, Concas and Fais, 2004; Tavukçuoğlu, *et al.*, 2005; Tavukçuoğlu and Caner-Saltık, 1999).

Whether used alone or in combination with other investigation methods, thermal imaging can be proved as a highly effective method in the general context of construction (Titman, 2001). According to the same author, IRT is most commonly used for the investigating aspects of building envelope – walls and roofs; in particular, in the context of energy conservation. The locations of missing, damaged, misplaced or saturated thermal insulation layer can be detached by IRT as the overall thermal conductivity of the element is altered locally at those locations. In addition to this, thermal bridge points can be detected and the severity of air leakage around doors, windows, and at construction joints, eaves etc. can be assessed with the use of this non-destructive method. Titman (2001) also adds that termography can be useful in the moisture/condensation investigations, when combined with other surface inspection methods. Roof leak investigations can also be successfully carried

out by this thermal gradient method. Moreover, it is functional when it is necessary to get information with regard to the internal construction of structures and finishes and the services buried within or hidden behind the structures (Titman, 2001).

There are some studies containing infrared thermography applications on the investigation of historic structures. According to Avdelidis and Moropoulou (2003), this non-destructive technique was used for the assessment of various traditional/historical materials and structures after they had been conserved, restored or repaired using different treatments. In addition, Grinzato, *et al.* (2002a) state that in the investigation of historical buildings IRT is applied for several important purposes, such as the monitoring of the thermal failures of the building components, the hidden structures, the finishing status, moisture content and crack mapping. This method is highly used in many studies for the examination of historical buildings, among them are Kandemir-Yucel, *et al.* (2007); Avdelidis and Moropoulou (2003); Cestari, Lombardi, Gubetti and Pignatelli (2002); Haralambopoulos and Paparsenos (1998); Grinzato, *et al.* (2002a, 2002b, 2004); Grinzato, Vavilov and Kauppinen (1998); Dişli (2008); Dişli, Tavukcuoğlu, Tosun and Grinzato (2008); Dişli, Tavukcuoğlu, Tosun, Grinzato, and Caner-Saltık (2007); Tavukcuoğlu, *et al.* (2007); Tavukçuoğlu, *et al.,* (2008); Tavukçuoğlu, *et al.*, (2005); Tavukçuoğlu and Caner-Saltık (1999) and Nappi and Cote (1997). The outcome of this kind of studies provides strong evidence that QIRT is an effective technique for the evaluation of historic buildings and sites.

In this study, the QIRT survey of Şengül Hamamı was done by single and sequential IR imaging in order to investigate the distribution of thermal failures; such as heat loss areas, thermal bridges and heat/air flow areas in the building components. The distribution of the damp zones was also searched by the use of this method. In addition to this, the effectiveness of the investigation was tried to be enhanced by the joint use of QIRT with heat transfer calculations, which is also a non-destructive technique. This combination is expected to give deeper information on the thermal performance of the building components of Şengül Hamamı at the present situation.

CHAPTER 3

MATERIAL AND METHOD

In this chapter are presented the material and method of the study. The first section describes Şengül Hamamı, which is examined as a case study. Included are those of its heating system and its roof and wall sections for both the *ORIGINAL* and the *AS-IS* cases. The following section provides a detailed account of the investigation methods used during the study. These cover the laboratory analyses and *in-situ* analyses, including microclimatic monitoring and infrared thermography together with heat transfer and water vapour transfer analyses.

3.1 Material: Şengül Hamamı

Şengül Hamamı, the focus of the study, is a typical 15th Century Ottoman bath of Anatolia (Figure 3.1) and is located in Ulus district, the historic center of Ankara. It is under the ownership and control of General Directorate of Pious Foundations (Vakıflar Genel Müdürlüğü) while being operated by a private manager. It still represents the continuous experience of hamam culture in Anatolia by keeping its original architecture and building technologies. Şengül Hamamı is a double bath composed of two separate parts, one for men and one for women. Both are composed of a changing section (cold space) and successive bathing sections called warm and hot spaces. The two parts of the bath have no communication with each other, but are supplied by the same service facilities.

As indicated in Figure 3.3, the changing sections of Şengül Hamamı are composed of the undressing rooms and entrances of the women's and men's parts. These sections have masonry walls, timber-framed mezzanine floors and higher timber upper structures with lanterns allowing for natural light and ventilation. The bathing section is composed of successive warm and hot spaces both for the men's and women's parts. This entire section has stone masonry walls and brick masonry upper structure. Both hot spaces are composed of rooms at the corners (*halvet*s) and at the sides (*iwans*) opening onto a central domed space. Like in many other Ottoman baths of Anatolia, the toilets and other service spaces,

like depilatory rooms, are also within the warm section. The service section composed of cold water and hot water storage rooms, a firewood storage room and a furnace, which are all located on the east side of the building. The furnace is located at the bottom of the hot water storage cistern.

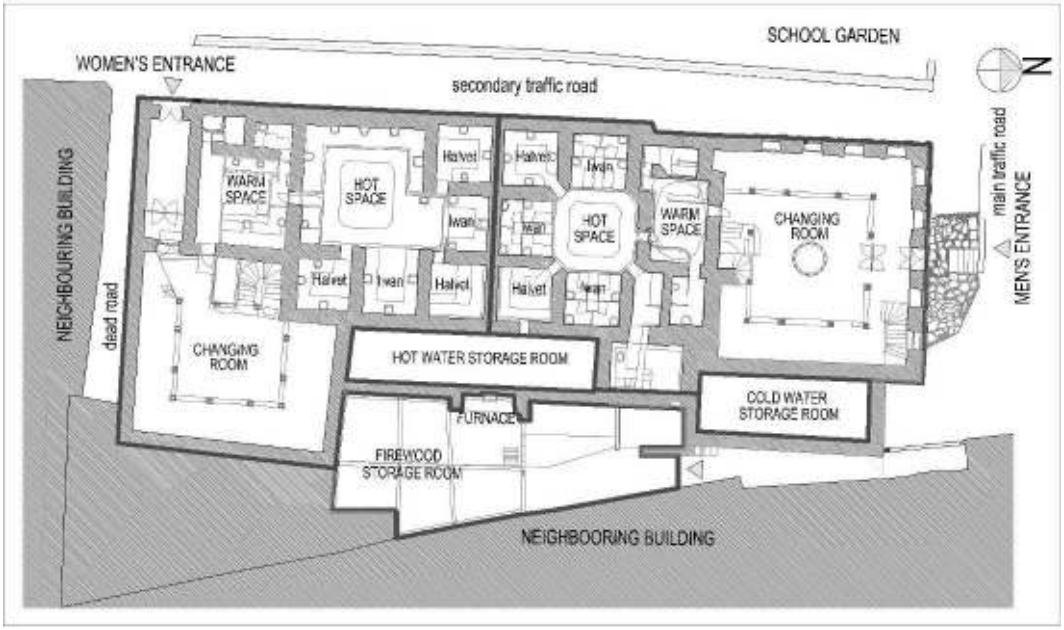

Figure 3.1 Plan of Şengül Hamamı showing sections for the women's and men's parts and service spaces (*Source: Archives of the General Directorate of Pious Foundations, 2008*)

3.1.1 The heating system of Şengül Hamamı

Şengül Hamamı exhibits the historical/original heating systems used in the Ottoman period baths in Anatolia. Like in many other historical baths in Anatolia, the traditional heating system has a direct effect on the plan organization. In this bath, the main architectural elements of the heating system are the firewood storage room, furnace, copper boiler, hot water storage room, hypocaust (*cehennemlik*) and draft chimneys (*tüteklik*). The furnace, by which water in the hot water storage room and the interiors of bathing spaces are heated, is placed in the firewood storage room. It has an arched opening in the form of a fireplace that opens from the outside for lighting the fire (Figure 3.2).

Figure 3.2 Views of the furnace in Şengül Hamamı (*Source: Archives of the Author and Gülşen Dişli*)

The interiors of bathing section are heated by the exhaust gases from the furnace. These gases circulate inside the hypocaust (Figures 3.3), which has links to the outlets of draft chimneys. The flow and orientation of the hot gases under the floor, as well as its pressure are controlled by the opening and closing the dampers of these chimneys. The elevated marble platform (*göbektaşı*) located at the centre of the hot areas are the hottest surfaces of the bath. The changing rooms are heated by means of stoves located at their centers.

Twenty draft chimneys are observed on the roof (Figure 3.4). The draft chimneys D1-D9 belong to the women's part, while those between D10-D19 belong to the men's part. D2 and D18 are connected to the stoves located in the changing sections of women's and men's parts, respectively. In addition to this, D20 is located above the furnace in the firewood storage room in order to expel the smoke coming out of the furnace. The draft chimneys D1, D4, D12 and D15 have a damper mechanism to adjust the flow and orientation of hot gases under the floor and to control its pressure (Figure 3.5), while the others were made out of use by tapping with cement mortar. Figure 3.6 shows two draft chimneys; one with a damper mechanism and one out of use.

Like other Ottoman baths of Anatolia, the hot water needed for the cleaning purposes is heated via a concave copper boiler placed over the fireplace and is stored in the hot water storage room (Figure 3.7). This hot water storage room lies along one side of the hot area and has a small window called "*observation window*" as a connection to one of the *halvets* of the hot area of men's part for the purpose of access for maintenance and control.

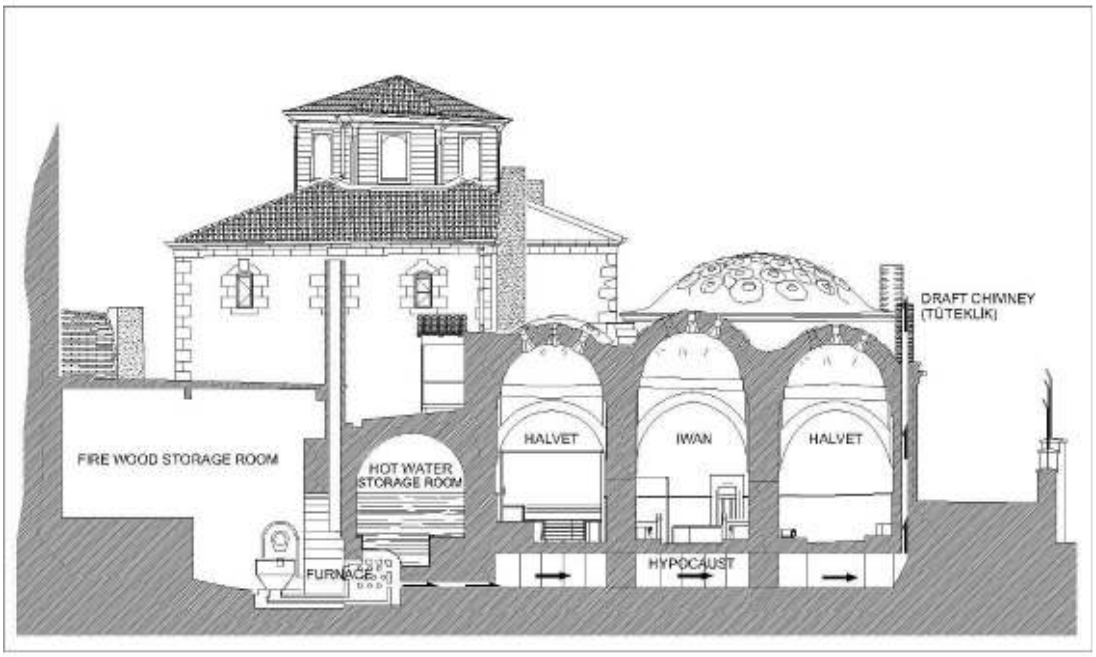

Figure 3.3 Section showing the heating system of Şengül Hamamı. (*Source: Archives of the General Directorate of Pious Foundations, 2008; produced by the author).*

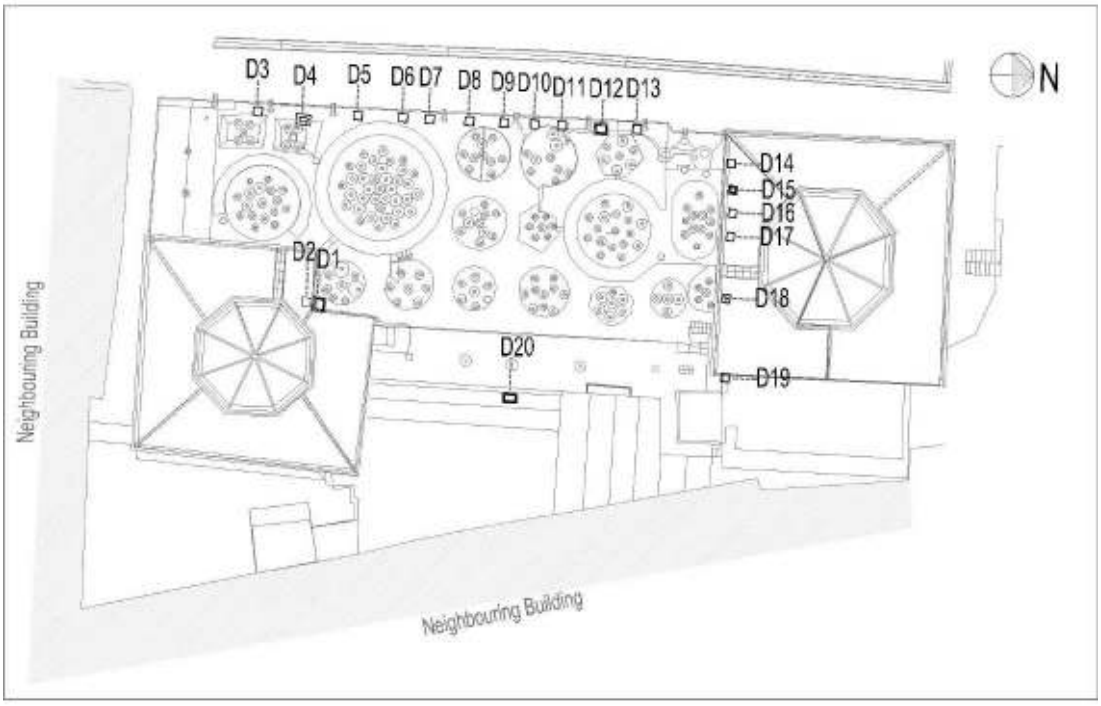

Figure 3.4 Roof plan showing the distribution of draft chimneys, *D*, in Şengül Hamamı (*Source: Archives of the General Directorate of Pious Foundations, 2008; produced by the author).*

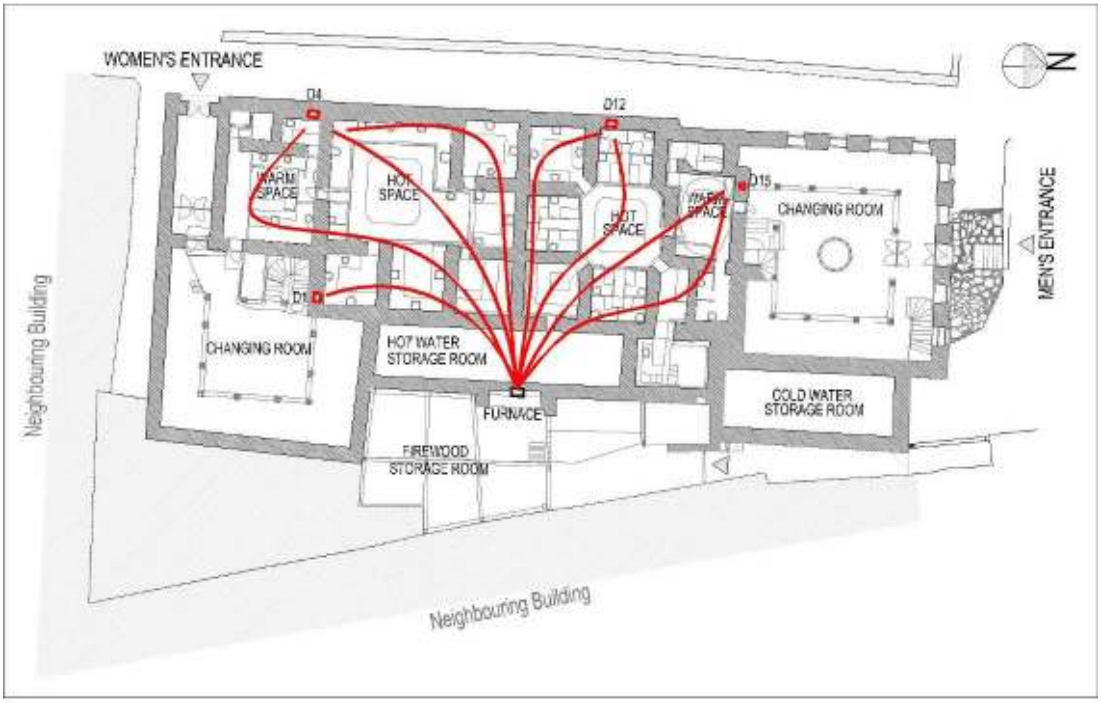

Figure 3.5 Representative drawing showing the diffusion of hot gases coming out of the furnace in the hypocaust of Şengül Hamamı and its orientation towards the outlets of draft chimneys. (*Source: Archives of the General Directorate of Pious Foundations, 2008; produced by the author).*

Figure 3.6 View of two draft chimneys; one out of use (on the left) and one with a damper mechanism to open and close the top (on the right) on the roof of Şengül Hamamı (*Source: Archives of Author*)

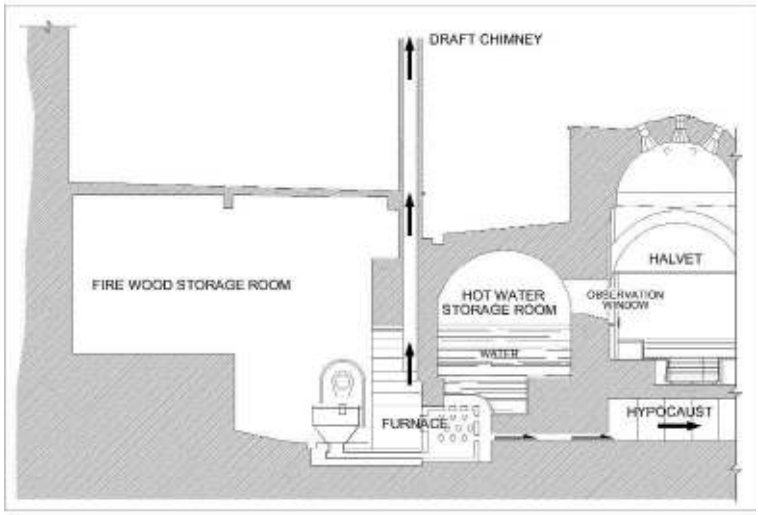

Figure 3.7 Section showing the location of furnace underneath the hot water storage room (*Source: Archives of the General Directorate of Pious Foundations, 2008; produced by the author)*

3.1.2 Roof and wall sections of Şengül Hamamı: *ORIGINAL* and *AS-IS cases*

Şengül Hamamı was originally constructed with stone masonry walls and brick domed upper structure. The changing rooms, roof surfaces and exterior walls of the bath were renewed in the 19th Century and in 1970's. The roof was covered by an 8 cm-thick mesh-reinforced concrete layer (Figure 3.8). In the bathing section, the floor surfaces and the walls up to the height of 150cm were clad by marble cladding and all the interior dome and higher wall surfaces were covered by cement-based plasters and oil paint.

Figure 3.8 Views of Şengül Hamam's roof covered by an 8 cm-thick mesh-reinforced concrete layer (*Source: Archives of the Author*)

In order to better understand the building envelope, two configurations/models of the dome and wall structures were produced: The first one is the "*ORIGINAL case*" representing the historic dome and wall structures and the second one is the "*AS-IS case*" of the dome and wall structures including the recent repairs with cement-based materials. The models of the *ORIGINAL case* were defined according to the historical masonry dome and wall structures of similar historical baths belonging to the same period with Şengül Hamamı, such as Yahsibey Bath (Urla, 15th cc.), Hersekzade Bath (Urla, 15th cc.), Amasya Hizir Pasa Bath (Amasya, 15th cc.), Çukur Bath (Manisa, 14th cc.), Yalinayak Bath (Tire, 16th cc.). The geometric descriptions of the models showing the order and thickness of the layers for the *ORIGINAL* and *AS-IS* cases of the dome structure of Şengül Hamamı were given in Figure 3.9 and those for the wall structure were given in Figure 3.10.

The historic dome masonry was composed of historic brick (HB) and historic mortar (HBM) in same amounts, and was assumed to be clad with three layers of protective roof plasters (HEP-L1, HEP-L2 and HEP-L3) while being internally covered with two layers of interior plasters (HIP-L1 and HIP-L2) (Caner *et al*., 2005; Caner-Saltik *et al*. 2003a, 2003b, 2005a, 2005b; Esen *et al*., 2004) (Figure 3.9). The roofs of those historical baths were covered with earth in certain thicknesses, except the high domes with dome lights (Önge, 1995). Considering the geometrical formation of the Şengül Hamam's roof, it was assumed that 59.2% of the roof surfaces were covered by a 30 cm-thick earth layer, except the high dome surfaces which occupies the 40.8% of the whole roof area. The model of the *AS-IS case* was composed of historic brick dome masonry which was externally-clad with 8 cm-thick mesh-reinforced concrete layer (MRC) and internally-covered by cement-based plaster layers (CBUC and CBFC) and oil paint.

The historic wall masonry was composed of historic stone (HS) and historic stone mortar (HSM), and was assumed to be left exposed externally while being internally covered with two layers of interior plasters (HIP-L1 and HIP-L2) (Caner-Saltik *et al*. 2003a, 2003b, 2005a, 2005b; Esen *et al*., 2004) (Figure 3.10). A decrease in the thickness of the plaster layers was observed above the height of 150 cm (Caner-Saltik *et al*., 2003b; Uğurlu, 2005). The model of the *AS-IS case* was composed of historic stone masonry wall which was internally-covered by cement-based plaster layers (CBUC and CBFC) and oil paint above the height of 150 cm. Below this height the walls were clad by 3 cm-thick marble cladding (MC) and 2 cm-thick marble mortar (MM).

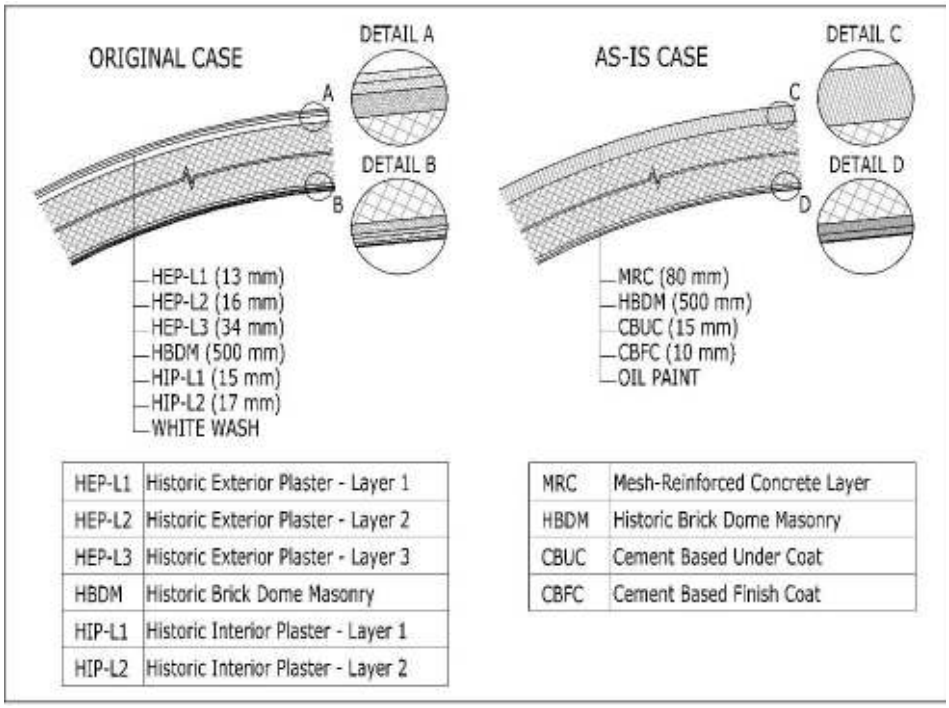

Figure 3.9 Geometric descriptions of dome models showing the order and thickness of the layers for the "*ORIGINAL case*" representing the historic dome structure of Şengül Hamamı (at left) and for the "*AS-IS case*" including the recent repairs with cement-based materials (at right).

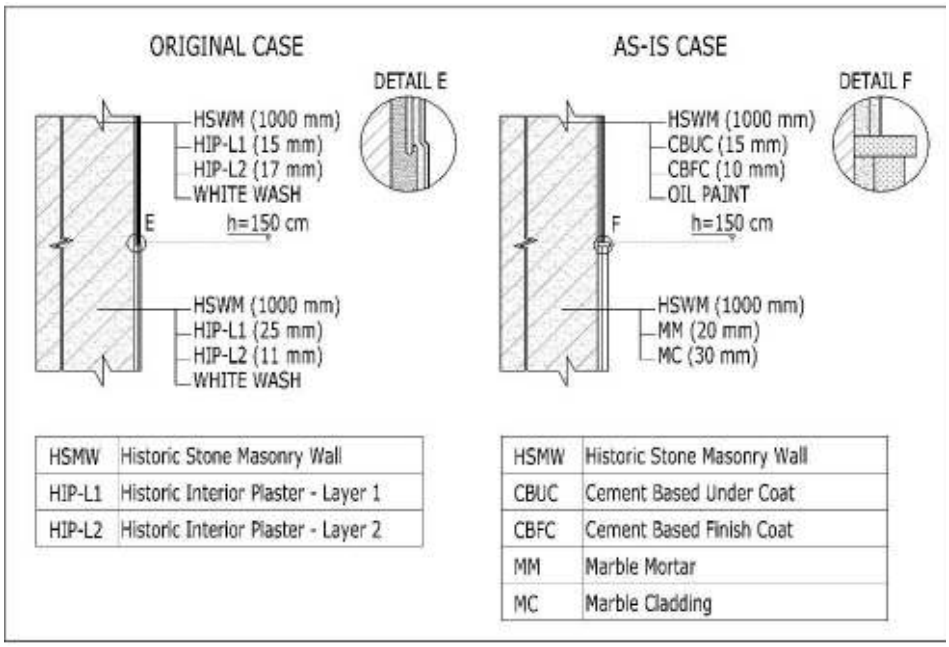

Figure 3.10 Geometric descriptions of wall models showing the order and thickness of the layers for the "*ORIGINAL case*" representing the historic wall structure of Şengül Hamamı (at left) and for the "*AS-IS case*" including the recent repairs with cement-based materials (at right).

3.2 Laboratory Analyses

Samples of historic materials including historic brick, stone, brick and stone mortar, interior and exterior plasters (Figure 3.11) forming the historic dome and wall masonry were collected from the historical baths belonging to the same period with Şengül Hamamı such as; Yahsibey Bath (Urla, 15th cc.), Hersekzade Bath (Urla, 15th cc.), Amasya Hizir Pasa Bath (Amasya, 15th cc.), Cukur Bath (Manisa, 14th cc.), Yalinayak Bath (Tire, 16th cc.), Kumacık Bath (Sivrihisar, 15th cc.), Hekim Bath (Tire, 15th cc.) and Yeniceköy Bath (Tire, 14th cc.) (Table 3.1). Basic physical properties as bulk density (ρ), porosity ($\varnothing$) and basic thermal properties as specific heat (c), thermal effusivity (e), thermal conductivity (k), thermal diffusivity (α) and volumetric heat capacity (VHC) of these samples were examined. The methods used to find the physical and thermal properties of historical materials were summarized below under respective headings.

Figure 3.11 Samples of historic brick, stone, brick and stone mortar, interior and exterior plasters collected from the historical baths belonging to the same period with Şengül Hamamı.

Table 3.1 Names and types of the samples of historic brick, stone, brick and stone mortar, interior and exterior plasters together with the historical buildings and cities they belong to.

SAMPLE NAME	TYPE	BUILDING	CITY
BRI.SI.M.DO.20	Dome Brick	Yalınayak Bath	İzmir-Tire
BRI.SO.M.07	Brick	Yalınayak Bath	İzmir-Tire
32B	Wall Brick	Çukur Bath	Manisa
HA-A3-VB-B	Vault Brick	Hersekzade Paşa Bath	İzmir-Urla
HA-A3-VB-C	Vault Brick	Hersekzade Paşa Bath	İzmir-Urla
HA-A1,2-DB	Dome Brick	Hersekzade Paşa Bath	İzmir-Urla
KuBCDE	Dome Brick	Kumacık Bath	Sivrihisar
YDB1b	Dome Brick	Yahşi Bey Bath	İzmir-Urla
27BM	Brick Mortar	Çukur Bath	Manisa
AHRM1	Brick Mortar	Hızır Paşa Bath	Amasya
YDM1c	Brick Mortar	Yahşi Bey Bath	İzmir-Urla
YDM1d	Brick Mortar	Yahşi Bey Bath	İzmir-Urla
HA-A3-FS	Stone	Hersekzade Paşa Bath	İzmir-Urla
KT2	Stone	Ankara Castle	Ankara
KT3	Stone	Ankara Castle	Ankara
MOR.SD.170	Stone Mortar	Yalınayak Bath	İzmir-Tire
HA-A3-VM	Stone Mortar	Hersekzade Paşa Bath	İzmir-Urla
CTI.SI.M.DO.210	Clay Tile	Yalınayak Bath	İzmir-Tire
PLA.DO.HE.807A	Exterior Dome Plaster	Hekim Bath	İzmir-Tire
PLA.DO.HE.807B	Exterior Dome Plaster	Hekim Bath	İzmir-Tire
PLA.DO.HE.808A	Exterior Dome Plaster	Hekim Bath	İzmir-Tire
PLA.DO.YE.812	Exterior Dome Plaster	Yeniceköy Bath	İzmir-Tire
HA-R (L)	Exterior Dome Plaster	Hersekzade Paşa Bath	İzmir-Urla
HA-R (U)	Exterior Dome Plaster	Hersekzade Paşa Bath	İzmir-Urla
PLA.SI.YE.811	Plaster of Hot Space	Yeniceköy Bath	İzmir-Tire
PLA.SI.M.060	Plaster of Hot Space	Yalınayak Bath	İzmir-Tire
PLA.SI.W.120	Plaster of Hot Space	Yalınayak Bath	İzmir-Tire
PLA.SI.YE.810	Plaster of Hot Space	Yeniceköy Bath	İzmir-Tire
HA.A4.PINT	Plaster of Hot Space	Hersekzade Paşa Bath	İzmir-Urla
PLA.IL.M.YA.804	Plaster of Warm Space	Yalınayak Bath	İzmir-Tire
PLA.IL.M.O50	Plaster of Warm Space	Yalınayak Bath	İzmir-Tire
AH.I2.AP4e	Plaster of Warm Space	Hızır Paşa Bath	Amasya
AH.I2.AP4c	Plaster of Warm Space	Hızır Paşa Bath	Amasya
AH.I2.AP4d	Plaster of Warm Space	Hızır Paşa Bath	Amasya
PLA.Ex.YE.813	Exterior Wall Plaster	Yeniceköy Bath	İzmir-Tire

3.2.1 Determination of basic physical properties

Basic physical properties such as bulk density (ρ) and porosity ($ø$) of historic materials were determined by using RILEM standard test methods together with other sources (RILEM, 1980; Teutonico, 1986 and TS 699, 1987).

In order to find out the physical properties of historic samples, firstly they were entirely saturated with distilled water during two days and then placed in vacuum by using HERAEUS vacuum chamber at 0.132 atm (100 torr) pressure for one hour. The weight of these samples were measured in air and recorded as saturated weight, M_{sat}. Following this, the weight of these saturated samples was measured in distilled water and recorded as Archimedes weight, M_{arc}. Finally, the samples were dried in the Erasmus oven at low temperatures (40°C) until reaching a constant weight, which was recorded as the dry weight of the sample, M_{dry}. All weights were measured with a balance sensitive to 0.1mg and used for the calculations of bulk density and porosity properties of the samples (RILEM, 1980; TS 699, 1987; Teutonico, 1986). The results were expressed in tables and/or diagrams.

Bulk density, "ρ", is the ratio of the mass to the bulk volume of the sample (RILEM, 1980; Teutonino, 1986). It is expressed in grams per cubic centimeters (g cm^{-3}) and calculated by using the Equation 1 given below (TS 699, 1987):

$$\rho = \frac{M_{dry}}{M_{sat} - M_{arc}} \qquad \text{g cm}^{-3} \tag{1}$$

where,
M_{dry}: dry weight, g
M_{sat}: saturated weight, g
M_{arc}: weight of the sample in water, g

Porosity, "$ø$", is the ratio of the pore volume of a solid mass to the bulk volume and expressed by the percentage (%) of volume (RILEM, 1980; Teutonico, 1986). The porosity was calculated by using the Equation 2 given below (TS 699, 1987):

$$\phi = \frac{M_{sat} - M_{dry}}{M_{sat} - M_{arc}} x100 \qquad \% \qquad (2)$$

3.2.2 Determination of thermal properties

Thermal effusivity, "*e*", is the capacity of a material to absorb and release heat and characterizes how easily heat can be absorbed or released at the surface of a material. It is expressed in W $s^{-1/2}m^{-2}K^{-1}$ (Goulart, 2004; http://www.beodom.com). The thermal effusivity measurements of the collected samples were done in the METU Central Laboratory with a sensitivity of 10-15%. The "*Perkin Elmer Pyris TC Probe*", which is a non-destructive device used in the determination of thermal properties of materials, was used in these measurements.

Specific heat capacity, "*c*", of a material defines the heat energy required to raise the temperature of the material by one degree per unit of weight and is expressed in J $kg^{-1}K^{-1}$ (TS 4048, 1984; Kumaran, 2001; Cook, 1978). The specific heat capacity of a material is constant while in a particular phase.

Experiments were done in order to find out the specific heat capacity, *c* values of the building materials belonging to the historic bath buildings. The main principle behind this experimental method is the rule of "conservation of energy" which is the first Law of Thermodynamics. When a definite amount of hot material is put into a definite amount of cold water, the temperature of the two becomes stable at an equilibrium point. Here, the quantity of heat taken by the water and the cup is equal to the quantity of heat given by the material. This enables the calculation of the specific heat capacity values of materials (TS 4048, 1984).

Heat, "*q*", is the energy that is transferred from one region to another when there is a temperature difference between the regions or when one of the regions is undergoing a phase change. It is a form of energy and a measurable quantity, which is expressed in Joule or Calorie and determined by the Equation 3 given below (TS 4048, 1984):

$$q = M\, c\, \Delta T \qquad \text{Calorie} \tag{3}$$

where,

M: the mass of the substance, g

c: the specific heat capacity, cal $g^{-1}°C^{-1}$

ΔT: the temperature change undergone by the sample, °C.

When two bodies, initially at different temperatures, are placed in intimate contact, in time they will come to equilibrium at some intermediate temperature. Provided no heat is lost to or gained from the surroundings, the quantity of heat gained by the colder body (q_{GAINED}) is equal to that lost by the hotter body (q_{LOST}). The equation is shown below (TS 4048, 1984):

$$q_{GAINED} = q_{LOST} \tag{4}$$

Calorimetry was generally used for the experimental determination of the energy transferred and so to determine the specific heat capacity values of the historic materials. The energy transfer, *q*, is measured by an apparatus called a *calorimeter*. A type of coffee cup calorimeter (Figure 3.12) was used in these experiments. Although it is a low tech device, it is possible to yield remarkably good results when used efficiently. This calorimeter has four basic components. The first one is an insulated container used for minimizing heat loss to the general surroundings. A Dewar Cup (Thermos) with a capacity of 1200 ml was used in this study. The second is an insulating lid with a hole for the insertion of thermometer. For this a thermal insulation material was used. The third one is a heat sink that can absorb or provide energy to the process being examined. Distilled water was used as heat sink or calorimeter liquid in the experiments. Finally, the last component of a calorimeter is a means of monitoring the temperature of the calorimeter. A digital insertion thermometer was placed through the hole on the lid; the accuracy of which was checked with another one.

The other equipments used in the experiments can be listed as a stirrer, an oven, a weighing machine and solid samples. A stirrer is a device that is used for maintaining uniform temperature inside the calorimeter. Instead of a stirrer, gently stirring the calorimeter system was done for the same purpose. As a heater, “Erasmus oven” with a temperature adjustment system was used. A Beckmann type mercury thermometer was placed inside the oven to make sure about the temperature. The experimental set up was placed next to this oven and

the climatic conditions in the room were kept stable during the experiment. For weighing the samples, a Chyo JL-200 type device with a balance sensitivity of 0.1mg was used. Since the bulk density of water is 1.00g cm^{-3}, the amount of water to be placed in the calorimeter was more conveniently measured by volume. Graduated cylinders were used for this purpose.

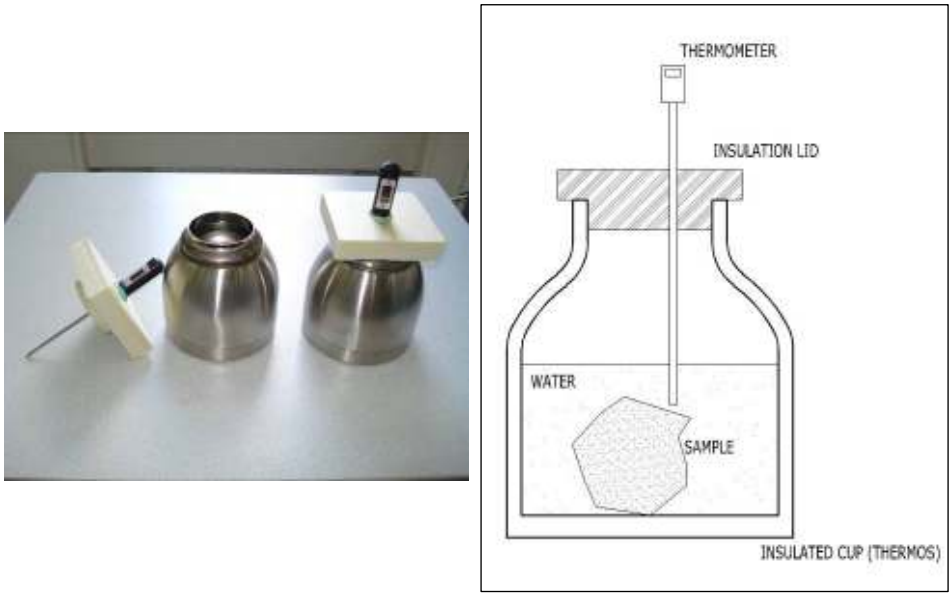

Figure 3.12 Views (at left) and schematic drawing (at right) of the calorimeters that were used in the experiments for the determination of specific heat capacity values of historic samples.

The solid samples, the specific heat capacities of which are to be measured, were chosen randomly from the historic materials and prepared as two pieces. Importance was given to having samples neither too small nor too big in dimension. It was also important for the sizes of the sample to be proportional to the calorimetric water and for the water to cover the whole sample by at least a centimeter (TS 4048, 1984).

After gathering all necessary equipment, the experiments were started by drying the samples of historic materials in the ERASMUS oven at low temperatures (40°C) until they reached a constant weight. This weight was then recorded as the weight of the sample, M_S (TS 4048, 1984). The samples were then placed in the same oven at a temperature of about 60˚C for one day in order to heat the samples to the temperature of the oven. The temperature of the oven, T_S, was recorded as the initial temperature of the samples.

Approximately 1000 grams – recorded as the mass of calorimeter water, M_W – of distilled water in the room temperature was placed in the calorimeter. Some time after closing the lid over the calorimeter cup, the cup and water system came to thermal equilibrium. Just before adding the hot sample into the water, the temperature was recorded as the initial temperature, T_W, of the cup and water system with the use of the thermometer placed through the lid.

After removing the lid from the calorimeter, the hot sample was transferred from the oven to the calorimeter as soon as possible, without physically touching it. The calorimeter was then covered with the lid as quickly as possible in order to prevent heat loss, taking care that the thermometer was only in contact with the water. The changes in temperature of the system were recorded at two minute intervals. During the experiment, the calorimeter system was stirred gently in order to retain the homogeneity of temperature of the water. The last and highest temperature that remained stable for three measurements was recorded as the equilibrium temperature of the system, T_E (TS 4048, 1984). Figure 3.13 shows the photographs of the experimental setup.

Figure 3.13 Photographs showing the experimental setup for the determination of specific heat capacity values of historic samples.

After completing the experiments for all the samples, calculations were done to find out the specific heat capacity values of historic samples. It was assumed that the transfer of heat between the thermometer and the system was small enough to be neglected. If the net heat exchange with the surroundings could be kept small, the energy transferred from the hot sample (q_{SAMPLE}) as its temperature drops must then equal the energy required by the insulated cup (q_{CUP}) and the cold water (q_{WATER}) to raise their temperature. For the experiments within the scope of this study, the heat emitted by the calorimeter cup (q_{CUP})

was neglected, so the main heat exchange was assumed to be between the sample and water (Equation 5). In this case, heat was gained by the water so the temperature change for the water was $\Delta T_1 = T_E - T_W$. In the same way, during the experiment heat was given by the historic samples, for which the temperature change was $\Delta T_2 = T_S - T_E$. Calculation of this change was carried out according to Equation 6, given below (TS 4048, 1984):

$$q_{WATER} = q_{SAMPLE} \tag{5}$$

$$M_W c_W \Delta T_1 = M_S c_S \Delta T_2 \tag{6}$$

where,

M_W: the mass of the calorimeter water, g

c_W: the specific heat capacity of the calorimeter water, cal g^{-1} $^oC^{-1}$

ΔT_1: the temperature change undergone by the calorimeter water, $T_E - T_W$, $^\circ$C.

M_S: the mass of the sample, g

c_S: the specific heat capacity of the sample, cal g^{-1} $^oC^{-1}$

ΔT_2: the temperature change undergone by the sample, $T_S - T_E$, $^\circ$C

The specific heat capacity value of a historic sample was found by solving this equation. The same stages were repeated for the second sample of the same material and the mean of the two values was determined to be the specific heat capacity of that historic material. In cases where the same sample was used for the repeated determinations, it was dried completely in the oven before reheating and weighed again to check for any particle or material loss during any point in the procedure (TS 4048, 1984).

Volumetric heat capacity, "*VHC*" is a measure of heat capacity of a particular material per unit volume. It represents how much heat can be stored in a given volume of a building material. It is expressed in J $m^{-3}K^{-1}$ and calculated by using Equation 7 given below (Goulart, 2004):

$$VHC = c\rho \qquad \text{J m}^{-3}\text{K}^{-1} \tag{7}$$

where,

c: specific heat capacity, J $kg^{-1}K^{-1}$

ρ: bulk density, kg m^{-3}

Thermal conductivity, *"k",* is the property that measures the effectiveness of a material to conduct heat. It is the time rate of heat flow through a body of unit thickness and unit area with a unit temperature difference between two surfaces (Strother & Turner, 1990; http://www.beodom.com). It is expressed in $W\ m^{-1}K^{-1}$ and calculated by using Equation 8 given below (Goulart, 2004; Grinzato *et al.,* 1994):

$$k = \frac{e^2}{c\rho} \qquad \text{W m}^{-1}\text{K}^{-1} \tag{8}$$

where,

e: thermal effusivity, W $s^{-1/2}m^{-2}K^{-1}$

c: specific heat capacity, J $kg^{-1}K^{-1}$

ρ: bulk density, kg m^{-3}

Thermal diffusivity, "α", indicates how easy a material undergoes temperature change and determines how rapidly heat will flow within it. It was expressed in $m^2\ s^{-1}$ and calculated by using the Equation 9 given below (Goulart, 2004; Strother & Turner, 1990; Grinzato *et al.,* 2002; http://www.beodom.com):

$$\alpha = \frac{k}{c\rho} \qquad \text{m}^2\,\text{s}^{-1} \tag{9}$$

where,

k: thermal conductivity, W $m^{-1}K^{-1}$

c: specific heat, J $kg^{-1}K^{-1}$

ρ: bulk density, kg m^{-3}

3.3 *In-Situ* Analyses

The *in-situ* analyses include the "Microclimatic Monitoring" and "Infrared Thermography" which were summarized below under respective headings.

3.3.1 Microclimatic monitoring

The microclimatic conditions for the indoor and outdoor of the structure were continuously-monitored (every five minutes) along a year by taking ambient temperature and relative humidity measurements from the entrance hall, undressing room, warm and hot spaces as well as from the outside. Similar measurements were also taken during the period of *in-situ* QIRT studies. The data were collected by means of data loggers, "*HOBOware Pro*" and the software, "*HOBOware Pro v.2.3*." Figure 3.14 shows the locations of 12 data loggers in different parts of Şengül Hamamı. The first six data loggers were located in the women's part to the entrance hall, undressing room lower and upper storey, warm space, hot space and a *halvet*, respectively. Other ones were located in the men's part to the undressing room lower and upper storey, hot space, *halvet*, pool and *sauna* rooms, respectively.

Figure 3.14 Plan showing the distribution of data loggers in different parts of Şengül Hamamı (*Source: Archives of the General Directorate of Pious Foundations, 2008; produced by the author)*.

3.3.2 Infrared thermography

In-situ infrared thermography (IRT) studies of Şengül Hamamı were done by single and sequential IR imaging. These studies were carried out at nights in February, July and November. The exterior wall and roof surfaces as well as the interior wall, dome and floor

surfaces were scanned in segments by taking single IR images together with their visible-light photographs. At some regions, especially at dome and exterior wall surfaces, the IR imaging was carried out by taking infrared sequences at 5-10 seconds intervals for a period of 5-10 minutes. The differential IR images were produced by taking the temperature differences as a function of time. The decrease and/or increase in surface temperature were evaluated during the cooling period of exterior surfaces at night while interior surfaces were exposed to a very hot and wet air. The IR sequences taken from interior and exterior surfaces of dome structures were also analyzed in order to produce the thermal models representing the real surface temperature distribution.

The Quantitative IRT survey was done by using the "*AGEMA ThermaCAM 550*" and *"FLIR ThermaCAM E65"* thermographic equipments. The camera was given inputs on ambient temperature, relative humidity, distance to target area and on emissivity of target surfaces to obtain accurate *in-situ* measurements. The climatic data were recorded by using an environmental meter, "*Kestrel 3000" and* dataloggers, "*HOBOware Pro*". Images were then analyzed by using the softwares of *"ThermaCAM Reporter 2000"* and *"ThermaCAM Researcher Professional"*.

3.4 Heat Transfer Analyses

In this part, the methods for "determination of total thermal resistance and transmittance values" and "heat transfer calculations" were given under respective headings.

3.4.1 Determination of the total thermal resistance and transmittance values

Thermal resistance, "R_n", is the resistance of a material for a given thickness to the thermal conduction/heat transfer. It is expressed in $m^2K\ W^{-1}$ and calculated by using the Equation 10 given below (Izocam, 2004; TS 825, 1998; Strother and Turner, 1990; Straaren, 1967; BRE, 1969; Örs, 2006):

$$R_n = \frac{l_n}{k_n} \qquad \text{m}^2\text{K W}^{-1} \tag{10}$$

where,

l_n: the thickness of the material, m

k_n: thermal conductivity coefficient of the material calculated with laboratory analyses or taken directly from literature, $\text{Wm}^{-1}\text{K}^{-1}$.

Total Thermal Resistance, "R_T", is the sum of thermal resistances of all materials/layers used in a building component, including the interior and exterior surface thermal resistances. Its unit is $\text{m}^2\text{K W}^{-1}$ and calculated by using the Equation 11 given below assuming the section had *n* layers (TS 825, 1998; Strother and Turner, 1990; Cook, 1978; BRE, 1969, Örs, 2006; Goulart, 2004):

$$R_T = R_{si} + R_1 + R_2 + \ldots + R_n + R_a + R_{se} \qquad \text{m}^2\text{K W}^{-1} \tag{11}$$

where,

R_{si}: thermal resistance of interior surface, $\text{m}^2\text{K W}^{-1}$

R_n: thermal resistance of the material, $\text{m}^2\text{K W}^{-1}$

R_a: thermal resistance of the air space, $\text{m}^2\text{K W}^{-1}$

R_{se}: thermal resistance of exterior surface, $\text{m}^2\text{K W}^{-1}$.

For the calculations, R_{si} and R_{se} values for the roof/dome structure were determined from Tables 2.3 and 2.4 given in the previous chapter. R_{si} was taken as 0.106 given for interior roof surfaces with high emissivity where the heat flow is upwards and R_{se} was the taken as 0.07 given for exterior roof surfaces with high emissivity where the stated exposure is sheltered (Hall, v.1, 1994).

Total Thermal Transmittance, "*U*", is the reciprocal of the total thermal resistance, "$1/R_T$". It represents the amount of heat transferred through a building section, between the indoor and outdoor climate, for a unit of surface and temperature. It is expressed in $\text{W m}^{-2}\text{K}^{-1}$ and determines the rate of heat flow through a given building component (Goulart, 2004; Cook, 1978; Hall, v.1, 1994; Strother and Turner, 1990).

Turkish Standards give the acceptable values required for the energy efficient buildings for the four climatic regions in Turkey (TS 825, 1998). Those values given for quality construction of the buildings situated in Ankara, which is in the 3rd region of Turkey, were given in Table 2.1 in the previous chapter.

3.4.2 Heat transfer calculations

For the heat transfer calculations of the dome sections, heat flow curves (temperature gradient curves) are produced for both the *ORIGINAL* and *AS-IS cases* of Şengül Hamamı. In order to draw these curves, first of all the temperature values at each layer in the dome section were calculated. For this purpose, temperature differences between interior and exterior, ΔT; thermal resistance values of all layers, R_n; the total thermal resistance of the dome section, R_T; heat flow, Q and temperature drop, ΔT_n between layers of the dome sections were determined (Izocam, 2004; TS 825, 1998; Strother and Turner, 1990; BRE, 1969; Örs, 2006). The way how these values were calculated was summarized below:

Temperature difference, "ΔT", is the difference between the interior and exterior air temperatures. It was expressed in degree ˚C and calculated by using the Equation 12 given below (Izocam, 2004; TS 825, 1998; Strother and Turner, 1990; BRE, 1969):

$$\Delta T = T_i - T_e \quad ^\circ\text{C} \tag{12}$$

where;
T_i: interior air temperature, °C
T_e: exterior air temperature, °C.

Heat flow, "Q", indicates the heat loss from the unit area of a building section at a unit time (one hour). It is expressed in W m^{-2} and calculated by using the Equation 13 given below (Izocam, 2004; TS 825, 1998; Strother and Turner, 1990; BRE, 1969).

$$Q = \frac{\Delta T}{R_T} \qquad \text{W m}^{-2} \tag{13}$$

where,

ΔT: temperature difference, °C

R_T: total thermal resistance, m^2°C W^{-1}

Temperature drop between layers of a building section, "ΔT_n", was calculated by using the Equation 14 given below (Izocam, 2004; TS 825, 1998; Strother and Turner, 1990; BRE, 1969):

$$\Delta T_n = Q \times R_n \qquad ^{\circ}C \qquad (14)$$

where,

Q: heat flow, W m^{-2}

R_n: thermal resistance of the layer, m^2°C W^{-1}.

A new non-destructive investigation method was developed by the joint use of heat transfer calculations and Quantitative Infrared Thermography. Here, the thermal models representing the real temperatures of interior and exterior dome surfaces for the *AS-IS* case were prepared by the analyses of IR sequences. Then, the heat flow curves presenting the reference temperature gradients through the dome sections calculated for steady state conditions were drawn. The reference interior and exterior surface temperatures calculated by the heat transfer equations were compared with the real surface temperatures obtained by the analysis of IR images in order to examine the thermal failures in the dome sections of Şengül Hamamı and their possible reasons.

3.5 Water Vapour Transfer Analyses

In this part, the calculation methods for and procedure of "analyses of water vapour transmission/flow" and "analyses of partial vapour pressure distribution" were given under respective headings.

3.5.1 Analyses of water vapour transmission/flow

Continuity of the water vapour transmission along the layers of the *ORIGINAL* and *AS-IS* dome sections were examined by the total S_D values, equivalent air layer thickness of water vapour diffusion. The total S_D value of a building section is the sum of the S_D values of its layers (TS prEN ISO 7783-2, 1999; TS 825, 1998; Izocam, 2004; Akkuzugil, 1997; Örs, 2006). It is expressed in meters (*m*) and calculated as shown in the Equation 15:

$$S_D = S_{D1} + S_{D2} + S_{D3} + \ldots + S_{Dn} \qquad \text{m} \qquad (15)$$

The classification of materials based on their S_D values is possible according to TS prEN ISO 7783-2 (1999). Table 2.2 given in the previous chapter was prepared in accordance with this standard and provides the ranges for low, medium or high water vapour permeable materials. The various materials forming the layers of *ORIGINAL* and *AS-IS* dome sections of historical bath buildings were analyzed according to their S_D values in order to make comparative results.

Figures were produced by adding up the S_D values of each layer as a function of layer thickness, where the slope of the line gave the μ value of each layer. The higher slope indicated higher μ value, in other words higher resistance to water vapour permeation. Increase in the slope of the line is mainly observed at the low permeable layers, where the water vapour flow is interrupted.

3.5.2 Analyses of partial vapour pressure distribution

In order to investigate the risk of condensation in the dome sections, partial vapour pressure (*p*) and equilibrium vapour pressure *(ps)* values through the sections were calculated for both the *ORIGINAL* and *AS-IS cases* of Şengül Hamamı (Izocam, 2004; TS 825, 1998; Strother and Turner, 1990; BRE, 1969; Örs, 2006). These calculations were done for the mean temperature and relative humidity (RH) values of all the months in order to check the condensation conditions in the building fabric through the year. The extreme cases having values above and below the monthly-means of exterior temperatures were also considered in

these calculations. The numerical values were achieved by the microclimatic data collected from the inside and outside of Şengül Hamamı during a year in 2007-2008 for the microclimatic analyses.

Partial vapour pressure, "*p*", indicates the pressure of water vapour at a given temperature and humidity conditions. It is expressed in Pascal and calculated by using the Equation 16 given below (Izocam, 2004; TS 825, 1998):

$$p = \varphi \times p_s \qquad \text{Pa} \tag{16}$$

where,
φ: relative humidity, %
p_s: equilibrium water vapour pressure at a given temperature, Pa (Appendix B).

The partial vapour pressure for the *ORIGINAL* and *AS-IS cases* was calculated for the interior and exterior dome surfaces. The results of these calculations were presented in figures with a linear decrease from interior to exterior.

On the other hand, **the equilibrium vapour pressure**, "*ps*", was found and presented as a distribution of values in the dome sections. In order to achieve this, temperature values at each layer in the dome section were calculated by using the methods and equations given in the previous pages. The equilibrium vapour pressure values at these temperatures for each layer surface were then calculated by the use of tables showing the water vapour pressure values at different temperatures (Appendix B).

The assessment of condensation risk through the dome sections was made by drawing the profiles of water vapour pressure for the partial and equilibrium vapour pressure through the structure independently. From these figures, the surfaces where equilibrium water vapour pressure was greater than partial water vapour pressure were found to have no risk of condensation (Figure 3.15a), whereas the surfaces where the equilibrium water vapour pressure was lower than the partial water vapour pressure or where these two pressures were equal to each other, condensation was inevitable (Figure 3.15b) (Izocam, 2004; TS 825, 1998; Strother and Turner, 1990; BRE, 1969).

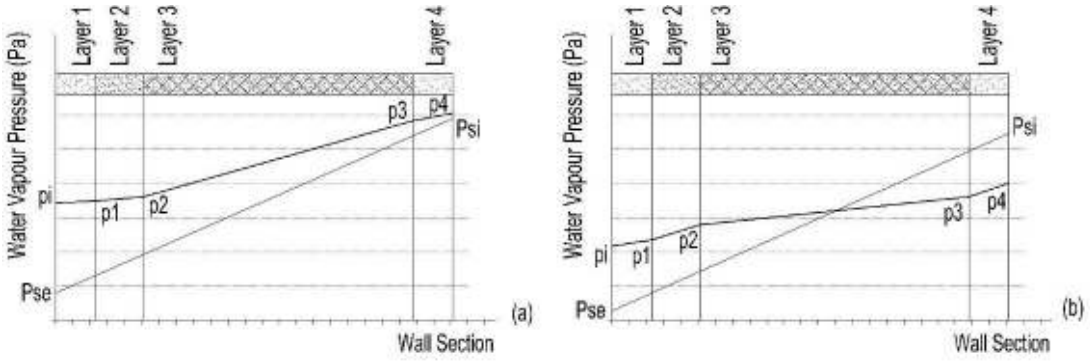

Figure 3.15 Partial and equilibrium water vapour pressure distribution in a wall where (a) there is no risk of condensation and where (b) condensation occurs.

CHAPTER 4

RESULTS

The results are summarized in this section together or in succession with figures and tables.

4.1 Basic Thermo-Physical Properties of Historic Materials

The results of laboratory analyses revealed the thermo-physical properties of historic brick, brick mortar, interior and exterior plasters in terms of bulk density (ρ), porosity ($\varnothing$), specific heat (c), thermal effusivity (e), thermal conductivity (k), thermal diffusivity (α) and volumetric heat capacity (VHC). Those values having the International System of Units (SI) were summarized in Table 4.1 and Figures 4.1 and 4.2. The conversion of SI units to the units of metric system was also given in Appendix C.

The basic physical properties of historic brick, HB1-HB3, and its mortar, HBM1 and HBM2, together with historic exterior plasters, HEP-L1 and HEP-L2, were obtained from the literature (Caner-Saltik *et al*., 2005b; Esen *et al*., 2004; Caner-Saltik *et al.*, 2003a and Caner *et al*., 2005) as summarized in Table 2.5. These sources gave the bulk density and porosity values of historic bricks within the range of 1310kg m^{-3} to 1520kg m^{-3} and 38.90% to 47.55%, respectively while being 1520kg m^{-3} to 1550kg m^{-3} and 38.10% to 38.30% for the historic brick mortars. Exterior historic plasters covering the roof, HEP-L1, HEP-L2 and HEP-L3 had bulk density values of 1480kg m^{-3}, 1390kg m^{-3} and 1700±80kg m^{-3}, with effective porosity values of 40.80%, 43.40% and 26.23±0.21%, respectively. For the historic interior plaster layers, HIP-L1 and HIP-L2, bulk density values were determined to be 1580±50kg m^{-3} and 1070±20kg m^{-3}, with porosity values of 45.29±3%, and 53.72±4.66%, respectively.

Table 4.1 Thermo-physical properties of historic brick (HB), brick mortar (HBM), exterior plasters (HEP) and interior plasters (HIP) in SI units forming the brick dome masonry.

Layers	**Samples**	ρ **kg m^{-3}**	ϕ **%**	c **J kg^{-1}K^{-1}**	e **W s$^{-1/2}$m^{-2}K^{-1}**	k **W m^{-1}K^{-1}**	α **m^2 s^{-1}**	VHC **Jm^{-3}K^{-1} x10^4**
HB1	BRI.SO.M.07	1310[(i)]	47.55[(i)]	879±35	800±9	0.56±0.02	4.8 10^{-7}±0.3 10^{-7}	115.2121±4.5199
HB2	32B	1470[(ii)]	39.84[(ii)]	1038±18	900±16	0.53±0.01	3.5 10^{-7}±0.1 10^{-7}	152.6063±2.5729
HB3	HA-A3-VB-C	1520[(iii)]	38.90[(iii)]	891±63	902±9	0.60±0.04	4.5 10^{-7}±0.6 10^{-7}	135.5003±9.4979
HBM1	YDM1c	1550[(iii)]	38.10[(iii)]	939±21	987±3	0.67±0.02	4.6 10^{-7}±0.2 10^{-7}	145.4966±3.3091
HBM2	YDM1d	1520[(iii)]	38.30[(iii)]	922±19	840±5	0.50±0.01	3.6 10^{-7}±0.2 10^{-7}	140.1450±2.9080
HEP-L1	HA-R (U)	1480[(iv)]	40.80[(iv)]	848±57	1068±7	0.91±0.06	7.3 10^{-7}±1 10^{-7}	125.4245±8.4345
HEP-L2	HA-R (L)	1390[(iv)]	43.40[(iv)]	1017±5	1073±8	0.81±0.00	5.8 10^{-7}±0.1 10^{-7}	141.4229±0.7133
HEP-L3	PLA.DO.HE.808A	1700±80	26.23±0.21	905±71	988±5	0.64±0.05	4.2 10^{-7}±0.7 10^{-7}	153.8744±12.0844
HIP-L1	AH.I2.AP4e	1580±50	45.29±3	983±82	756±22	0.37±0.03	2.4 10^{-7}±0.4 10^{-7}	155.1294±12.9411
HIP-L2	AH.I2.AP4d	1070±20	53.72±4.66	956±27	816±12	0.65±0.02	6.4 10^{-7}±0.4 10^{-7}	102.2333±2.8772

NOTE.-The ρ *and* ϕ values of some samples were taken from the literature: [(i)]Caner-Saltik *et al*. 2005b; [(ii)]Esen *et al*., 2004; [(iii)]Caner-Saltik *et al.*, 2003a and [(iv)]Caner *et al*., 2005.

The bulk density and porosity values of historic materials obtained from literature and by laboratory analyses were presented in Figure 4.1 together with the bulk density and porosity values of contemporary cement-based repair materials used in Şengül Hamamı, such as mesh-reinforced concrete and cement based plaster layers taken from the literature (TS 825, 1998; Örs, 2006). The bulk density value of mesh-reinforced concrete layer (MRC) covering the roof surfaces of Şengül Hamamı was given as 2400kg m^{-3} (TS 825, 1998). For the cement based under coat (CBUC) and cement based finish coat (CBFC) layers covering the interiors of bathing spaces, bulk density values were given to be 1850kg m^{-3} and 1940kg m^{-3}, respectively with porosity values of 25.4% and 25.5% (Örs, 2006). The historic materials were seemed to be less dense and more porous than the contemporary materials.

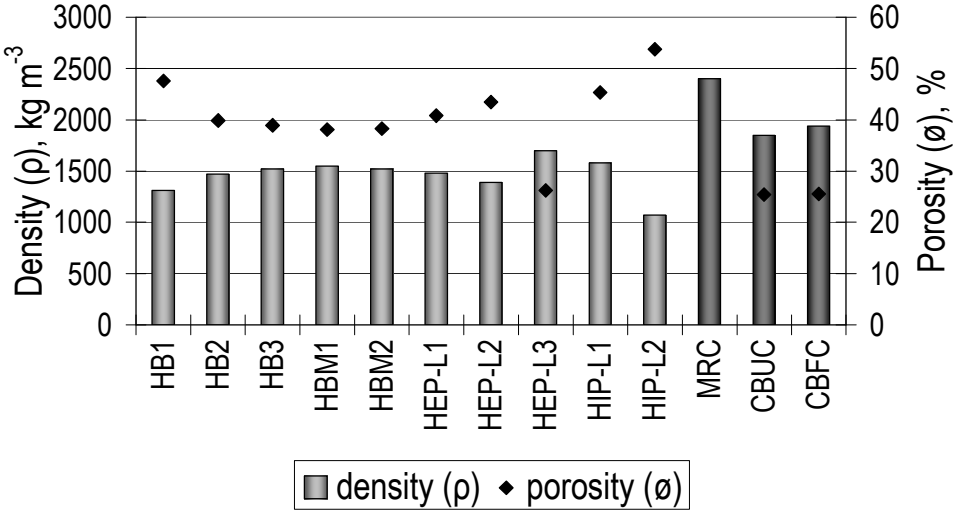

Figure 4.1 Bulk density (ρ) and porosity ($\varnothing$) of historic and cement-based repair materials; *except HEP-L3, HIP-L1 and HIP-L2, bulk density and porosity values were obtained from the literature (Caner-Saltik et al., 2005b; Esen et al., 2004; Caner-Saltik et al., 2003a and Caner et al., 2005; TS 825, 1998 and Örs, 2006)*.

The mean thermal conductivity values of historic brick, HB and brick mortar, HBM were found to be 0.56±0.04W $m^{-1}K^{-1}$ and 0.59±0.1W $m^{-1}K^{-1}$, being in the range of 0.50±0.01W $m^{-1}K^{-1}$ and 0.67±0.02W $m^{-1}K^{-1}$. The *k* values of the protective roof plasters of HEP-L1, HEP-L2 and HEP-L3 were determined as 0.91±0.06W $m^{-1}K^{-1}$, 0.81±0.00W $m^{-1}K^{-1}$ and 0.64±0.05W $m^{-1}K^{-1}$, respectively. The two layers of interior plasters, HIP-L1 and HIP-L2 were found to have *k* values of 0.37±0.03W $m^{-1}K^{-1}$ and 0.65±0.02W $m^{-1}K^{-1}$, respectively. The thermal conductivity values of historic materials obtained by the laboratory tests were

presented in Figure 4.2 together with the thermal conductivity values of contemporary cement-based repair materials used in Şengül Hamamı, such as mesh-reinforced concrete and cement based plaster layers taken from the literature (TS 825, 1998; Örs, 2006). The thermal conductivity values were given as 2.1W $m^{-1}K^{-1}$ for mesh-reinforced concrete layer (MRC) (TS 825, 1998) and 1.4W $m^{-1}K^{-1}$ for the cement based under coat (CBUC) and cement based finish coat (CBFC) layers (Örs, 2006). The historic materials were seemed to be less thermal conductive than the contemporary materials.

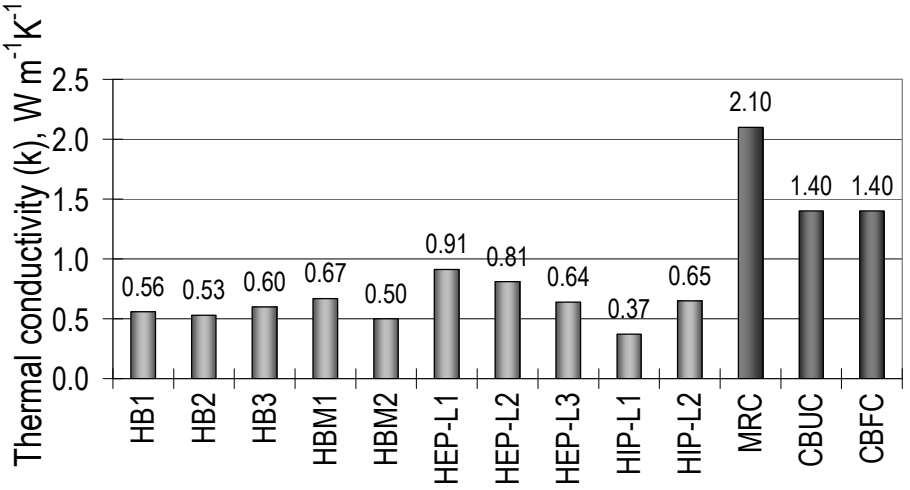

Figure 4.2 Thermal conductivities of historic and cement-based repair materials; *the k values of the MRC, CBUC and CBFC were obtained from the literature (TS 825, 1998 and Örs, 2006).*

The historic dome brick and its mortar were determined to have specific heat values in the range of 879±35J $kg^{-1}K^{-1}$ and 1038±18J $kg^{-1}K^{-1}$, with mean *c* values of 936±86J $kg^{-1}K^{-1}$ and 930±19J $kg^{-1}K^{-1}$, respectively. The mean *c* values of the protective roof plasters, HEP-L1, HEP-L2 and HEP-L3, were determined as 848±57J $kg^{-1}K^{-1}$, 1017±5J $kg^{-1}K^{-1}$ and 905±71J $kg^{-1}K^{-1}$, respectively. The two layers of interior plasters, HIP-L1 and HIP-L2, were found to have mean *c* values of 983±82J $kg^{-1}K^{-1}$ and 956±27J $kg^{-1}K^{-1}$, respectively.

The mean thermal effusivity and diffusivity values of the historic dome brick were determined to be 867±52W $s^{-1/2}m^{-2}K^{-1}$ and 4.3 10^{-7}±0.7 $10^{-7}m^2$ s^{-1}, being 914±85W $s^{-1/2}m^{-2}K^{-1}$ and 4.1 10^{-7}±0.6 $10^{-7}m^2$ s^{-1} for historic brick mortar, respectively. The mean *e* and α values of protective roof plasters were determined as 1068±7W $s^{-1/2}m^{-2}K^{-1}$ and 7.3 10^{-7}±1 $10^{-7}m^2$ s^{-1} for

HEP-L1, 1073±8W $s^{-1/2}m^{-2}K^{-1}$ and 5.8 10^{-7}±0.1 $10^{-7}m^2$ s^{-1} for HEP-L2 and 988±5W $s^{-1/2}m^{-2}K^{-1}$ and 4.2 10^{-7}±0.7 $10^{-7}m^2$ s^{-1} for HEP-L3, respectively. The two layers of interior plasters were found to have mean *e* and α values of 756±22W $s^{-1/2}m^{-2}K^{-1}$ and 2.4 10^{-7}±0.4 $10^{-7}m^2$ s^{-1} for HIP-L1 and 816±12W $s^{-1/2}m^{-2}K^{-1}$ and 6.4 10^{-7}±0.4 $10^{-7}m^2$ s^{-1} for HIP-L2, respectively.

The volumetric heat capacity values of historic dome brick and its mortar were determined to be in the range of 115.2121 10^4 ± 4.5199 10^4J $m^{-3}K^{-1}$ and 152.6063 10^4 ± 2.5729 10^4J $m^{-3}K^{-1}$, with mean *VHC* values of 134.4396 10^4 ± 17.4296 10^4J $m^{-3}K^{-1}$ and 142.8208 10^4 ± 4.0019 10^4J $m^{-3}K^{-1}$, respectively. The mean *VHC* values of the protective roof plasters, HEP-L1, HEP-L2 and HEP-L3, were determined as 125.4245 10^4 ± 8.4345 10^4J $m^{-3}K^{-1}$, 141.4229 10^4± 0.7133 10^4J $m^{-3}K^{-1}$ and 153.8744 10^4 ±12.0844 10^4J $m^{-3}K^{-1}$, respectively. The two layers of interior plasters, HIP-L1 and HIP-L2, were found to have mean *VHC* values of 155.1294 10^4 ± 12.9411 10^4J $m^{-3}K^{-1}$ and 102.2333 10^4 ± 2.8772 10^4J $m^{-3}K^{-1}$, respectively.

4.2 Microclimatic Analyses

In this section are presented the results of microclimatic analyses of Şengül Hamamı, which revealed the microclimatic characteristics of the structure. According to the microclimatic data, there were three different spaces in the structure, having particular microclimatic characteristics in terms of ambient temperature, relative humidity and monthly temperature fluctuations. From outside to inside, in an order from the entrance hall, undressing room, warm space and hot space of the women's part, an increase in ambient temperature was determined while the large range of temperature fluctuations getting lower (Figure 4.3).

The monthly means of ambient temperatures from undressing room to the warm space and then to the hot space of Şengül Hamamı showed a gradual increase in temperature, with the annual mean of 23.1°C±2.1°C for the undressing room, 28.2°C ±2.0°C and 36.0°C ±1.0°C for the warm and hot spaces, respectively. However, a considerable temperature difference was determined at the entrance hall, being the transition space between the outside and the inside of the structure. The annual mean temperature of 16.0°C ±6.8°C for the entrance hall presented a large range of temperature fluctuation since that space was in close contact with the outside climatic conditions having annual mean of 13.3°C ±9.3°C.

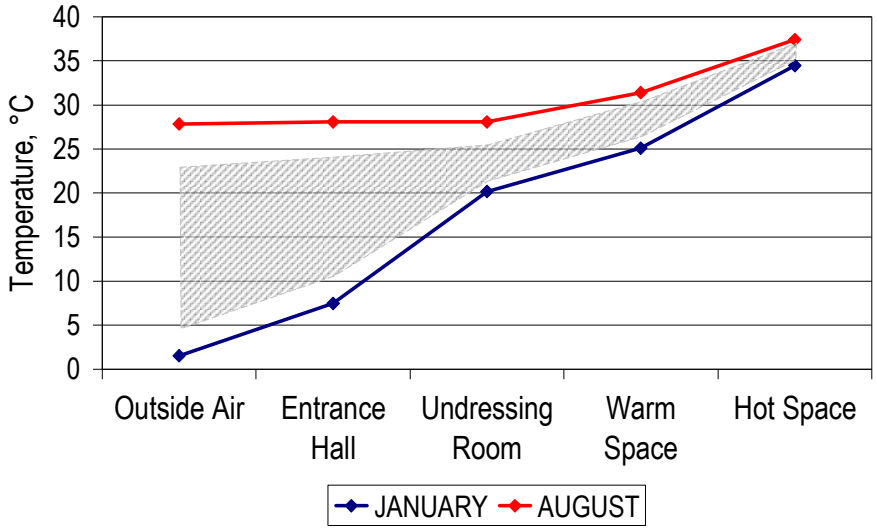

Figure 4.3 The monthly means of ambient temperatures, showing the gradual increase in temperature between the spaces, starting from the outside air to the entrance hall, then to the undressing room, and to the warm and hot bathing spaces of the women's part.

The historical baths have particular microclimatic features having very hot and humid indoors. The microclimatic analyses showed that the indoor climate of hot spaces was quite constant for all seasons while the exterior climate exhibited seasonal temperature and RH fluctuations considerably (Figure 4.4). At women's and men's hot spaces, the annual mean of ambient temperature were found to be 36.0°C ± 1.0°C and 35.5°C ± 1.2°C, respectively, while those of relative humidity were 95% ± 2%RH and 100% ± 0%RH.

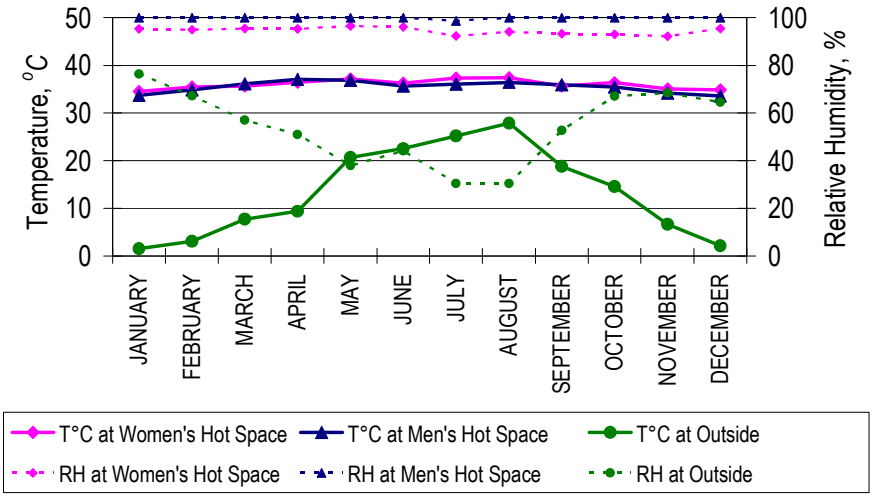

Figure 4.4 The monthly means of ambient temperature and relative humidity in the women's and men's hot spaces and at outside during a year.

The maximum difference in interior ambient temperature was observed between summer and winter. According to the daily means of ambient temperatures, a temperature differences of 2.9°C ± 0.7°C and 2.7°C ± 0.6°C were determined between the months of August and January in the women's and men's hot spaces, respectively (Figure 4.5) while the humidity conditions remained the same. This data also showed the presence of considerable heat loss problems in the dome structure.

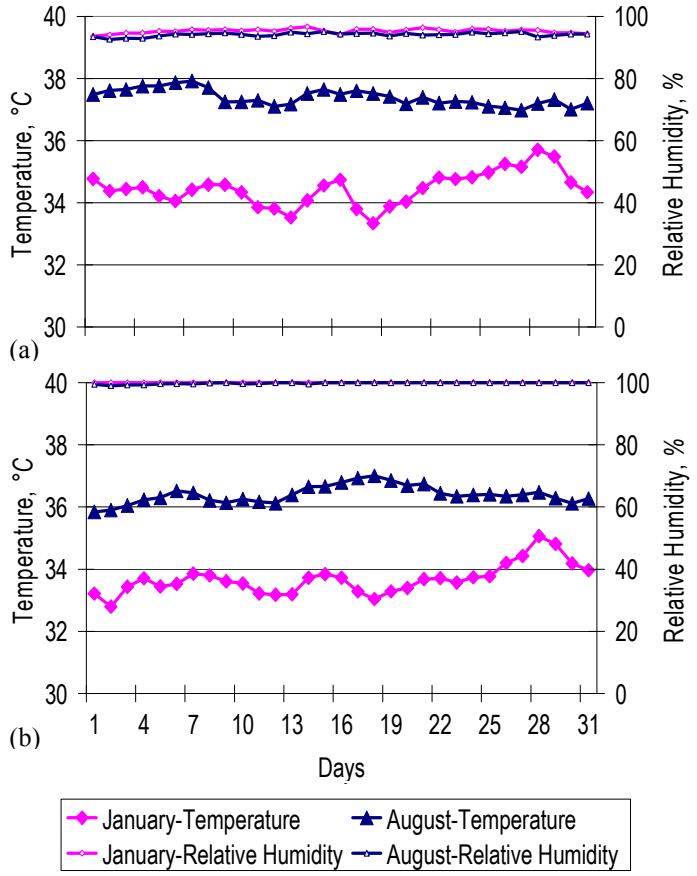

Figure 4.5 The daily means of ambient temperature and relative humidity at women's and men's hot spaces in January and August; showing the interior ambient temperature differences of 2.9°C ±0.7°C and 2.7°C ±0.6°C measured between the months of August and January at women's (a) and men's (b) hot spaces, respectively, while the humidity conditions were remained the same.

In addition, the warm dome surfaces were found to heat the neighbouring outside air due to the insufficient thermal resistance of the dome structure. For instance, in February the air close to the dome surfaces was warmer than the outside air temperature with a mean

temperature difference of 3.1°C ± 0.5°C (Figure 4.6). This data clearly showed the existence of a temperature difference between the outside air and the air neighboring the exterior dome surfaces. The measurements were taken especially to discover whether there was a temperature difference or not. One data logger was left very close to the exterior dome surface and the other was hanged on the wall at the roof storey level to measure the outside air during the period of IR survey in February.

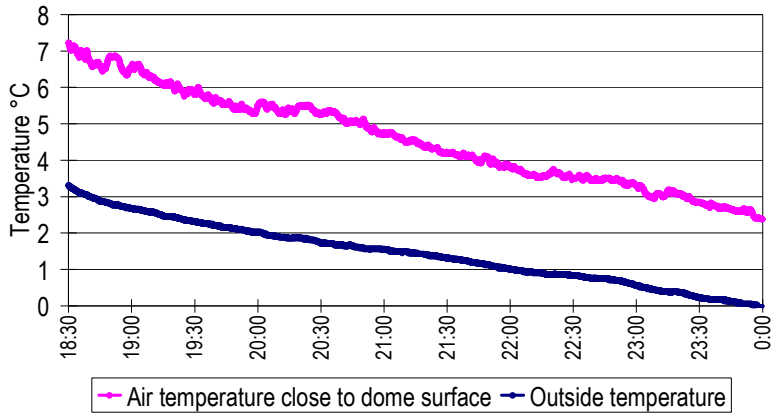

Figure 4.6 The curves of air temperature close to the exterior dome surface and outside air temperature for a period of three-and-a-half hours in February at night, showing that the air temperature close to the dome surfaces was warmer than the outdoor temperature with a temperature difference of 3.1°C ± 0.5°C.

The hot spaces of Şengül Hamamı showed daily temperature and relative humidity fluctuations both in winter and in summer. According to the microclimatic data collected at 5 minutes intervals, in January the daily ambient temperature fluctuations were determined to be 0.72°C±0.12°C and 0.56°C±0.20°C for the women's and men's hot spaces, respectively (Figure 4.7) while the daily outside temperature fluctuations were 11.91°C±2.41°C. In August, when the outside temperature fluctuations in a day were 12.83°C±1.34°C, the daily ambient temperature fluctuations at the women's and men's hot spaces were determined to be lower, being in the range of 0.57°C±0.16°C and 0.23°C±0.09°C, respectively. The daily fluctuations in the temperature and relative humidity values of hot bathing spaces were in relation with the working hours of Şengül Hamamı starting from 5:00am to the 23:00pm for the men's part and from 6:00am to 19:00pm for the women's part.

In January, the mean ambient temperatures of the women's and men's hot spaces measured at the weekend were found to be higher than those measured in weekdays in the range of 0.51°C and 0.94°C, respectively (Figure 4.7). This was mainly because of the fact that at the weekends more energy/coal was introduced to the heating system in winter. Furthermore, at the weekends one more draft chimney (D15) was added to the functioning ones, resulting in a considerable increase in the mean ambient temperature of the men' hot space. The necessity of introducing more heat to the bath and opening the damper of one more draft chimney at the weekends arose due to the fact that the baths were used by more people on Saturday and Sunday.

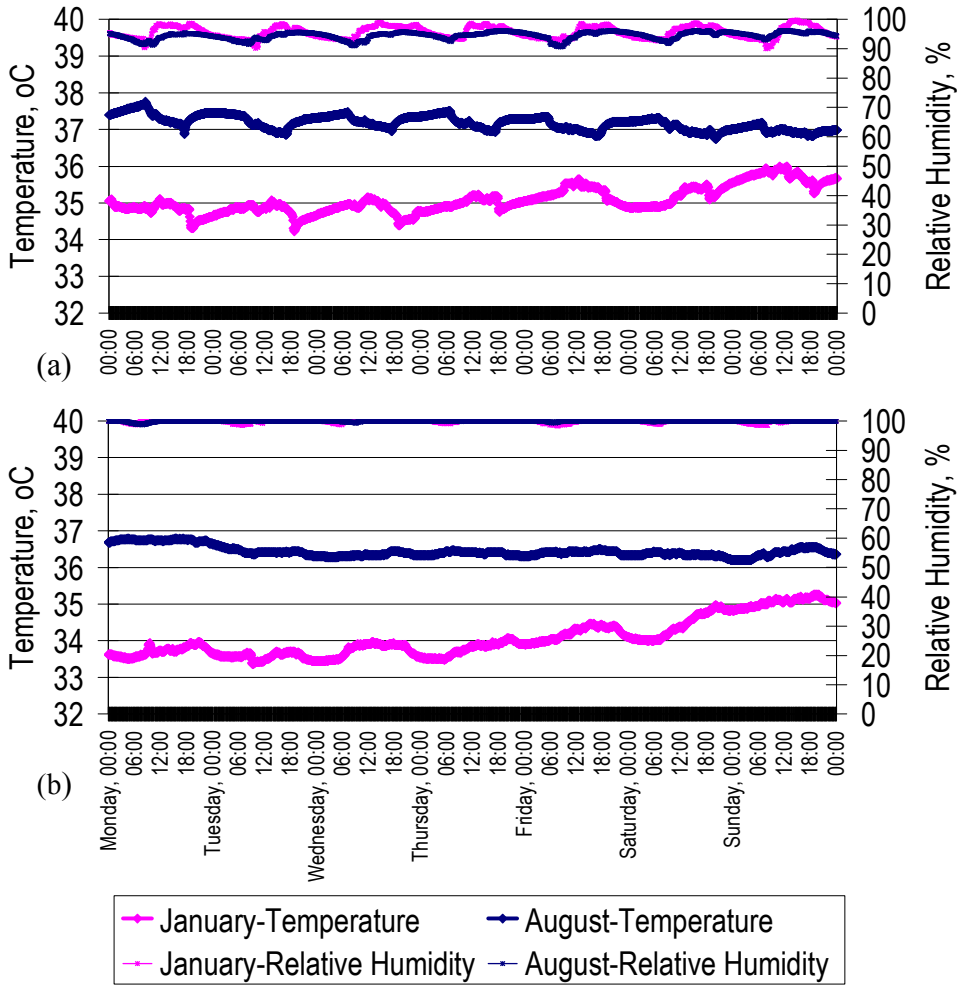

Figure 4.7 The daily temperature and relative humidity fluctuations at the women's and men's hot spaces for a period of one week in January and August; showing the daily ambient temperature fluctuations in the range of 0.72°C±0.12°C and 0.57°C±0.16°C in the women's hot space (a) and in the range of 0.56°C±0.20°C and 0.23°C±0.09°C in the men's hot space (b) in January and August, respectively.

4.3 Quantitative Infrared Thermography Analyses

In this section are presented the results of Quantitative Infrared Thermography analyses, which revealed the types of thermal failures, their distribution on dome and wall structures and the extent of problems (Figures 4.8-4.13). In the infrared images, most exterior surfaces of walls and concrete-clad roof were observed to be considerably warmer than outside air temperature (Figure 4.8). In these images, the circular dome lights were seemed to be the hottest areas while cement mortar peripheries encircling these dome lights were colder surfaces. Some false alarms have been considered due to the initial warming of these exposed surfaces by solar radiation and still keeping this heat for a period of time after sunset. However, the differential IR images showed that warmer dome surfaces were definitely due to heat loss from the very hot interior to the outside. For instance, at the dome of women's hot space, the heat loss from the concrete-clad surfaces was determined with an average temperature increase of 0.2°C during the cooling period of night for 322s in November (Figure 4.9).

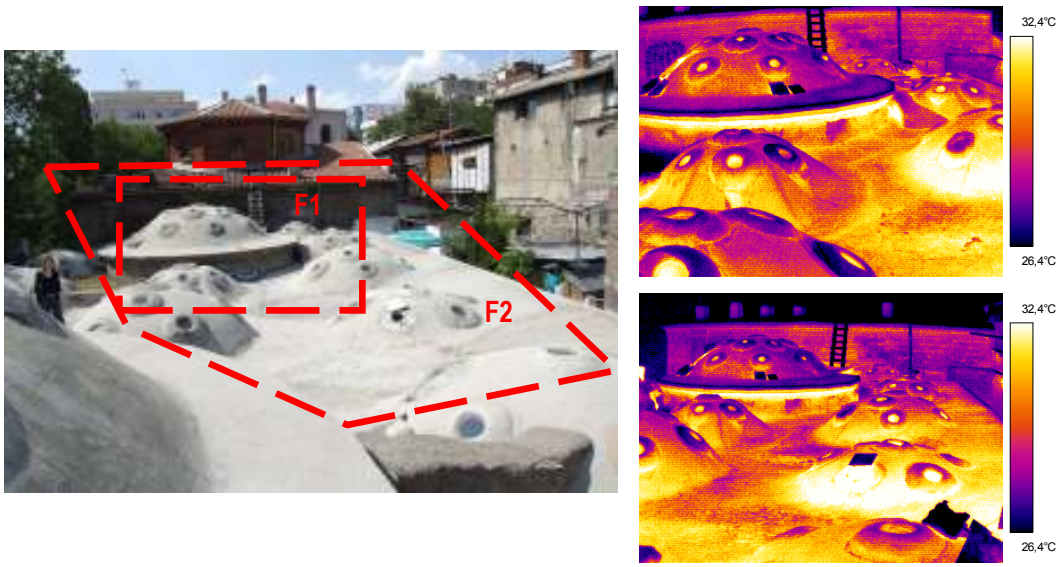

Figure 4.8 The IR images of the selected regions; F1 (at top) and F2 (at bottom) were taken at night in July at the boundary conditions of 26°C and 30% RH while the interiors' conditions being around 38°C and 95%RH. The concrete-clad roof surfaces were warmer than the outside air temperature; the circular dome lights seemed to be the hottest areas indicating heat loss/air leakage from these regions while cement mortar peripheries encircling these dome lights being colder surfaces.

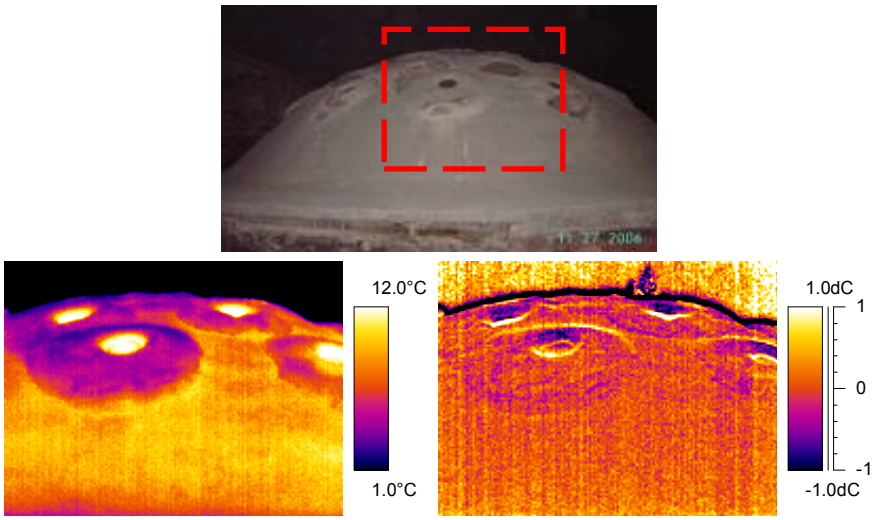

Figure 4.9 The IR image taken from the north side of the dome of the women's hot space at outdoor ambient air conditions of 10.7°C and 40%RH in November; and its differential IR image (at bottom right), that is the temperature difference between the last and first IR images in the sequence, showing the heat loss from the concrete-clad dome surfaces with ΔT=+0.2°C in 322s during the cooling period at night.

For the exterior walls, the warmer surfaces seemed to correspond to the severely-deteriorated areas due to the dampness and soluble salt problems introduced to the structure by incompatible repairs done with cement-based materials. The surface temperatures of the walls were found to be warmer than the ambient temperature of 2.8°C in February, with a temperature difference of 6.5°C on the west wall of the men's undressing room (Figure 4.10) and 12.5°C on the west wall of men's hot space on the axis of chimney (Figures 4.11). Furthermore, heat loss appeared to be higher at the lower parts of the structure where the hot subterranean path was located.

Figure 4.10 A partial view from the west wall of the men's undressing room and its IR image showing that surface temperatures of the wall were warmer than the ambient temperature of 2.8°C in February, at night, with a temperature difference of 6.5°C.

Figure 4.11 A partial view from the west wall of men's hot space on the axis of chimney and its IR image showing that surface temperatures of the wall were warmer than the ambient temperature of 2.8°C in February, at night, with a temperature difference of 12.5°C.

In addition, a significant heat loss was observed at the circular dome lights and lower parts of chimneys (Figures 4.12 and 4.13). An increase in temperature at the bottom edge of the chimney stack was determined in the differential IR images, reaching to 6.3^{o}C in 420s during cooling period of night. This may be due to their improper detailing causing thermal bridges at the connection of chimney stack with the roof cladding layers. The other significant zone of heat loss was determined at the edges of circular dome lights with a temperature increase in differential IR images reaching to 3.2^{o}C in 420s (Figures 4.13). Some cracks were observed both on the concrete layer above the roof and cement-based mortars surrounding the dome lights. Most surfaces of cement-based mortars were colder areas, quite below the outside air temperature (Figures 4.8, 4.9, 4.12, 4.13). These colder surfaces should suffer from dampness and salt weathering problems due to the condensation of hot and wet air leaking from the edges of dome lights (Figures 4.8 and 4.13). All these indications

demonstrate that the use of cement mortar, reducing the vapor transmission through the structure creates the main problems due to the interstitial localized condensation.

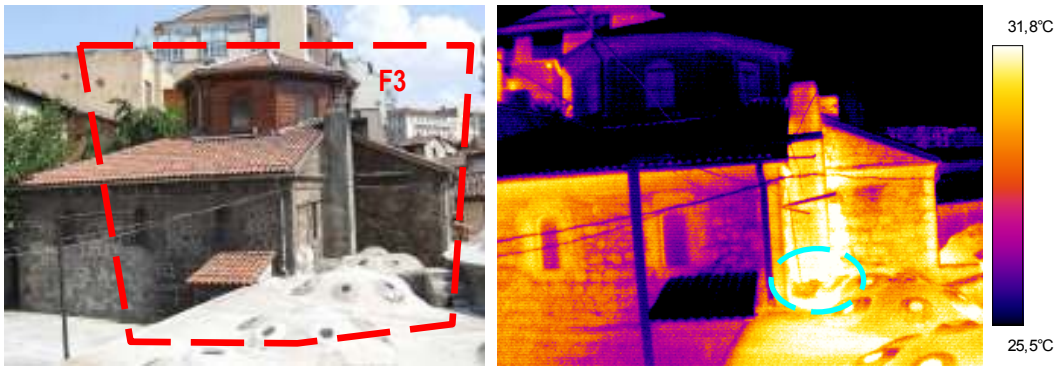

Figure 4.12 A partial view from the north side of the women's undressing room and its IR image taken at the boundary conditions of 26°C and 30% RH at night in July, showing significant heat loss at the lower parts of the chimney and circular dome-lights.

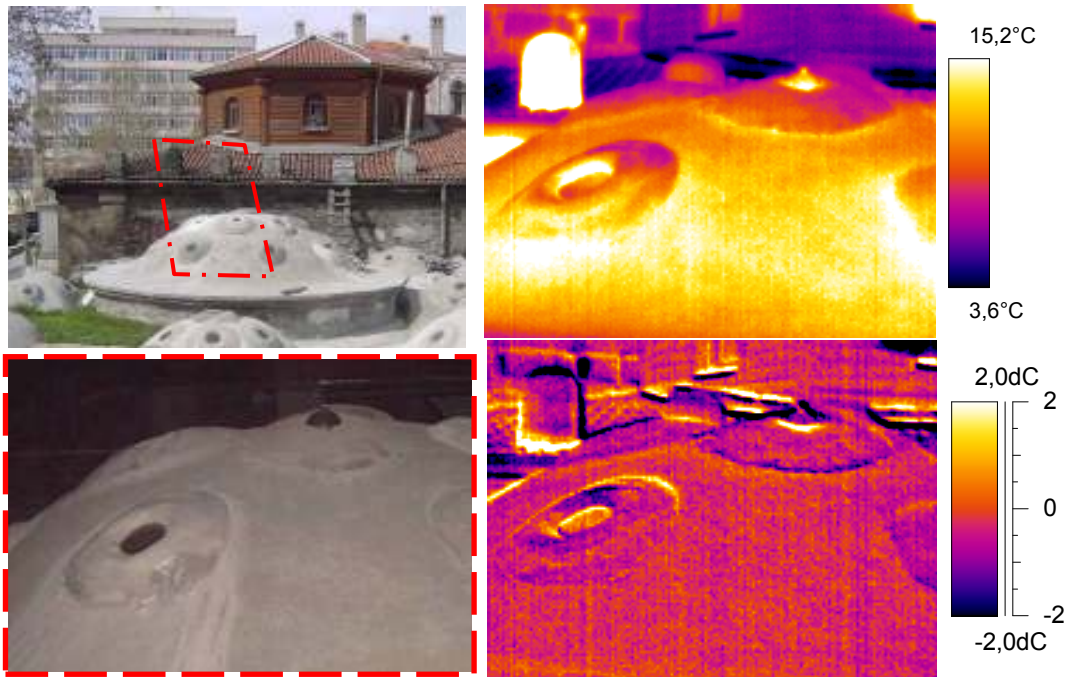

Figure 4.13 The IR and differential IR images taken from the dome of the men's hot space at the boundary conditions of 12.7°C and 40%RH in November, showing the significant heat loss at the circular dome-lights and at the bottom edge of the chimney stack, reaching ΔT = 3.2°C and ΔT = 6.3°C in 420s, respectively, during the cooling period of night in November. The dampness and salt weathering problems were also visible at the immediate periphery of circular dome lights due to the condensation of the hot and wet air leaking from the tiny cracks on cement-based mortars.

4.4 Heat Transfer Analyses

In this part, the results of *"Total thermal resistance and transmittance values of the dome section*" and "*Heat transfer analyses through the dome section*" were given under respective headings.

4.4.1 Total thermal resistance and transmittance values of the dome section

The total thermal resistance of the dome section, R_D, considering the thermal resistance of each layer and of the adjacent air layers was calculated to be 1.20$m^2K\ W^{-1}$. The R_T value of roof section, R_R, including the 30 cm-thick earth cover was calculated to be 1.78$m^2K\ W^{-1}$. The weighted mean of the R_T value for the overall roof surfaces was determined as 1.54$m^2K\ W^{-1}$. On the other hand, the R_T value of the *AS-IS* dome/roof section, $R_{AS\text{-}IS}$, was determined to be 1.10$m^2\ K\ W^{-1}$, which was quite lower than the mean $R_{ORIGINAL}$ value estimated as 1.54$m^2K\ W^{-1}$ calculated for the *ORIGINAL* dome/roof section. The thermal resistance values, *R*, of all layers forming the *ORIGINAL* and *AS-IS* roof/dome sections of Şengül Hamamı were given in Table 4.2.

The thermal transmittance through the dome section, U_D, considering the thermal resistance of each layer and of the adjacent air layers was calculated to be 0.83$W\ m^{-2}K^{-1}$. The *U* value of roof section, U_R, including the 30 cm-thick earth cover was calculated to be 0.56$W\ m^{-2}K^{-1}$. For the overall roof surfaces, the weighted mean of the *U* value was determined as 0.67$W\ m^{-2}K^{-1}$. The *U* value of the *AS-IS* dome/roof section, $U_{AS\text{-}IS}$, was determined to be 0.91$W\ m^{-2}K^{-1}$, which was quite higher than the mean $U_{ORIGINAL}$ value estimated as 0.56 $W\ m^{-2}K^{-1}$ calculated for the *ORIGINAL* dome/roof sections.

Temperature gradients through the layers forming the domes of the women's hot space were calculated according to the thermal conductivity values and thicknesses of each layer for the *AS-IS case* and the *ORIGINAL case* with and without the earth cover. The calculations were done for the steady-state conditions considering the dry state of materials. The curves showing the temperature gradients, given in Figure 4.14, were drawn for the months of January and August, when the temperature difference between the indoor and outdoor

climate was the most and the least in a year, respectively. In January and August, the mean values of interior temperatures for the women's hot space were measured to be 34.5°C and 37.4°C, respectively, with mean exterior temperatures of 1.5°C and 27.8°C, respectively.

This curves show that in the *AS-IS case*, the main insulation layer in the dome/roof section was the historic brick dome masonry (HBDM) composed of historic brick and its mortar. Similarly in the *ORIGINAL case*, in the dome section where there is no earth layer covering the exterior surfaces, HBDM is the major layer of insulation with an *R* value of 0.87$m^2K\ W^{-1}$. The contribution of earth cover to the thermal resistance of the *ORIGINAL* roof structure was significant as proved by the thermal gradients through the historic dome section by heat transfer calculations. The removal of this earth cover and the addition of concrete and cement-based layers, having considerably-higher thermal conductance values than the historic exterior and interior plasters, accelerated the heat flow through the dome section. A fairly constant mean heat flux (U x ΔT) across the dome of the women's hot space were estimated as 0.91 x 33 = 30W m^{-2} in January and as 0.91 x 9.6 = 8.7W m^{-2} in August.

Table 4.2 The thermal resistance values, *R*, of all layers forming the *ORIGINAL* and *AS-IS* roof/dome sections of Şengül Hamamı.

Layers of *ORIGINAL* roof/dome section	***l*, m**	***k*, W $m^{-1}K^{-1}$**	***R*, $m^2K\ W^{-1}$**
R_{se}			0.070
Earth Cover	0.300	0.52[(i)]	0.577
HEP-L1	0.013	0.91	0.014
HEP-L2	0.016	0.81	0.020
HEP-L3	0.034	0.64	0.053
HBDM	0.500	0.58	0.870
HIP-L1	0.015	0.37	0.041
HIP-L2	0.017	0.65	0.026
R_{si}			0.106

Layers of *AS-IS* roof/dome section	***l*, m**	***k*, W $m^{-1}K^{-1}$**	***R*, $m^2K\ W^{-1}$**
R_{se}			0.070
MRC	0.080	2.10[(ii)]	0.038
HBDM	0.500	0.58	0.870
CBUC	0.015	1.40[(iii)]	0.011
CBFC	0.010	1.40[(iii)]	0.007
R_{si}			0.106

NOTE 1-The *k* values of some layers were taken from the literature: [(i)]Strother and Turner, 1990; [(ii)] TS 825, 1998; and [(iii)]Örs, 2006.

NOTE 2-The thermal resistance values of interior and exterior surfaces, R_{si} and R_{se}, were obtained from the literature as 0.106 for interior roof surfaces with high emissivity where the heat flow is upwards and as 0.07 for exterior roof surfaces with high emissivity where the stated exposure is sheltered, respectively (Hall, v.1, 1994).

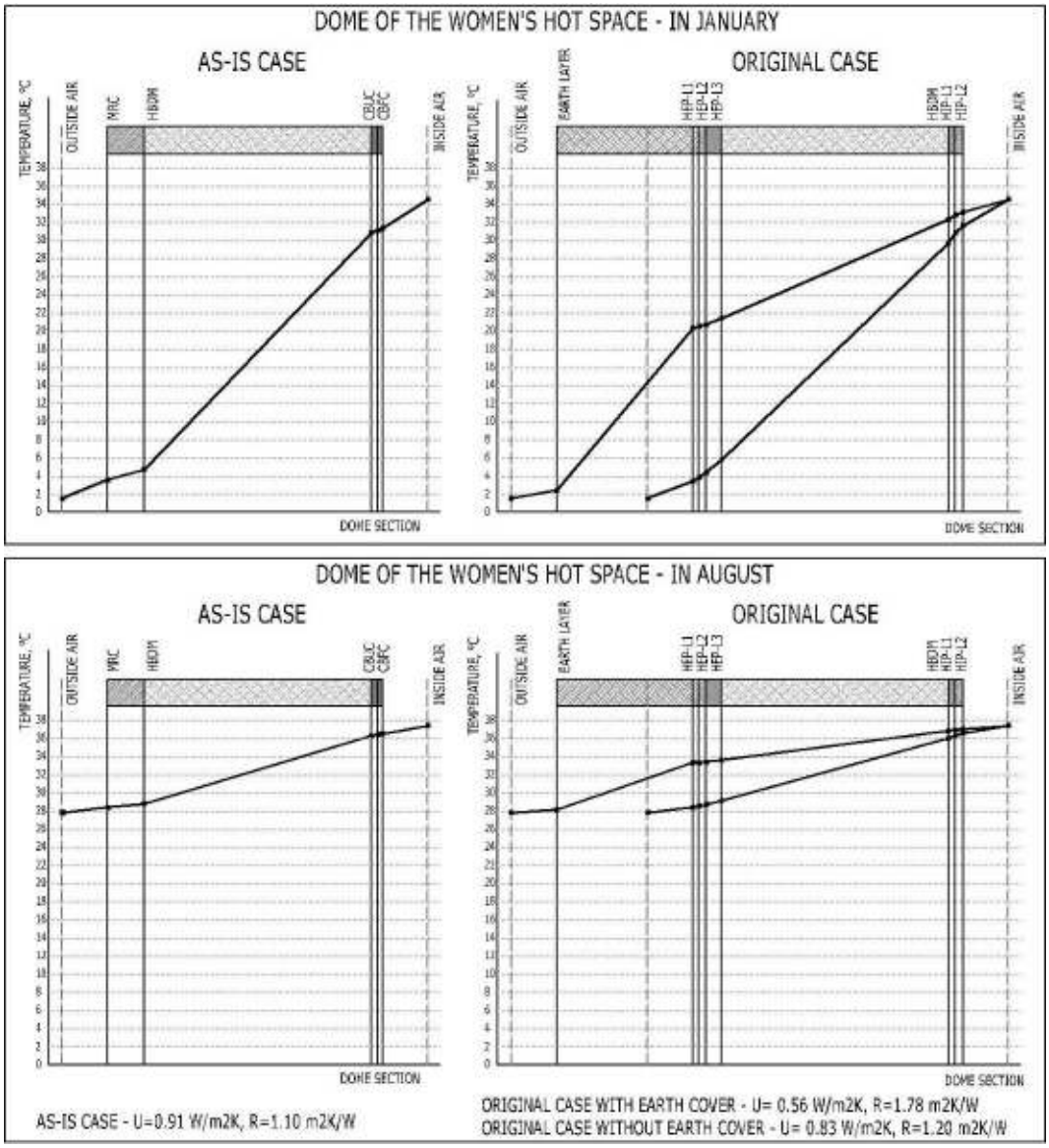

Figure 4.14 The curves showing the temperature gradients through layers forming the domes of the women's hot space in January (at top) and in August (at bottom), calculated according to the thermal conductivity values and thicknesses of each layer at the steady state conditions for the *AS-IS case* (at left); and *ORIGINAL case* (at right) with and without earth cover.

4.4.2 Heat transfer analyses through the dome section

The reasons of thermal failures were investigated by joint analysis of heat transfer calculations and IR sequences. Here, the real thermal conditions of surfaces and the neighboring air inside and outside were compared with the thermal gradients produced by heat transfer calculations.

The IR images taken from the interior and exterior surface of the domes of women's warm and hot spaces were shown in Figures 4.15 and 4.16, respectively. The thermal models of dome sections produced from these IR images were given in Figure 4.17, representing the real interior and exterior surface temperatures of the dome sections and real heat flow between inside and outside. The heat flow curves presenting the temperature gradients through the dome sections calculated for steady state conditions were presented in Figure 4.18. In addition, the graphs showing the real surface temperatures of some exterior and interior regions of the dome surfaces were produced from the thermal models and presented in Figures 4.19 and 4.20, respectively for a cooling period of 300s in February.

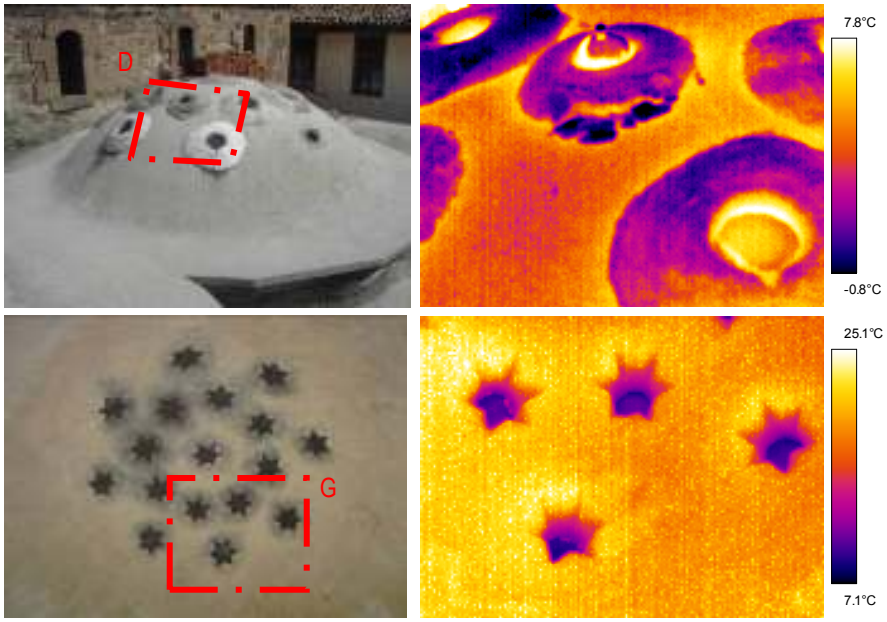

Figure 4.15 Visible light photographs taken from the dome of women's warm space and the IR images of selected regions: the exterior views (at top) and the interior views (at bottom). Here, the temperature scales are in the range of -0.8 ºC - +7.8ºC and +7.1 ºC - +25.1 ºC.

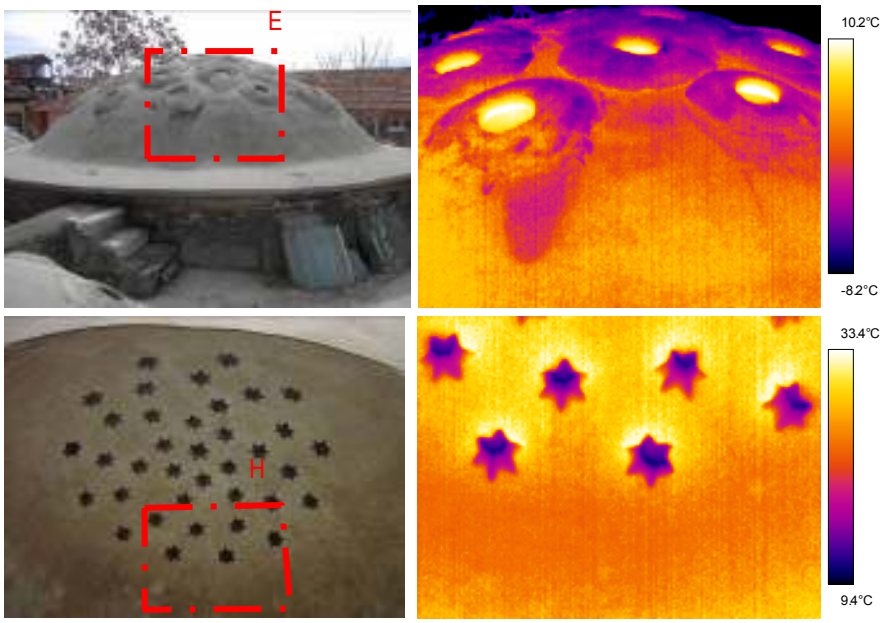

Figure 4.16 Visible light photographs taken from the dome of the women's hot space and the IR images of selected regions: the exterior views (at top) and the interior views (at bottom). Here, the temperature scales are in the range of -8.2ºC - +10.2ºC and +9.4 ºC - +33.4ºC.

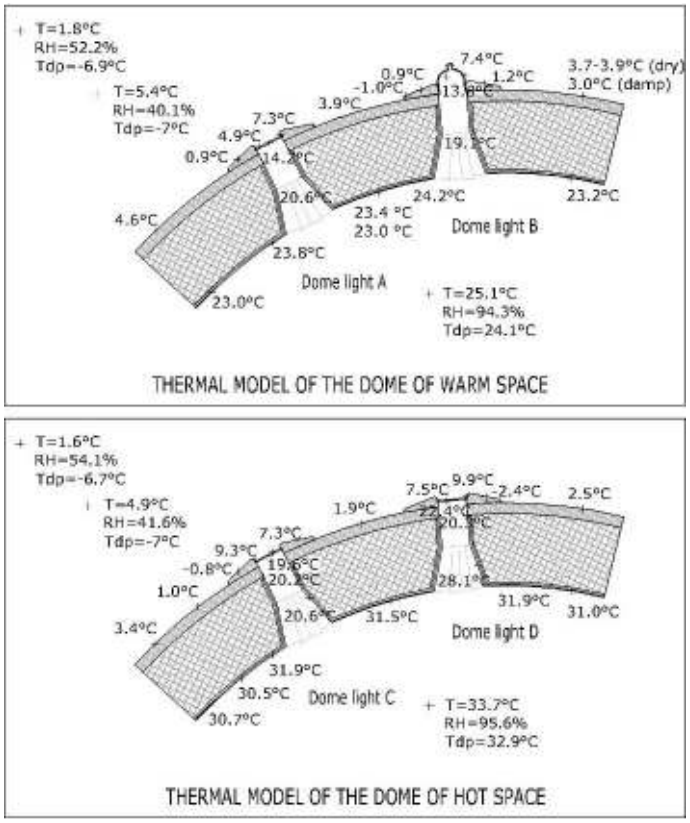

Figure 4.17 The thermal models of the domes of women's warm (at top) and hot (at bottom) spaces representing the real interior and exterior surface temperatures of dome sections.

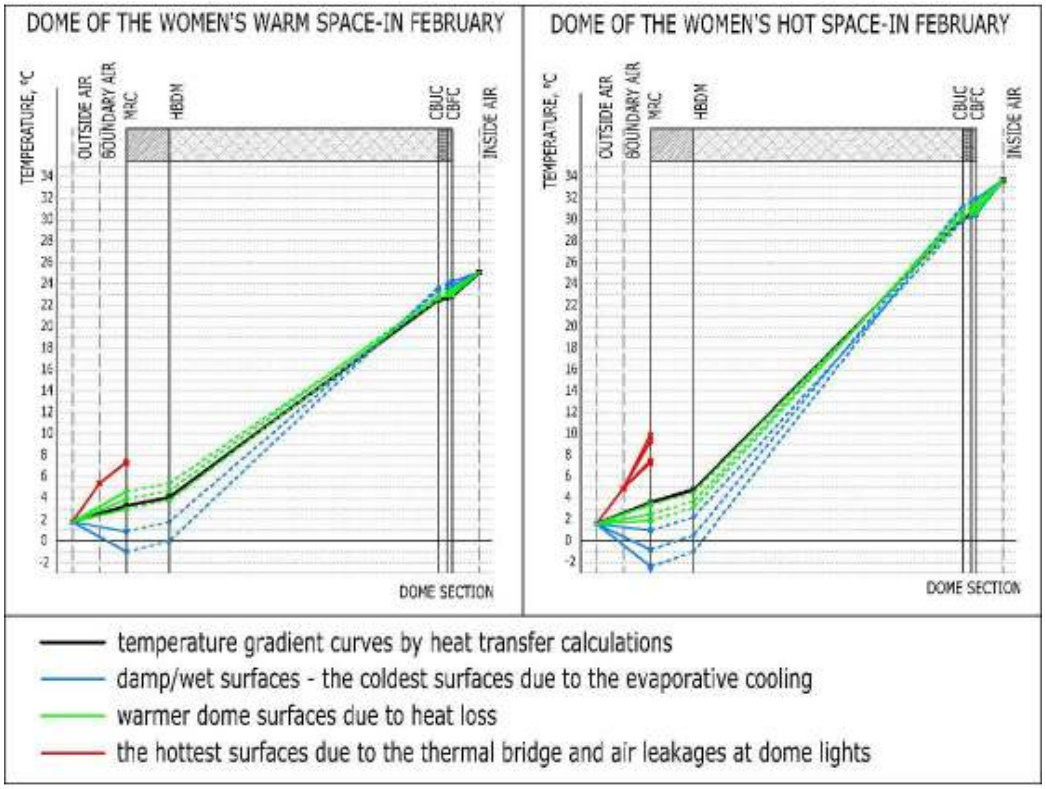

Figure 4.18 Sections through the domes of the women's warm (at left) and hot (at right) spaces, showing temperature gradients through each component calculated according to the thermal conductance and thickness of each layer (lines in black); and heat flow curves produced according to the real surface temperatures measured at inside and outside surfaces of the dome structures.

The reference heat flow curves and real thermal situations, shown in Figure 4.18 were found to be different. The interior and exterior surface resistances, R_{si} and R_{se}, seemed to be lower than the expected situation according to the reference heat flow curves. This may be due to the high humidity conditions.

At the dome of hot space, the warmer exterior surfaces being below the reference outside surface temperature were interpreted as damp surfaces and evaporation reduced its temperature (Figure 4.18). Also, evaporation from these surfaces seemed to increase the humidity in the boundary air. However, at the dome of warm space, the warmer surfaces being above the reference outside surface temperature indicated the heat loss due to the lower overall thermal resistance of the dome section when compared to the reference temperature gradient curves (Figure 4.18). This should be due to the interstitial condensation in the deeper zones of the dome section causing thermal bridges.

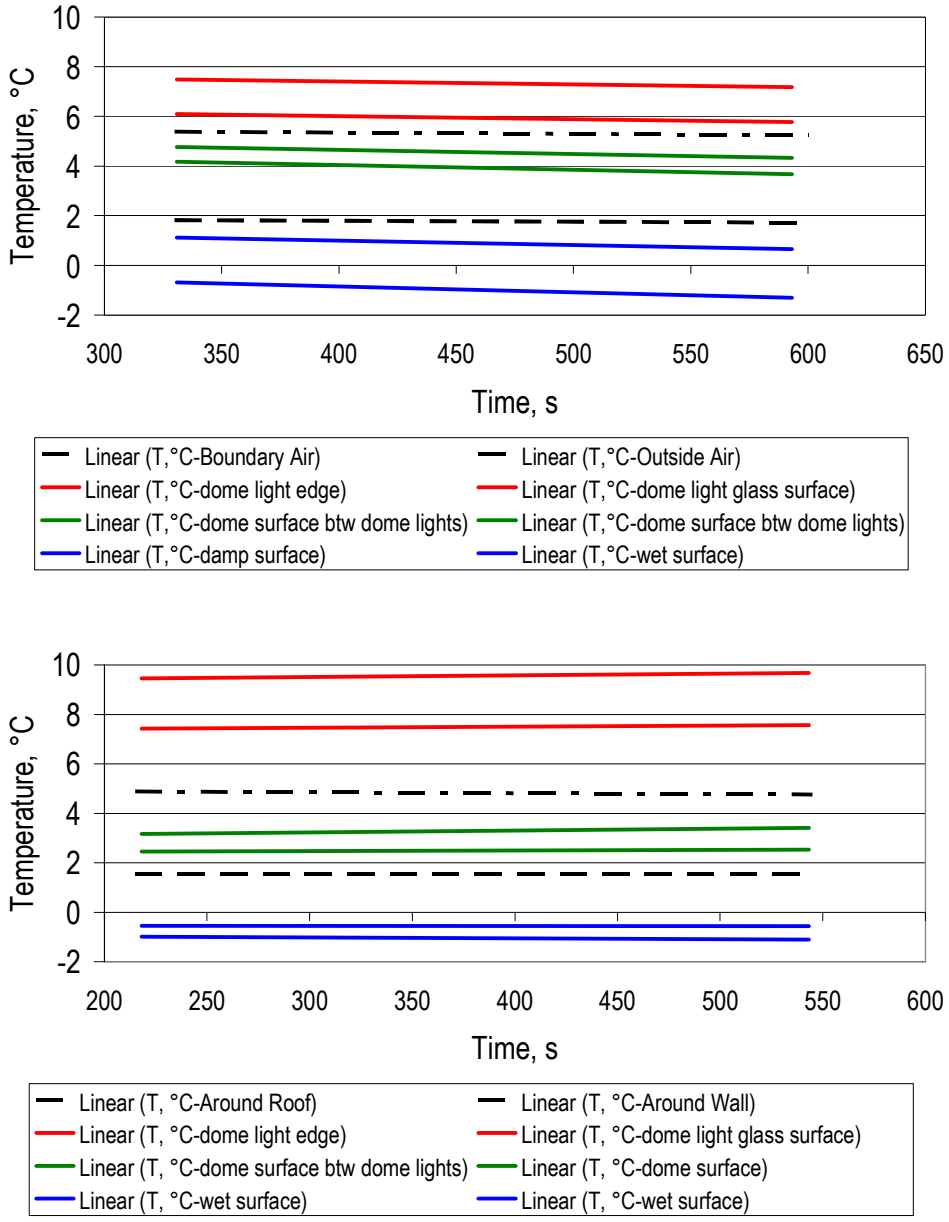

Figure 4.19 Real surface temperatures of some regions selected from the exterior dome surfaces of the women's warm (at top) and hot (at bottom) spaces, taken during the cooling period of night for 300s in February, showing their relationship with the outside air and warm boundary air temperatures.

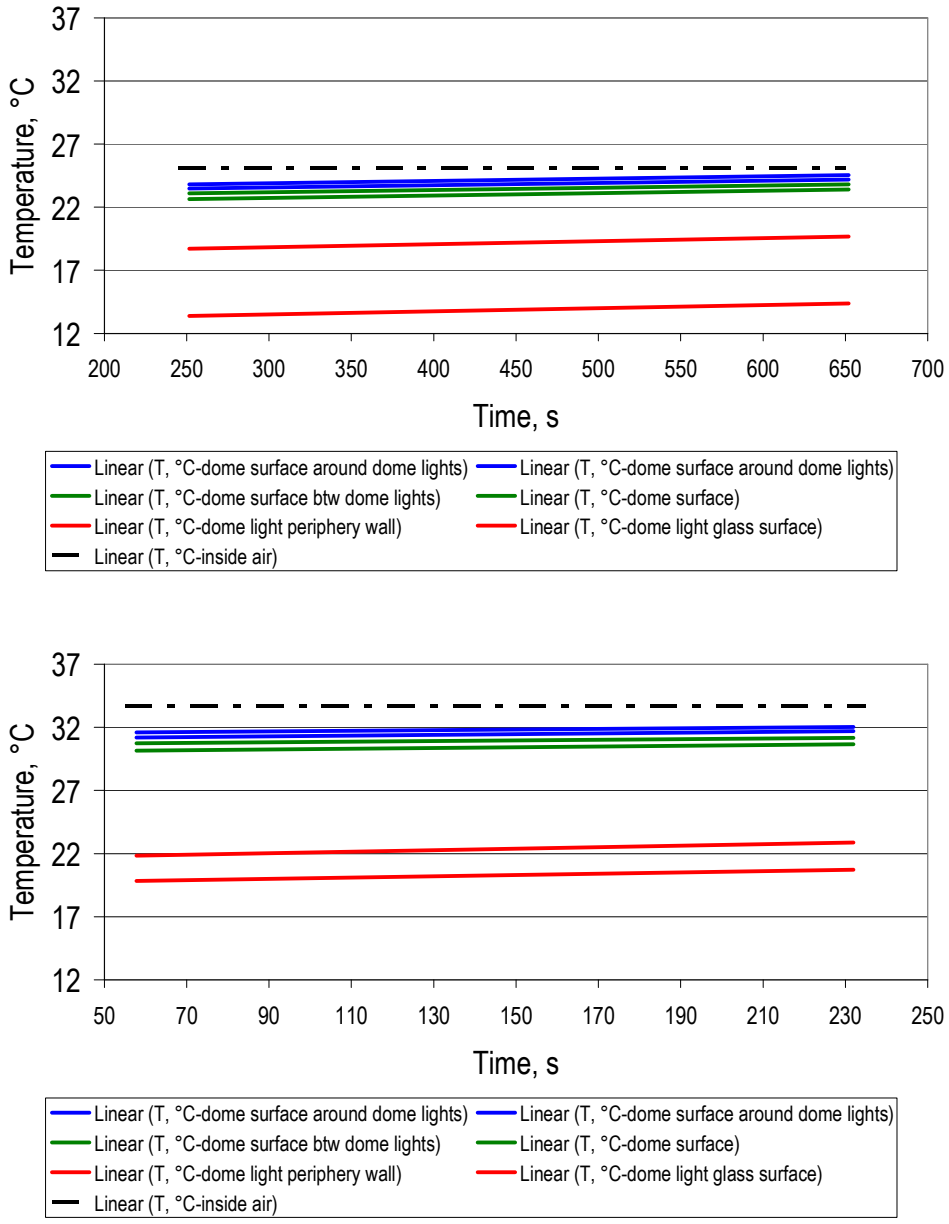

Figure 4.20 Real surface temperatures of some regions selected from the interior dome surfaces of women's warm (at top) and hot (at bottom) spaces, taken during the constant interior ambient temperatures during the cooling period of night for 300 s in February.

The dome light surfaces acting like thermal bridges as well as the air leakages from their edges were found to be the main sources of heat loss increasing the temperature of boundary air close to the dome surfaces (follow the curves in Figures 4.18 and the red lines in figures 4.19). For instance, at the edges of dome lights of the hot space, surface temperatures were determined to reach to 10.4°C, being highly above the outside air temperature of 1.6°C and boundary air temperature of 4.9°C (Figure 4.17). Moreover, warm concrete-clad dome surfaces having temperatures above reference outside surface temperature seemed to contribute to warming up the boundary air (follow the green lines in Figures 4.18 and 19).

The coldest exterior surfaces having temperatures below the outside air temperature corresponded to the wet/damp surfaces (see the top views at Figures 4.15 and 4.16; follow the blue lines in Figure 4.18). This was due to the evaporative cooling of exposed surfaces. Those wet/damp surfaces mostly seen on cement-based mortars surrounding the dome lights. The main source of moisture was the condensed water on the interior surfaces of all dome lights, which were the coldest surfaces at interior (follow the red lines in Figure 4.20). This moisture seemed to leak to the outside dome surfaces following slope and to the deeper layers of concrete layer by means of capillary cracks. The cracks on the concrete layer and cement-based mortar were observed visually as well, causing entrapped moisture in the dome section. The monitoring of the same problem areas by IR images in July (Figure 4.8) and November (Figure 4.9) showed that the condensation problem on the cement-based mortars surrounding dome lights was continuous throughout a year.

The overlapped IR images taken from the interior and exterior surfaces of the same region at the same time showed that the coldest wet areas on the exterior surfaces corresponded to the hottest interior surfaces (follow blue lines in Figure 18). During the cooling period of 300s at the outside in February and during the constant boundary conditions at the inside, the wet exterior surfaces was observed to slightly-cool down while the hottest interior surfaces slightly-warming up (follow the blue lines in Figures 4.19 and 4.20). Evaporative cooling on the exterior wet surfaces seemed to accelerate the heat flow/transfer from the dome section. Therefore, the heat loss is more severe at the sections having wet exterior surfaces.

4.5 Water Vapor Transfer Analyses

In this part of the study the results of *"Continuity of water vapour permeability through the dome section"* and *"Partial vapour pressure distribution through the dome section*" were given under respective headings.

4.5.1 Continuity of water vapour permeability through the dome section

The equivalent air layer thickness of water vapour diffusion values, S_D, for layers forming the dome sections of Şengül Hamamı in the *ORIGINAL* and *AS-IS* cases were calculated by using their water vapour diffusion resistance values, μ, and real thicknesses and given in Table 4.3 and Figure 4.21. The μ values of historic and cement-based repair materials forming the layers of *ORIGINAL* and *AS-IS* dome sections were obtained from the literature (Caner-Saltik *et al.*, 2003a; Caner-Saltik *et al*., 2005b; Esen *et al*., 2004; TS 825, 1998 and Örs, 2006) as summarized in Table 2.6 and 2.7.

The S_D values of historic materials were found to be in the range of 0.06m and 1.39m, with μ values in the range of 2.3 and 10.3 (Table 4.3 and Figure 4.21). These layers were observed to be either high or medium vapour permeable according to their S_D values (TS prEN ISO 7783-2, 1999). The S_D values of HB and HBM layers were determined to be 1.39m and 1.15m, respectively, which were in the range of 0.14m and 1.4m defined for the medium vapour permeable materials. This was due to their thick application of 0.5m in the dome section. The historic exterior plaster layers, HEP-L1, HEP-L2 and HEP-L3 were found to have S_D values of 0.01m, 0.13m and 0.28m, respectively. Although μ values of these roof covering plaster layers were high, being in the range of 8.0-8.3, they were found to be high water vapour permeable according to their S_D values, which was provided by their application in thin layers. In addition, the historic interior layers, HIP-L1, was high vapour permeable with an S_D of 0.06m, whereas HIP-L2, having an S_D value of 0.17m, was a medium vapour permeable layer due to its high μ value.

The μ and S_D values of historic materials obtained from the literature or via calculations were presented in Figure 4.21 together with the μ and S_D values of cement-based repair materials

used in the *AS-IS* case of Şengül Hamamı, such as mesh-reinforced concrete and cement based plaster layers. The S_D values of these materials were found to be in the range of 0.22m and 12.00m, with μ values in the range of 21.5 and 150. The S_D value of 8cm thick mesh-reinforced concrete layer (MRC) covering the roof surfaces was calculated to be 12m, showing that it is a low vapour permeable layer. The cement based under coat (CBUC) and cement based finish coat (CBFC) layers were found to be medium vapour permeable with S_D values of 0.41m and 0.22m, respectively. The historic roof covering plaster layers were seemed to be more water vapour permeable than the mesh-reinforced concrete layer, which have the highest S_D value of 12m. In the same way, the historic interior plaster layers were found to be more water vapour permeable than the cement-based plaster layers, which have higher μ and S_D values than those of historic plasters.

Continuity of the water vapour transmission along the layers of the *ORIGINAL* and *AS-IS* dome sections were examined by comparing their total S_D values (Figure 4.22). These figures were produced by adding up the S_D values of each layer as a function of layer thickness and the slope of the line gave the μ value of each layer. The higher slope indicated higher μ value, in other words higher resistance to water vapour permeation. The interruption of continuity in water vapour permeability with a considerable increase in the slope of the line was mainly observed at the layers of mesh-reinforced masonry and cement-based plasters, MRC, CBUC and CBFC, where water vapour flow was disrupted by these medium and low permeable layers.

A considerable difference was determined between the total S_D values of the *ORIGINAL* and *AS-IS* dome sections. The total S_D value of the dome section in the *ORIGINAL case* was calculated to be 2.01m. On the other hand, total S_D values of the *AS-IS* dome/roof section was calculated to be 13.90m, which was quite higher than that of the original one. The breathing capability of the historic dome section was found to be about 7 times more than that of the *AS-IS* dome section. The continuity of the water vapour transmission through the dome section was completely destroyed by the vapour impermeable concrete layer (MRC) and cement-based plaster layers (CBUC and CBFC).

Table 4.3 The equivalent air layer thickness of water vapour diffusion values, S_D, for layers forming the dome sections of Şengül Hamamı in the *ORIGINAL* and *AS-IS* cases calculated with their resistance to water vapour permeation values, μ, and real thicknesses.

Layers of *ORIGINAL* roof/dome section	***l*, m**	**μ**	**S_D, m**
HEP-L1	0.013	8.0[(i)]	0.10
HEP-L2	0.016	8.3[(i)]	0.13
HEP-L3	0.034	8.2[(i)]	0.28
HB	0.500	2.8[(ii)]	1.39
HBM	0.500	2.3[(iii)]	1.15
HIP-L1	0.015	3.9[(iv)]	0.06
HIP-L2	0.017	10.3[(iv)]	0.17

Layers of *AS-IS* roof/dome section	***l*, m**	**μ**	**S_D, m**
MRC	0.080	150.0[(v)]	12.00
HB	0.500	2.8[(ii)]	1.39
HBM	0.500	2.3[(iii)]	1.15
CBUC	0.015	27.6[(vi)]	0.41
CBFC	0.010	21.5[(vi)]	0.22

NOTE.-The μ values of some samples were taken from the literature: [(i)]Caner-Saltik *et al.*, 2003a; [(ii)]Caner-Saltik *et al.*, 2003a and 2005b; [(iii)]Esen *et al.*, 2004; [(iii)]Caner-Saltik *et al.*, 2005b; [(v)]TS 825, 1998 and [(vi)]Örs, 2006.

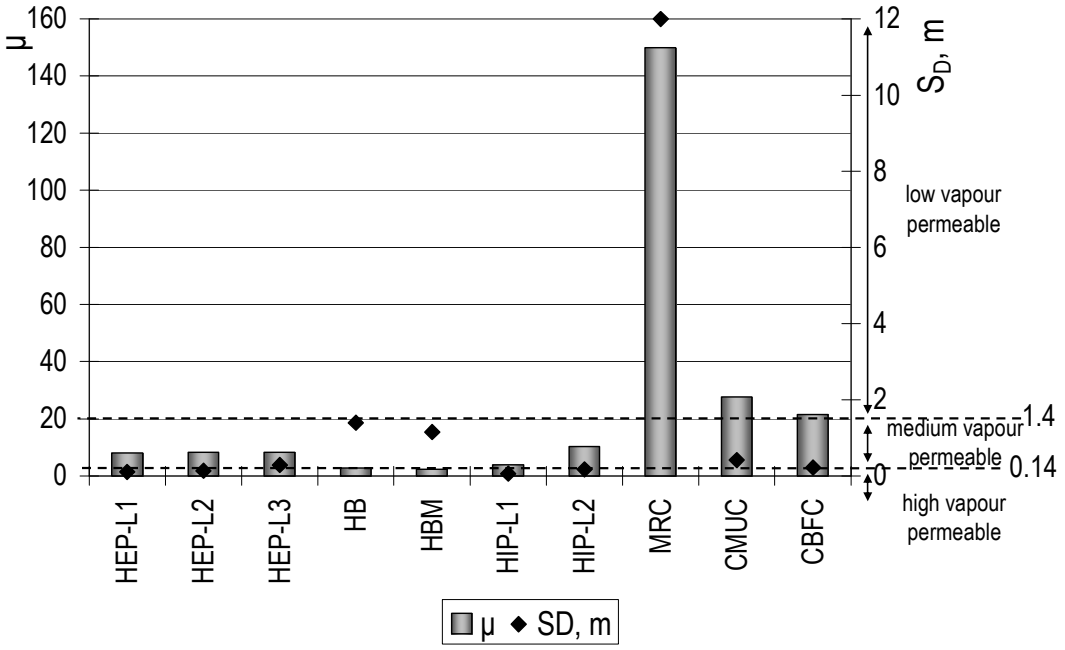

Figure 4.21 μ values of historic and cement-based repair materials with their S_D values calculated by their layer thickness, showing that the mesh-reinforced concrete layer had the highest μ value and the cement-based plaster layers had higher μ values than those of historic brick, brick mortar and plasters. *The μ values were obtained from the literature (Caner-Saltik et al., 2003a; Caner-Saltik et al., 2005b; Esen et al., 2004; TS 825, 1998 and Örs, 2006).*

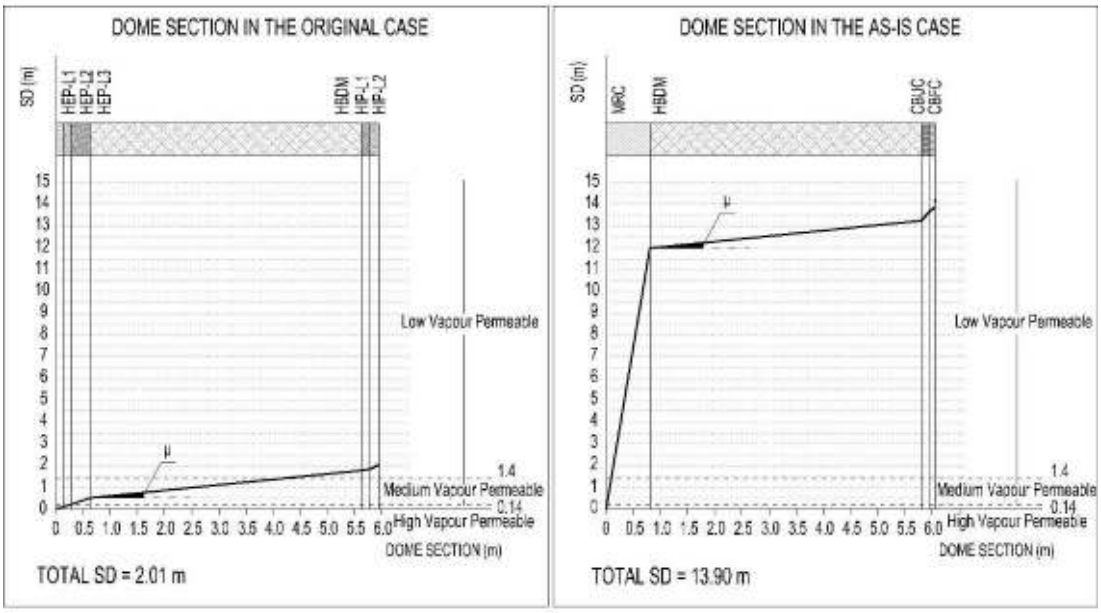

Figure4.22 Total S_D values of the dome sections of Şengül Hamamı in the *ORIGINAL* (at left) and *AS-IS* (at right) cases.

4.5.2 Partial vapour pressure distribution through the dome section

The water vapour pressure calculations were done for the historic/*ORIGINAL* and *AS-IS* cases of the dome structure covering the interiors of women's hot space. The partial vapour pressure distribution analyses of the dome sections of both cases were done for all months to observe the risk of condensation in the dome section during a year. Figures were produced by using the monthly-mean temperature and relative humidity values, together with the extreme cases with values above and below these monthly-means and given in Appendix D. The thermal conductivity values of each layer, which were calculated during the laboratory analyses or taken directly from literature, were taken into account for the determination of temperature differences between the layers. In these figures, the distribution of partial water vapour pressures from interior (*pi*) to exterior (*pe*) and equilibrium water vapour pressure (*ps*) were shown in figures of water vapour pressure (Pa) as a function of S_D (m).

In the *AS-IS* case, the partial pressures of the dome were found to be higher than the equilibrium vapour pressures along the dome section, showing that it was either partially or completely damp during the whole year. The dome section was determined to be under the risk of interstitial condensation all through the year. On the other hand, in the *ORIGINAL*

case condensation risk was observed in the dome section for 7 months, for the months of January, February, March, April, October, November and December. In these months, the partial pressures of the dome were found to be higher than the equilibrium vapour pressures. The historic dome section was found to be dry in the remained months of May, June, July, August and September, when the partial pressures of the dome were found to be lower than the equilibrium vapour pressures along the dome sections. In these months, there was no risk of condensation in the dome section (Appendix D).

January and August were decisive months for the analyses of partial water vapour pressure distribution in the dome section, as the temperature difference between the interiors of women's hot space and exterior were calculated to be the highest and lowest in these months being 33.0°C and 9.6°C, respectively. Figure 4.23 was drawn for the monthly-mean temperature and relative humidity values of January, which were 1.5°C and 76.3% RH at the exterior and 34.5°C and 95.3% RH at the interior. In the same way, Figure 4.24 was drawn for the same values measured in August, which were 27.8°C and 30.5% RH at the exterior and 37.4°C and 94.1% RH at the interior.

In January, the partial pressures of both historic/*ORIGINAL* and *AS-IS* dome sections were found to be higher than the equilibrium vapour pressures along the dome sections. While in the boundary conditions of January the dome section was seemed to be totally under the risk of interstitial condensation in the *ORIGINAL* case, it was seemed to be extremely wet in the *AS-IS* case. On the other hand, in August the partial pressures of historic/*ORIGINAL* dome section were found to be lower than the equilibrium vapour pressures along the dome section, indicating no risk of interstitial condensation. While in August the dome section was determined to be dry in the *ORIGINAL* case, it was found to be partially under risk of interstitial condensation in the *AS-IS* case. In this case the historic masonry was found to be extremely wet while the concrete cover was partially-wet. Moreover, the exterior surface of concrete cover was seemed to dry while concealing the extreme wetness at the backing masonry.

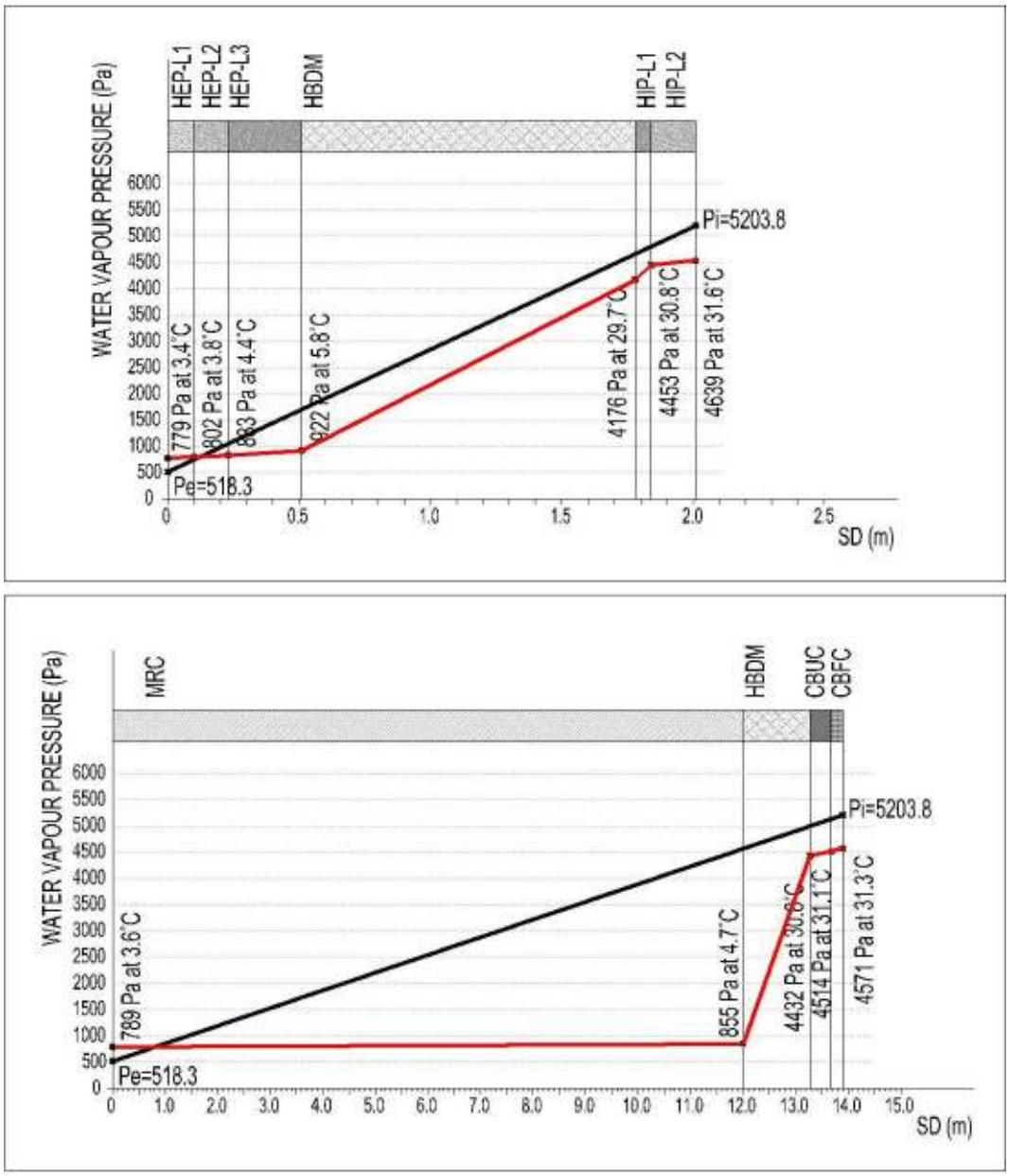

Figure 4.23 Partial (*pi* and *pe*) and equilibrium (*ps*) water vapour pressure distributions of the dome sections of Şengül Hamamı for the *ORIGINAL* (at top) and *AS-IS* (at bottom) cases; according to the mean values of January – exterior conditions of 1.5°C and 76.3% RH and interior conditions of 34.5°C and 95.3% RH; showing that in both cases the dome section was totally under the risk of interstitial condensation, being extremely wet in the *AS-IS* case.

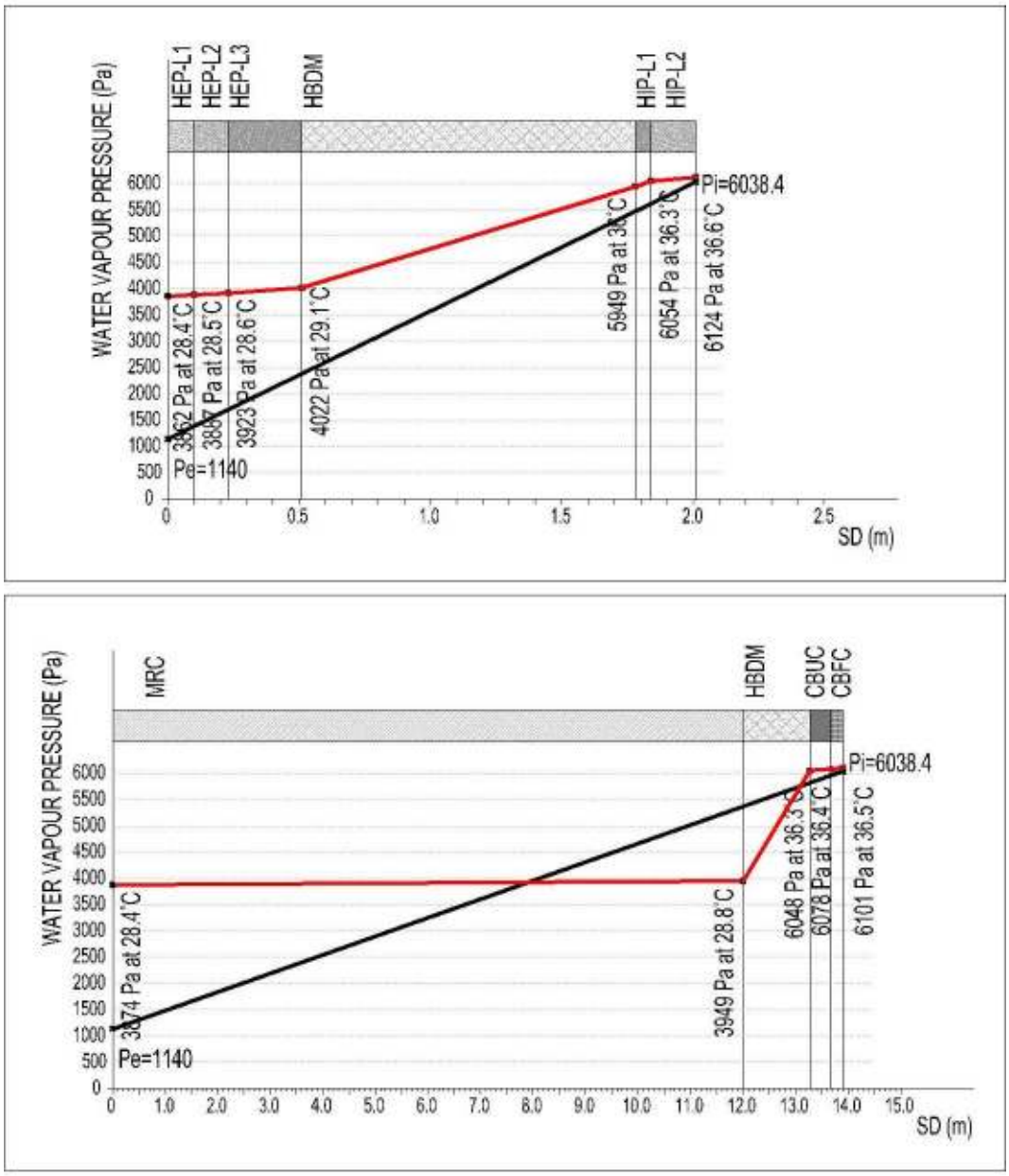

Figure 4.24 Partial (*pi* and *pe*) and equilibrium (*ps*) water vapour pressure distributions of the dome sections of Şengül Hamamı for the *ORIGINAL* (at top) and *AS-IS* (at bottom) cases; according to the mean values of August – exterior conditions of 27.8°C and 30.5% RH and interior conditions of 37.4°C and 94.1% RH; showing that the dome section was completely dry in the *ORIGINAL* case while it was under the risk of interstitial condensation in the *AS-IS* case.

CHAPTER 5

DISCUSSION AND CONCLUSIONS

In this chapter the results are interpreted in terms of thermal properties of historic materials, microclimatic characteristics of the historic bath structure, its original thermal performance and thermal failures due to the improper recent repairs. The evaluation of the investigation methods, particularly the joint use of quantitative IR thermography and heat transfer calculations at steady state conditions, was done for the purpose of thermal failure assessment of the real situation. At the end are given the conclusions followed by the suggestions for further studies.

5.1 Thermal Properties of Historic Materials Used in Historical Turkish Baths

In this section, some thermo-physical properties of historic materials are discussed with an emphasis on their bulk density (ρ), porosity ($\varnothing$) and thermal conductivity (k) properties. In addition, they are compared with other historic and contemporary masonry materials.

The historic dome masonry of the bath seemed to be composed of lightweight and porous materials/layers establishing a homogeneous and lightweight upper structure. The historic dome brick and its mortar seemed to have inherently good thermal insulation properties. Those light and porous materials having similar thermo-physical properties were determined to have low thermal conductivities in the range of 0.50±0.01 $Wm^{-1}K^{-1}$ and 0.67±0.02 $Wm^{-1}K^{-1}$ when compared with concrete and cement-based materials (Figure 4.2). The historic brick and brick mortar were found to have mean k values of 0.56±0.04 $Wm^{-1}K^{-1}$ and 0.59±0.1 $Wm^{-1}K^{-1}$, respectively. These k values were similar to those of other lightweight construction materials, such as tuffs, mud-brick, aerated concrete and porous light brick, all of which contributing to the thermal performance of buildings in terms of energy efficiency with their low thermal conductivity values. For instance the k values for Nevşehir and Cappadocia tuffs were given in the range of 0.28W $m^{-1}K^{-1}$ – 0.73W $m^{-1}K^{-1}$. (Erdoğan, 1986; Erguvanlı and Yüzer, 1977), for the mud-brick being in a wide range of 0.23W $m^{-1}K^{-1}$ and

0.93 W $m^{-1}K^{-1}$ (Houben and Guillaud, 1994), for the aerated concrete being the range of 0.22W $m^{-1}K^{-1}$ and 0.36W $m^{-1}K^{-1}$ (Kurama, Topcu, Karakurt, 2009; TSE 825, 1998); and contemporary hollow and hand-made bricks (having the densities between 1200kg m^{-3} - 1800kg m^{-3}) being in the range of 0.50W $m^{-1}K^{-}$ and 0.81W $m^{-1}K^{-}$ (TSE 825, 1998).

The cement-based repair materials, such as mesh-reinforced concrete layer (MRC) covering the exterior roof surfaces of Şengül Hamamı and the cement based under coat (CBUC) and cement based finish coat (CBFC) layers covering the interior surfaces of bathing spaces, were not compatible with the neighbouring historic materials due to their considerably-high density, low porosity and high thermal conductivity (Figures 4.1 and 4.2). Their thermal conductivity values were given in literature as 2.1 $Wm^{-1}K^{-1}$ for the mesh-reinforced concrete (TS 825, 1998) and 1.4 $Wm^{-1}K^{-1}$ for cement-based plasters (Örs, 2006). The mesh-reinforced concrete cover above the roof surface seemed to be almost four times more thermal conductive than the historic brick and almost 2.5 times more thermal conductive than historic roof covering plasters. The cement-based plaster layers at the interior surfaces of roof were almost three times more thermal conductive than historic interior plasters. Those *k* values of cement-based materials were considerably-high when compared with those of historic materials which definitely introduced moisture and thermal failures to the structure.

The thermal performance of the historic bath structure was closely related with the thermal properties of materials, such as bulk density, thermal conductivity and specific heat values in acceptable ranges providing satisfactory thermal characteristics to the masonry. Both historic masonry and earth cover seemed to have good thermal properties and thermal masses contributing to keep the particular microclimatic conditions of the bath structure stable during the day. The historic upper structure, thus, had proper thermal mass characteristics good enough to store the heat at the interior in its fabric and then to release it back to inside at night while still acting as a good thermal insulator. Here, the earth cover acting as an exterior thermal insulation layer contributed to its thermal performance by minimizing the heat loss from the exposed surfaces of the dome masonry. Therefore, the earth layer of the roof structure was one of the fundamental components keeping the good thermal performance of the historic dome masonry.

The interior and exterior finishing plaster layers also had thermo-physical properties similar to historic masonry materials (Table 4.1, Figures 4.1 and 4.2). The similar thermal

characteristics of those neighbouring layers provided a healthy situation for the upper structure where a uniformity was achieved throughout the roof section in terms of thermo-physical properties and thermal inertia characterictics. That uniformity seemed to be disrupted by the repairs with cement-based materials being denser, less porous, highly thermal conductive and less vapour permeable than the historic roof/dome masonry. The materials failure was inevitable under such unhealthy boundary condition and differential thermal behaviours/movements.

5.2 Microclimatic Characteristics of the Structure

Şengül Hamamı is a unique structure establishing three different microclimates at its interiors by means of a well-functioning heating system in collaboration with its historic fabric providing a good/satisfactory thermal insulation. The undressing room, warm and hot spaces had particular microclimatic characteristics in terms of ambient temperature, relative humidity and monthly temperature fluctuations (Figure 4.3), with the annual mean ambient temperatures of 23.1°C±2.1°C, 28.2°C ±2.0°C and 36.0°C ±1.0°C, respectively. The hot space was found to present the lowest temperature fluctuations during the year followed by the warm space and undressing room. The warm and hot bathing spaces were continuously heated by the traditional heating system of the bath, while the undressing rooms were heated only in winter months by means of a stove. The temperature fluctuation at the undressing room was determined to be the highest since that space was in direct contact with the entrance hall of the women's part.

The monthly means of ambient temperature and relative humidity data have shown that the indoor climate of the hot space of Şengül Hamamı was quite constant for all seasons when compared with the monthly means of the prevailing outside climatic conditions of the region, which exhibited considerable seasonal temperature and RH fluctuations (Figure 4.4). In bath structures, always hot and very humid air during a year is an expected situation. For Şengül Hamamı, the indoor climatic conditions during a year was found to be 36.0°C±1.0°C and 95%±2%RH for the women's hot space and 35.5°C±1.2°C and 100%±0%RH for the men's hot space. These values represent the thermal characteristics of Şengül Hamam's interiors.

On the other hand, the maximum difference in the ambient temperature was observed between the months of August and January. The detailed analysis of the microclimatic data collected at 5 minute intervals during a year allowed us to compare the daily means of ambient temperature for each month (Figure 4.5) and to examine the microclimatic variations in a day (Figure 4.7). The daily means of these months have shown the seasonal temperature fluctuations in the women's and men's hot spaces with the ambient temperature differences of 2.9°C ±0.7°C and +2.7°C ±0.6°C, respectively.

The interiors of the hot bathing spaces of Şengül Hamamı were found to present very low daily temperature fluctuations both in winter and summer. For instance, in January and August the daily ambient temperature fluctuations at women's and men's hot spaces were found to be similar to each other, being in the range of 0.23°C±0.09°C and 0.72°C±0.12°C (Figure 4.7). These small fluctuations in the daily ambient temperature and RH values at the hot spaces of Şengül Hamamı had direct relations with the good thermal insulation properties of the historic materials composing the building envelope. Moreover, in January at the weekends the interiors of women's and men's hot spaces were determined to be hotter than in weekdays with an ambient temperature difference of 0.51°C and 0.94°C, respectively. This was mainly due to the amount of energy introduced to the heating system, the number of functioning draft chimneys and the working hours of the bath.

5.3 Thermal Characteristics of the Historic Structure and Its Comparison with the Present Situation

The evaluation of the thermal characteristics of historic upper structure was done in terms of the total thermal resistance, R_T , and total thermal transmittance, U, values of the roof/dome section. The total thermal resistance values for the dome section, R_D, and for the roof section including the 30 cm-thick earth cover, R_R, were calculated to be 1.20$m^2K\ W^{-1}$ and 1.78$m^2K\ W^{-1}$, respectively. The weighted mean of the R_T value for the overall roof surfaces was determined as 1.54 $m^2K\ W^{-1}$. In the same way, the thermal transmittance values through the dome section, U_D and of roof section, U_R were calculated to be 0.83W $m^{-2}K^{-1}$ and 0.56W $m^{-2}K^{-1}$, respectively. The weighted mean of the U value for the overall roof surfaces was determined as 0.67W $m^{-2}K^{-1}$. This overall U value seemed to be in acceptable ranges for a historic structure. However, when compared with the acceptable U value of 0.50W $m^{-2}K^{-1}$

required for the walls of energy efficient houses at the same climatic region, the overall *U* value of the historic roof/dome structure was found to be moderately-higher (TS 825, 1998).

These R_T and *U* values were calculated by considering both the thermal resistance of each layer forming the roof/dome sections and the interior and exterior surface resistances specified for various exposures and emissivity conditions (Table 4.2). The thermal properties of materials/layers, such as thermal conductance and thermal resistance values were significant in providing satisfactory thermal insulation characteristics to the building section and in improving the thermal performance of the historic bath structure. It was clear in both Table 4.2 and Figure 4.14 that in the *ORIGINAL* case, the earth layer covering the roof surfaces and the historic brick dome masonry (HBDM) were the main thermal insulation layers having good thermal properties with thermal resistance, *R* values of 0.577 $m^2K\ W^{-1}$ and 0.870$m^2K\ W^{-1}$, respectively. Here, especially the earth layer contributed much to the thermal performance of the historic dome masonry by minimizing heat loss from the exposed surfaces of the roof structure.

On the other hand, in the *AS-IS* case the removal of the earth layer from the structure and the addition of concrete layer resulted in a decrease in the total thermal resistance, R_T value of the roof/dome structure. The R_T value was found to be 1.10$m^2K\ W^{-1}$, being quite lower than the overall R_T value of 1.54$m^2K\ W^{-1}$ calculated for the *ORIGINAL* dome/roof section. Similarly, the *U* value of the *AS-IS* roof/dome section was determined to be 0.91$W\ m^{-2}K^{-1}$, which was quite higher than the overall *U* value estimated as 0.67 $W\ m^{-2}K^{-1}$ for the *ORIGINAL* dome/roof section.

The thermal performance of the structure seemed to be destroyed by the cement-based repair materials such as mesh-reinforced concrete layer (MRC) covering the exterior of roof surfaces of Şengül Hamamı and the cement based under coat (CBUC) and cement based finish coat (CBFC) layers covering the interior surfaces of bathing spaces, having high thermal conductance and low thermal resistances values (Table 4.2 and Figure 4.17). Their *R* values were calculated to be 0.04$m^2K\ W^{-1}$ for MRC layer and 0.011$m^2K\ W^{-1}$ and 0.07$m^2K\ W^{-1}$ for CBUC and CBFC layers, respectively. These values were considerably-lower than the earth layer and historic exterior and interior plaster layers, accelerating the heat flow through the roof/dome section.

5.4 Thermal Failures due to Improper Recent Repairs

The joint interpretation of various investigation methods, namely the microclimatic investigations, quantitative IR thermography together with the heat and water vapour transfer analyses clearly exhibited thermal failures in the structure, such as heat loss, thermal bridges, air leakages and condensation problems and the reasons of these failures.

The analyses of microclimatic data showed the presence of considerable heat loss problems in the structure (Figures 4.5 and 4.6). The maximum decrease in interior ambient temperature reaching 3ºC in the hot spaces of Şengül Hamamı was observed between the months of January and August, indicating the presence of significant heat loss problem in winter (Figure 4.5). Another microclimatic data proving such problems included the existence of a temperature difference between the outside air and the air neighboring the exterior dome surfaces in winter. In February, the air close to the dome surfaces was found to be warmer than the outside air temperature with a mean temperature difference of 3.1°C ± 0.5°C (Figure 4.6). This data was also vital in showing that the warm dome surfaces of the bath were heating the neighboring outside air due to the insufficient thermal resistance of the dome structure.

The quantitative analysis of IR images and/or sequences also revealed the types of thermal failures, their distribution on dome and wall structures and the extent of problems (Figures 4.8 to 4.13). In these analyses, the exterior surfaces of walls and concrete-clad roof were found to be considerably warmer than the outside air temperature showing that the thermal insulation properties of the dome/wall sections were not enough to resist the heat flow and above all, these problems were systematically located. According to the differential IR images given in Figure 4.9, the heat loss from the concrete-clad surfaces at the dome of women's hot space was determined with an average temperature increase of +0.2^{o}C during the cooling period of night for 322s in November, indicating that the warmer dome surfaces were due to heat loss from very hot interiors to outside. The 50 cm-thick historic brick dome masonry underneath the concrete layer was found to still have a certain thermal insulation capacity with thermal resistance, R, of 0.87m^{2}K W^{-1}; however, the progressive cooling at night was prevented due to heat transfer from inside to outside of the dome.

The thermal performance of the exterior walls in the present situation was determined to be severely destroyed by unconscious interventions done with cement-based repair materials (Figure 4.10 and 4.11). In these figures, the warmer wall surfaces seemed to match the severely-deteriorated areas due to the dampness and soluble salt problems introduced to the structure by cement-based mortars. Moreover, heat loss from the lower parts of the structure was found to be higher, as these parts were close to the hot hypocaust (*cehennemlik*) space at the subterranean area of the bath where the heating of the bathing spaces were done.

In QIRT analyses, the main heat loss areas were found to be the edges of circular dome lights and lower parts of the chimneys, which were seemed to be hottest surfaces in the infrared images (Figures 4.12 and 4.13). The IR sequences given in Figure 4.13 showed that during cooling period of night in November, there was a temperature increase in differential IR images reaching 3.2^{o}C and 6.3^{o}C in 420s at the edges of circular dome lights and the bottom edge of the chimney stack, respectively. These results indicated the existence of significant thermal failures such as heat loss and air leakage from the edges of dome lights and thermal bridges caused by the improper detailing in the connection of chimney stack with the roof structure.

Thermal insulation characteristics of the dome surfaces were seemed to be severely-destroyed by the use of cement-based repair materials, such as the cement-based mortar layers encircling the circular dome lights. In the IR analyses, these surfaces were seemed to be colder areas quite below the outside air temperature, suffering from dampness and salt weathering problems due to the condensation of hot and wet air leaking from the edges of dome lights (Figures 4.8 and 4.13). Failures in the thermal performance of the structure were mainly introduced by recent incompatible repairs done with cement-based materials, which seemed to reduce the vapor transmission through the structure and create problems due to interstitial localized condensation.

The water vapour transfer analyses clearly exhibited the condensation risk in the dome structure. The historic dome seemed to be composed of high and medium permeable layers, with S_D values in the range of 0.06m and 1.39m, allowing the passage of water vapour through the dome section (Table 4.3 and Figure 4.21) (TS prEN ISO 7783-2, 1999). In other words, a continuity of water vapour permeability along the dome section was achieved allowing the passage of water vapour back and forth through the section and ensuring the

evaporation of any entrapped water and/or water vapour within the section. However, the permeability characteristics of the dome section seemed to have destroyed by the use of impermeable layers, such as mesh-reinforced concrete cover and cement-based mortars/plasters, with S_D values in the range of 0.22m and 12m. These layers having high resistance to water vapour permeation, μ, were not compatible with the breathing historic dome section (Table 4.3 and Figure 4.21). Any failure, such as tiny cracks on these impermeable layers, would inevitably-cause the accumulation of entrapped moisture in the dome section and would prevent its evaporation from its exterior surfaces.

A considerable difference was determined between the total S_D values of the *ORIGINAL* and *AS-IS* roof/dome sections of Şengül Hamamı (Figure 4.22). The breathing capability of the historic dome section, with a total S_D value of 2.01m, was about 7 times more than that of the *AS-IS* dome section, which have a total S_D value of 13.90m. Therefore, the continuity of the water vapour transmission through the dome section was completely destroyed by the vapour impermeable concrete layer (MRC) and cement-based plaster layers (CBUC and CBFC).

The partial water vapour distribution curves clearly exhibited that in the *AS-IS* dome section the impermeable concrete and cement-based plaster layers were the main reasons of the entrapped moisture accumulated in the historic dome masonry, acting like impermeable skins (Figures 4.23-4.24). The dome section was under the risk of interstitial condensation all through the year, being either partially or completely damp. On the other hand, in the *ORIGINAL* case the dome section was under high risk of condensation for 7 months of a year (October, November, December, January, February, March, April) while being dry in the months remained (May, June, July, August and September). This is mainly due to its being composed of high vapour permeable layers providing a continuous passage of water vapour transition following with evaporation from its exposed surfaces; in other words, preventing the accumulation of moisture in the section. That highly-permeable section was also an advantage for the critical months preventing the extreme wetting of dome section.

This highly breathing dome section was covered with an impermeable skin by cladding outside of the historic structure with mesh-reinforced concrete. The backing of masonry and the deeper parts of mesh-reinforced concrete layer were found to be wet although the exposed surfaces seemed to be dry, showing that the dry surfaces of concrete cover at roof concealed the extreme entrapped moisture problem at the backing masonry. This meant that,

the structure was left to corrode as its evaporating surface was completely closed. As the outside skin was the only chance for the historic fabric to dry out or to remove its moisture, the historic brick masonry is now a great threat for its structure.

5.5 Joint Use of QIRT and Heat Transfer Calculations for the Thermal Failure Assessment of Real Situations

Simplified 1D steady state heat transfer calculations and *in-situ* analyses of quantitavive IR thermography were used together in order to assess thermal failures which affect the overall thermal resistance of building envelopes on a quantitative basis. Being a non-destructive method, it was found to be useful for the *in-situ* assessment of the real thermal conditions at monuments. It allowed us to compare the real surface temperatures of the buildings achieved by IR thermography method when a stable thermal gradient existed between the outside and inside with the neighbouring air and dew point temperature values as well as the reference surface temperatures obtained by heat transfer calculation methods at the steady-state conditions when the wall/dome section was assumed to be dry. It was also possible to compare the thermal resistance of the inside and outside surfaces at real situations with those values given in the standards.

For Şengül Hamamı, the interior and exterior surface resistances, R_{si} and R_{se}, of the dome section were found to be lower than the expected situation according to the reference heat flow curves given in Figure 4.18. This may be due to the high humidity conditions. More important, the found discrepancies are due to the adopted simplified one-dimensional, steady state model, which contains obviously a lack of similarity with the present situation. This issue gives the hints for a deeper study about relationship of the interior's dampness and thermal problems at the particular microclimatic conditions.

The joint use of QIRT and heat transfer calculations was also found to be useful in clearly-identifying thermal failures, such as damp/wet surfaces, air and moisture leakages, thermal bridges, entrapped moisture, interstitial condensation, *etc.* affecting the thermal insulation performance of these sections, their location in the structure and their possible reasons. For this, thermal models of dome sections were produced by QIRT analyses in order to assess the real heat flow curves along these sections, which were then compared with the reference

heat flow curves produced by heat transfer calculations for the steady-state condition of the structure. The use of different materials/layers in the wall/dome section and the absence or presence of thermal insulation layers could also be detected by this method as such failures change the overall thermal resistivity of the structure.

The analyses of Şengül Hamamı done with this new method revealed such thermal failures in the dome structure. In the domes of the women's hot and warm spaces the warmer exterior dome surfaces being below the reference outside surface temperature were interpreted as damp surfaces, while those being above the reference outside surface temperature indicated heat loss due to the lower overall thermal resistance of the dome section (green lines in Figures 4.18 and 4.19). The interstitial condensation in the deeper zones of the dome section may have caused thermal bridges in these areas. In addition, the dome light surfaces having surface temperatures considerably higher than the outside air and reference outside surface temperatures were found to be thermal bridge areas and also the main source of heat loss increasing the boundary air temperature due to air leakages from their edges (red lines in Figures 4.18 and 4.19). Moreover, the cement-based mortars surrounding the dome lights having the coldest exterior surfaces with temperatures below the outside air and reference outside surface temperatures were found to correspond to the wet/damp surfaces (blue lines in Figures 4.18 and 4.19). In these areas serious condensation and entrapped moisture problems were detected due to moisture leakages from inside to outside by means of capillary cracks on the concrete layer and cement-based mortars.

The analyses of the overlapped IR images of the exterior and interior dome surfaces showed that the coldest wet areas on the exterior surfaces corresponded to the hottest interior surfaces (blue lines in Figure 4.18). The analyses of IR sequences of these regions taken in February have shown that the wet exterior surfaces were slightly-cooling down while the interior surfaces were slightly-warming up during the cooling period at outside and constant boundary conditions at inside (blue lines in Figure 4.19 and 4.20). This revealed that the heat loss is more severe at the dome sections having wet exterior surfaces due to evaporative cooling.

5.6 Conclusions

The study exhibited that the historic brick dome structure of Şengül Hamamı was originally configured to provide sufficient thermal insulation characteristics due to the good thermal properties of its materials. It seemed that the components of the historic upper structure, mainly the historic brick masonry and the earth cover on roof, established a healthy relationship providing a good thermal performance under the harsh interior and exterior climatic conditions. That success was due to the conscious use of less thermal conductive and high vapour permeable historic masonry materials in association with each other. The knowledge on historical materials also revealed the experience of materials technology achieved in the past establishing successful thermal performance of bath structures.

The original thermal performance of the roof structure, however, has been severely-destroyed by the recent repairs, removing the earth cover and using mesh-reinforced concrete cover and cement-based interior plasters which were incompatible with the historic fabric of the structure due to their different thermo-physical properties. Due to their considerably-high density, low porosity and high thermal conductivity when compared with the historic materials, the use the cement-based materials caused a significant increase in the total thermal transmittance value of the roof structure. This meant that, the heat flow through the roof/dome section of Şengül Hamamı was accelerated due to the wrong repairs. Due to the low water vapour permeability characteristics of cement-based materials when compared with the highly vapour permeable historic materials, the continuity of the water vapour transmission through the layers of dome section was completely blocked by the vapour impermeable concrete and cement-based plaster layers.

The partial water vapour distribution analyses revealed that water vapour penetration into the dome section was inevitable in varying ranges depending on season. The highly-breathing capability of the historic dome section was the main precaution to prevent entrapped moisture problem in that dome section. However, covering the exterior surface of historic roof with the impermeable skin made of mesh-reinforced concrete definitely-damaged the original breathing feature of historical masonry structure and caused entrapped moisture and thermal breaks in the historic dome section followed by material failures. At present conditions, the problem of interstitial condensation is inevitable since the moisture escape from the historic brick dome masonry was prevented by the impermeable concrete skin. This

meant that, the roof structure was left to corrode due to the entrapped moisture since its only evaporating surface was completely closed to breathe. The concrete cover is a great threat for the historic brick masonry structure.

The thermal failures and damp regions detected on roof/dome surfaces were the indicators of significant heat loss fro the structure. The quantitative analysis of infrared data together with the heat transfer calculations and microclimatic investigations revealed the thermal and moisture failures, their location and extent in the structure as well as their reasons. The monitoring of those failures during a year by thermography were also useful to better-understand the extent of the problems. In short, the dome structure in *AS-IS* case, suffer from considerable heat losses, especially from dome surfaces: The condensed water on the glass surfaces of the dome lights was determined to leak out from the cement-based mortar surrounding the dome light and the concrete cover. Those problem areas acting like thermal bridges were visible on concrete cover as cracks associating with salt deposits and discoloration. The heat escape from the dome lights and their surroundings were the main source of heat loss from roof structure. The entrapped moisture in the roof/dome section (interstitial condensation) was the next source of the extensive heat loss, which decreased the inherent thermal resistance of historic roof/dome section.

The quantitative analyses of infrared data together with the heat transfer calculations was useful to define the thermal insulation characteristics of a masonry section and to identify thermal and moisture failures. The IR images taken in sequences at mutually corresponding (interior and exterior) surfaces of dome section at the same time made it possible to produce the thermal models of dome structure. Those models allowed us to achieve the real temperature gradients between inside and outside through the dome section and to compare that data with the temperature gradient calculated in consideration with thermal conductivity of dry materials, their thicknesses and real inside and outside air temperatures one representing the heat flow through the dome section. The calculated one accepted as the reference temperature gradient obtained by heat transfer calculations at the steady-state conditions. In brief, a simplified 1D steady state heat transfer calculations combined with the *in-situ* surface temperature extensively measured by IR thermography seemed to be a promising alternative to assess the overall thermal resistance of the historic building envelope. That approach allowed to assess the heat flow through dome/wall sections and to make reasonable hypothesis on the reasons of thermal failures and the restoration.

This study helped us to better understand the thermo-physical properties of historic materials and thermal insulation characteristics of the historic roof/dome structure in terms of the thermal transmittance value, U, and thermal resistance value, R, all of which should be fulfilled by restorations. Comprehensive studies on thermo-physical properties of building materials collected from many historic bath structures as well as on the overall thermal transmittance/resistance values of those structures are also needed to define the inherent thermal performance of historic baths and the thermal specifications expected from the new repair materials.

Due to the high humidity conditions in the bathing spaces, the materials under direct exposure of those wet/damp boundary conditions should be expected to be damp to certain extent. Further laboratory analyses, therefore, are needed to examine the thermo-physical properties of historic materials in relation to the moisture content. The relation between the resistance to water vapour permeation value, μ, and water permeability was another subject of interest, particularly for the interior and exterior historic plasters of historic baths.

Further studies are needed to examine the performance of heating system in terms of its energy consumption capacity, heating capacity and adequacy in order to define its functioning principles, to better understand its contribution to the overall thermal performance of the historic structure and to establish maintenance programs for keeping its authentic technological features.

REFERENCES

AKKUZUGIL, E. 1997. A Study on Historical Plasters, *Unpublished MSc Thesis*, Department of Architecture, Building Science Graduate Program, METU, Ankara, Supervisor: Türel Saranlı, Co-supervisor: E. N. Caner-Saltık.

AKYAZI, M. 1998. A Proposal for the Repair and Conservation of Haraçoğlu Konak in Bursa, *Unpublished MSc. Thesis*, Department of Architecture, Restoration Graduate Program, METU, Ankara, Supervisor: Neriman Şahin Güçhan, Co-supervisor: E. N. Caner-Saltık.

ANDOLSUN, S. 2006. A Study on Material Properties of Autoclaved Aerated Concrete (AAC) and its Complementary Wall Elements: Their Compatibility in Contemporary and Historical Wall Sections, *Unpublished MSc Thesis*, Department of Architecture, Building Science Graduate Program, METU, Ankara, Supervisor: Ayşe Tavukçuoğlu.

Archives of the General Directorate of Pious Foundations, 2008.

ARU, K. A. 1949. *Türk Hamamları Etüdü*, İstanbul Matbaacılık, İstanbul.

AVDELIDIS, N. P. and A. Moropoulou. 2003. Emissivity Considerations in Building Thermography, in: *Energy and Buildings*, v. 35, pp: 663-667.

BAŞARAN, T. 1995. Thermal Analysis of the Heating Systems of Roman Baths, *Unpublished MSc. Thesis*, Department of Mechanical Engineering, Dokuz Eylül University, İzmir, Supervisior: Zafer İlken.

BAŞARAN, T. and Z. İlken. 1998. Thermal Analyses of the Heating System of the Small Bath in Ancient Phaselis, in: *Energy & Buildings*, v. 27, pp: 1-11.

BRE. 1969. Condensation. *BRE Digest,* (Digest 110), October, 1969. The Blackburn Times Press, Great Britain.

BRE. 1992. Interstitial Condensation and Fabric Degradation. *BRE Digest,* (Digest 369), February, 1992. The Blackburn Times Press, Great Britain.

CANER, E. 2003. Archaeometrical Investigation of Some Seljuk Plasters, *Unpublished MSc Thesis*, Archaeometry Graduate Program, METU, Supervisor: Şahinde Demirci, Co-supervisor: E. N. Caner-Saltık.

CANER E., G. K. Akoglu, E. N. Caner-Saltik, S. Demirci and T. Yasar. 2005. Bazı Ortaçağ Çatı Örtüsü Sıvalarının Hammadde Özellikleri, in: *Proceedings of the 23rd International Symposium on Excavation, Research and Archeometry; Meeting of Research Results*, v.2, Antalya, Turkey, May 30-June 03, 2005, Ankara, Ministry of Culture and Tourism, DÖSİM Press, pp. 417-428.

CANER-SALTIK E. N., S. Demirci, A. Guney, G. K. Akoglu and E. Caner. 2003a. METU Research Fund project BAP-2003.02.01.02: Technological properties of some plasters used as roof covering material in historic structures, *Unpublished Final Research Report*, METU Faculty of Architecture, Ankara, 25 pages.

CANER-SALTIK E. N., A. Tavukcuoğlu, G. Akoglu, A. Guney. 2003b. The Material Analyses of Amasya Hızır Pasa Bath, *Unpublished Analyses Report in the context of REST 555 Course*, METU, Ankara.

CANER-SALTIK E. N., S. Demirci, G. K. Akoğlu, E. Caner and A. Guney. 2005a. METU Research Fund project BAP-2005.02.01.07: Consolidation of Historic Plasters with Nano-Dispersive Solutions, *Unpublished Final Research Report*, METU Faculty of Architecture, Ankara, 15 pages.

CANER-SALTIK E. N., A. Tavukcuoglu, G. Akoglu, A. Guney. 2005b. The Material Analyses of Yalınayak Bath, *Unpublished Analyses Report in the context of REST 555 Course*, METU, Ankara.

CANER-SALTIK, E. N. 2008. Kültürel ve Mimari Miras Olarak Hamamların Önemi: Ankara Örneği. In: O. Yildirim (ed.), *Osmanlının Peşinde Bir Yaşam – Suraiya Faroqhi'ye Armağan*, Ankara, Türkiye, İmge Kitapevi, pp: 135-165.

CANER-SALTIK E. N., A. Tavukcuoglu, G. Akoglu, A. Guney. 2009. The Material Analyses of Tabaklar Bath, *Unpublished Analyses Report in the context of REST 509 Course*, METU, Ankara.

ÇAKMAK, C. 2002. Tire Hamamları. Kültür Bakanlığı Yayınları, Ankara.

CESTARI, C. B., C. Lombardi, E. Gubetti and O. Pignatelli. 2002. Arsenal Project – The Timber Roof of Tesone '111': Technological Characteristics, Dating and Assessment of Thermo-Hygrometric Behavior for a Restored Functionality Proposal, in: *Journal of Cultural Heritage*, v. 3, pp: 53-57.

CLARK, M. R., D. M. McCann and M. C. Forde. 2003. Applications of Infrared Thermography to the Non-Destructive Testing of Concrete and Masonry Bridges, in: *NDT & E International*, v. 36, pp: 265-275.

COOK, H. K. 1978. Thermal Properties, in *Significance of Test and Properties of Concrete and Concrete Making Materials*. ASTM STP 169B-EB/Dec. American Society for Testing and Materials, Philadelphia, Chapter 39: 695-707.

ÇİZER, Ö. 2004. Investigation of Lime Mortar Characteristics for the Conservation of the Ottoman Baths in Seferihisar-Urla Region, *Unpublished MSc. Thesis*, Department of Architecture, İzmir Institute of Technology, İzmir, Supervisor: Başak İpekoğlu.

DARGA, M. 1985. *Hitit Mimarlığı* / I. Yapı Sanatı, İstanbul, pp:157-158.

DATCU, S., L. Ibos, Y. Candau and S. Mattei. 2005. Improvement of Building Wall Surface Temperature Measurements by Infrared Thermography, in: *Infrared Physics & Technology*, v. 46, pp: 451-467.

DIN 52615, 1987. *Determination of Water Vapour (Moisture) Permeability of Construction and Insulating Materials*. November, 1987. Deutsches Institut für Normung, Berlin.

DİŞLİ, G. 2008. An Investigation on the Water Supply and Drainage Systems of Historical Turkish Baths, *Unpublished MSc Thesis*, Middle East Technical University, Department of Architecture, Building Science Graduate Program, Ankara, Supervisor: Ayşe Tavukçuoğlu.

DİŞLİ, G., A. Tavukcuoğlu, L. Tosun, E. Grinzato, and E. N. Caner-Saltık. 2007. Rainwater Drainage System Investigation of an Historical Hamam By Using Non-Destructive Methods, in: *Water And Cultural Heritage, Proceedings - 7th International Symposium on the Conservation of the Monuments in the Mediterranean Basin*, June 6-9, 2007, Orleans , France, pp: 153-165.

DİŞLİ, G., A. Tavukcuoglu, L. Tosun, E. Grinzato. 2008a. The Assessment of Roof Drainage System of a Historical Turkish Bath: Sengul Hammam, in: *11 DBMC International Conference on Durability of Building Materials and Components*, İstanbul, Turkey, 11-14 May 2008, v. 3, pp: 1287-1297. İstanbul, Turkey: İstanbul Technical University Press

DİŞLİ, G., A. Tavukcuoglu, L. Tosun. 2008b. An Investigation on Water Consumption and Waste Water Discharge Systems for Historical Turkish Baths, in: *8th International HVaC-R Technology Symposium*, 12-14 May, 2008, Istanbul, Turkey, pp: 556-565. Turkish Society of HVAC & Sanitary Engineers.

ESEN S, N. Tunç, S. Telatar, A. Tavukcuoglu, E. N. Caner-Saltık and S. Demirci. 2004. Manisa Çukur Hamam'ın Onarımına Yönelik Malzeme Çalışmaları, in: *Proceedings of 2nd National Congress and Exhibition on Building Materials.* İstanbul, Turkey, 6-8 October, 2004, TMMOB Chamber of Architects - Istanbul Branch, pp: 494-505.

ERDOĞAN, M. 1986. Nevşehir-Ürgüp Yöresi Tüflerinin Malzeme Jeolojisi Açısından Araştırılması. *Unpublished Phd Thesis*. Istanbul Technical University. Maden Fakültesi.

ERGUVANLI, A. K., A. E. Yüzer. 1977. Past and Present Use of Underground Openings Excavated in Volcanic Tufts at Cappadocia area. Proc. on Rock Storage, Oslo, Norway, pp: 15-17.

FANG, X., A. K. Athienitis and P. P. Fazio. 2009. Methodologies for shortening test period of coupled heat-moisture transfer in building envelopes, in: *Applied Thermal Engineering*, v. 29, pp:787-792.

GOULART S. V. G. 2004. Thermal Inertia and Natural Ventilation – Optimisation of Thermal Storage as a Cooling Technique for Residential Buildings in Southern Brazil. *Unpublished Phd. Thesis,* Architectural Association School of Architecture, Graduate School.

GRINZATO E., P. G. Bison and S. Marinetti. 2002a. Monitoring of the Ancient Buildings by Thermal Methods, in: *Journal of Cultural Heritage*, v. 3, pp: 21-29.

GRINZATO E., C. Bressan, S. Marinetti, P. G. Bison and C. Bonacina. 2002b. Monitoring of the Scrovegni Chapel by Infrared Thermography: Giotto at Infrared, in: *Journal of Cultural Heritage*, v. 3, pp: 21-29.

GRINZATO E., V. Vavilov and T. Kauppinen. 1998. Ouantitative Infrared Thermography in Buildings, in: *Energy & Buildings*, v. 29, pp: 1-9.

GRINZATO, E., P. G. Bison, S. Marinetti, M. Concas and S. Fais. 2004. Comparison of Ultrasonic Velocity and IR Thermography for the Characterisation of Stones, in: *Infrared Physics & Technology*, v. 46, Issues 1-2 December 2004, pp: 63-68.

Hamam. 1964. İslam Encyclopedia, İslam Alemi Tarih, Coğrafya, Etnografya ve Biyografya Lügatı, v. 5, part 1, pp:174, Milli Eğitim Basımevi, İstanbul.

HALL F. 1994. Heat Losses, in: *Building Services and Equipment*, v.1, 3rd edition, Longman Group UK Limited.

HALL F. 1994. Heating, in: *Building Services and Equipment*, v.3, 3rd edition, Longman Group UK Limited.

HARALAMBOPOULOS, D. A., and G. F. Paparsenos. 1998. Assessing the Thermal Insulation of Old Buildings-The Need for In Situ Spot Measurements of Thermal Resistance and Planar Infrared Thermography, in: *Energy Conrers. Mgmt*, v. 39, number 1-2, pp. 65-79, Great Britain.

HENS, H. 2007. Building Physics – Heat, Air and Moisture, Berlin, Germany.

HOFFMANN, D. & K. Niesel. 1996. Relationship between Pore Structure and Other Physico-Thecnical Characteristics of Stone, in: *Proceedings of the 8th International Congress on Deterioration and Conservation of Stone*, v 1, pp: 461-470. Germany.

HOUBEN, H. & H. Guillaud. 1994. *Earth Construction – A Comprehensive Guide*. Intermediate Technology Publications, London, UK.

HUGHES, P. 1986. The Need for Old Buildings to "Breathe". Society for the Protection of Ancient Buildings: Information Sheet 4, 37 Spital Square, London E1 6DY: 01 377 1644

IŞIK, F. 1995. A Study on the Changing Turkish Bathing Culture under the Western Influences, *Unpublished MSc. Thesis*, Department of Architecture, History of Architecture Graduate Program, Middle East Technical University, Ankara, Supervisor: İnci Aslanoğlu.

İzocam. 2004. *İzolasyon-Isı, Ses ve Yangın*, İzocam, İzmit.

KANDEMIR-YÜCEL, A., A. Tavukçuoğlu and E. N. Caner-Saltık. 2007. In situ Assessment of Structural Timber Elements of a Historic Building by Infrared Thermography and Ultrasonic Velocity, in: *Infrared Physics & Technology*, v. 49, Issue 3 January 2007, pp: 243-248.

KUMARAN, M. K. 2001. *Hygrothermal Properties of Building Materials*. MNL40-EB/Jan. 2001.

Kurama, H., I. B. Topcu and C. Karakurt. 2009. Properties of the Autoclaved Aerated Concrete Produced From Coal Bottom Ash, in Journal of Materials Processing Technology, v. 209, pp: 767–773.

LANGLAIS, C., A. Silberstein and P. I. Sandberg. 1994. Effects of Moisture on the Thermal Performance of Insulating Material. in: *Moisture Control in Buildings,* chapter 4, Heinz R. Trechsel, ed. The American Society for Testing and Materials, Philadelphia, pp. 54-71.

MEOLA, C., R. Di Maio, N. Roberti and G. M. Carlomagno. 2005. Applications of Infrared Thermography and Geophysical Methods for Defect Detection in Architectural Structures, in: *Engineering Failure Analysis*, v. 12, Issue 6 December 2005, pp: 875-892.
MOSS, K. J. 2007. Heat and Mass Transfer in Buildings. London and New York.

NAPPI, A. and P. Cote. 1997. Non-destructive Test Methods Applicable to Historic Stone Structures, in: N.S. Baer & R. Snethlage (ed.), *Saving Our Architectural Heritage: The Conservation of Historic Stone Structures*, Dahlem Workshop Report, John Wiley & Sons; New York, pp: 151-166.

ÖRS, K. 2006. An Investigation on Compatibility Properties of Exterior Finish Coats For Insulated Walls in Terms of Water Vapour Permeability and Modulus of Elasticity, *Unpublished MSc. Thesis*, Department of Architecture, Building Science Graduate Program, METU, Ankara, Supervisor: Ayşe Tavukçuoğlu.

ÖNEY, G. 1971. *Ankara'da Türk Devri Dini ve Sosyal Yapıları*, Ankara Üniversitesi Dil ve Tarih-Coğrafya Fakültesi Yayınları, number: 209, Ankara.

ÖNGE, M. Y. 1995. *Anadolu'da XII-XIII. Yüzyıl Türk Hamamları*, Vakıflar Genel MüdürlüğüYayınları.

ÖNGE, M. Y. 1988. Anadolu Türk Hamamları Hakkında Genel Bilgiler ve MimarKoca Sinan'nın İnşa Ettiği Hamalar (General Information on Anatolian Turkish Hamas and the Hamams Built by Mimar Koca Sinan), in: Sadi Bayram (ed.), *Mimarbaşı Koca Sinan Yaşadığı Çağ ve Eserleri I*, T.C. Başbakanlık Vakıflar Genel Müdürlüğü ve Vakıflar Bankası Genel Müdürlüğü Yayınları, Ankara.

REYHAN, K. 2004. Construction Techniques and Materials of Ottoman Period Baths in Urla-Seferihisar Region, *Unpublished MSc. Thesis*, Department of Architecture, İzmir Institute of Technology, İzmir, Supervisor: Başak İpekoğlu.

REYHAN, K. and B. İpekoğlu. 2004. Osmanlı Dönemi Bir Grup Hamam Yapısında Malzeme Kullanımı (Material Use in a Group of Otoman Period Hamam Buildings), in: *2. Ulusal Yapı Malzemesi Kongresi ve Sergisi Bildiriler Kitabı*, 3-17 Ekim 2004, İTÜ, Taşkışla, İstanbul, pp: 482-493.

RILEM. 1980. Tentative Recommendations, in: *Commission-25-PEM, Recommended Test to Measure the Deterioration of Stone and to Assess the Effectiveness of Treatment Methods, Materials and Structures*, v. 13, number 73, pp:173-253.

SANTOS G.H. and N. Mendes. 2008. Heat, air and moisture transfer through hollow porous blocks, in: *International Journal of Heat and Mass Transfer*, doi:10.1016/j.ij heatmasstransfer.2008.11.003.

STRAAREN, J.F. 1967. *Thermal Performance of Buildings*. Elsevier Publishing Company. Amsterdam, London and New York.

STROTHER E.F. and W. C. Turner. 1990. *Thermal Insulation Building Guide*, Malabar, Florida, Robert E. Krieger Publishing Company.

TAŞÇIOĞLU, T. 1998. *The Turkish Hamam*, İstanbul.

TAVUKÇUOĞLU, A. and E. N. Caner-Saltık. 1999. Mapping of Visual Decay Forms and Infrared Imaging of Stone Structures for the Maintenance and Monitoring Studies, in: M.A. Lacasse and D.J. Vanier (edt.), *Durability of Building Materials and Components 8*, NRC Research Press, Canada. v. 1, pp:613-623.

TAVUKÇUOĞLU, A., A. Duzgunes, Ş. Demirci and E. N. Caner-Saltık. 2005. Use of IR Thermography for the Assessment of Surface Water Drainage Problems in a Historical Building, Ağzıkarahan (Aksaray), Turkey, in: *NDT & E International*, v. 38, pp: 402-410.

TAVUKCUOĞLU, A., A. Düzgüneş, Ş. Demirci and E.N. Caner-Saltık. 2007. The Assessment of a Roof Drainage System for an Historical Building, in: *Building and Environment*, v. 42, pp: 2699-2709.

TEMIZSOY, A., S. Esen, K. Şahlan, N. Tunç and S. Telatar. 2003. Original Water Supply & Heating Systems in a 14th Century. Bath: Çukur hamam in Manisa, Turkey, *Unpublished Term-Paper of Rest 506 Course*, Department of Restoration, Faculty of Architecture, METU, 13 pages.

TEUTONICO, J.M. 1986. *A Laboratory Manual for Architectural Conservators*, ICCROM, Rome, pp: 32-122.

TITMAN, D.J. 2001. Applications of Thermography in Non-Destructive Testing of Structures, in: *NDT&E International*, v. 34, pp: 149-154.

TS 4048. 1984. *Determination of Specific Heat for Thermal Insulating Materials*, September 1984. Turkish Standards Institution, Ankara.

TS 699. 1987. *Methods of Testing For Natural Building Stones*. Türk Standartları Enstitüsü, Ankara.

TS 7847. 1990. *Wall Coating Emulsions for Exteriors-Polymer based*. February, 1990. Türk Standartları Enstitüsü, Ankara.
TS 825. 1998. *Rules of Thermal Insulation in Buildings*, April 1998. Turkish Standards Institution, Ankara.

TS prEN ISO 7783-2. 1999. *Paints and Varnishes-Coating Materials and Coating Systems for Exterior Masonry-Part 2: Determination and Classification of Water-Vapour Transmission Rate (Permeability).* March, 1999. Türk Standartları Enstitüsü, Ankara.

TS EN 1745. 2004*., Masonry and Masonry Products - Methods for Determining Design Thermal Values*, April 2004. Turkish Standards Institution, Ankara.

TS EN ISO 6946. 2007*., Yapı bileşenleri ve yapı elemanları - Isıl direnç ve ısıl geçirgenlik hesaplama metodu - Building components and building elements - Thermal resistance and thermal transmittance - Calculation method*, April 2007. Turkish Standards Institution, Ankara.

TYE, Ronald P. 1994. Relevant Moisture Properties of Building Construction Materials. *Moisture Control in Buildings*, p. 35-53, Chapter 3. Heinz R. Trechsel, ed. The American Society for Testing and Materials, Philadelphia.

UĞURLU, E. 2005. Characterization of Horasan plasters from some Ottoman baths in İzmir, *Unpublished MSc. Thesis*, Department of Architecture, Architectural Restoration Graduate Program, İzmir Institute of Technology, İzmir, Supervisior: Hasan Böke.

WILLIAMS, M. F. and B. L. Williams. 1994. *Exterior Insulation and Finish Systems*: Current Practices and Future Considerations. The American Society for Testing and Materials, Philadelphia

YEGÜL, F. 1992. *Baths and Bathing in Classical Antiquity*, Architectural History Foundation. MIT Press, New York.

YEGÜL, F. 2006. *Antik Cağ'da Hamamlar ve Yıkanma*. Homer Kitabevi, Istanbul.

Beodom web page, http://www.beodom.com/en/journal/entries, access date: 19 May 2008.

Wikipedia home page, http://en.wikipedia.org/wiki, access date: 17 May 2008.

Publications:

CANER-SALTIK, E.N., A. Tavukçuoğlu, K.G. Akoğlu, G. Dişli, A. Aydın, P. Çiçek, L. Tosun, M. Çalışkan, E. Caner-Özler, T. Yaşar. In Press. *Methods of Conservation for Şengül Hammam with a Priority to its Authenticity*. (18 pages). Submitted in February 2009 to be published in the proceedings of EU Project HAMMAM - 517704: Aspects and Multidisciplinary Methods for the Mediterranean Region. Syria, Damascus.

TAVUKCUOGLU, A., P. Çiçek, E. Grinzato. 2008. Thermal Analysis of a Historical Turkish Bath by Quantitative IR Thermography, in: *9th International Conference on Quantitative InfraRed Thermography*, Proceedings, July 2-5, 2008, (pp.659-660), Krakow, Poland: Technical University of Lodz, Institute of Electronics.

TAVUKCUOGLU, A., P. Cicek, E. Grinzato. 2008. Thermal Analysis of a Historical Turkish Bath by Quantitative IR Thermography, in: *Quantitative Infrared Thermography Journal*, v. 5(2), pp: 151-173.

APPENDIX A

THECNICAL SPECIFICATIONS OF INSTRUMENTS USED IN THE STUDY

A.1 AGEMA 550 Camera - Radiometric Handheld Infrared Camera

Imaging and Measurement Capabilities:

System Type	Focal plane array infrared camera
Spectral Range	3.6 – 5.0 microns
Detector	PtSi, 320 x 240
Temperature Measurement Accuracy	± 2% of range or 2°
Temperature Measurement Range	–20°C to +2000°C (–4°F to +3600°F)
Field of View	20°x15°
Cooling	> 10,000 hour MTBF Stirling cooler
Spatial Resolution	76,800 pixels
Minimum Discernable Temperature	0.1°C at 30°C
Image Update Rate	30/25 Hz NTSE/PAL and 60 Hz Digital
Infrared Dynamic Range	12 bits
Image Optimization	Continuous automatic or manual
Emissivity Setting	Yes
Color/Grey Levels	256
Palettes	Multiple color or monochrome, user selectable
Display	Type Built-in, high-resolution color LCD viewfinder
Image Storage Capacity	1000 images (12 bit) on 170 MByte PC Card disk

Additional Specifications

Interfaces	RS-232 interface for remote camera control; Voice annotation – headset connection; PC Card - type II or III

Video Outputs	RS 170 EIA/NTSC or CCIR/PAL, composite or S-video
Power	NiMH battery, 6 hours continuous operation
Operating Temperature	–15°C to +50°C (5°F to +120°F)
Camera Weight (w/lens & viewfinder)	2 kg (4.4 lbs)
Camera Size	220 x 132 x 140mm (8.7 x 5.2 x 5.5 inches)
Enclosure	IP54 rated (NEMA 13), completely water- and dust-proof

Optional Image Analysis Features Include:

Auto hot spot; continuous image storage; automatic temperature difference readout etween target and reference temperatures; automatic display of minimum, maximum and average value in defined AOI.

Accessories

Standard: 20° lens, AC power supply, operating manual and shipping case, multiple language support.

Optional: Software: IRwin Report for image analysis and reporting. Optics: additional lenses, filters. Video & Recording Accessories: recorders, printers, visual light cameras, 30sec. digital voice annotation per image with on-screen prompts, high-resolution 4" LCD display. Power Accessories: batteries, chargers, DC to DC adapter. Other: desktop/ laptop PCs, additional PC Cards, tripod.

A.2 FLIR ThermaCAM E65 Infrared Camera

Imaging Performance

Field of view/min focus distance	Interchangeable; 25° x 19° / 0.3 m, 12° x 9°/1.2m or 45° x 36° / 0.1m
Thermal sensitivity	0.10° C at 30° C
Detector type	Focal plane array (FPA) uncooled vanadium oxide microbolometer, 160x120 pixels, 50/60 Hz
Spectral range	7.5 to 13µm

Image Presentation

Display	2.5" color LCD, 320 x 240 pixels in IR image
Image Controls	Palettes (Iron, Rainbow, B/W, B/W inv), Level, Span, Auto adjust (continuous/ manual)

Measurement

Temperature ranges	-20°C to +250°C (-4°F to +482°F) (standard)
Accuracy	+250°C to +900°C (+482°F to +1,652°F) (optional) ± 2°C or ± 2% of absolute temperature in °C
Measurement modes	3 movable spots, area max, area min, area average, temp difference, color alarm above or below
Set-up controls	Date/time,Temperature units °C/°F, Language (English, Spanish), Scale, Info field, LCD intensity (high/normal/low)
Measurement corrections	Reflected ambient. Automatic, based on user-input

Image Storage

Digital storage functions	Freeze, Standard Calibrated JPEG images, Delete all images, Delete image, Open
Image storage capacity	Approx. 200 Calibrated JPEG Images with image gallery
Text annotation of images	Predefined text selected and stored together with image

Laser LocatIR TM

Classification	Class 2
Type	Semiconductor A1GaInP Diode Laser: 1mW/635 nm (red)

Power Source

Battery type	Li-Ion; rechargeable, field replaceable
Battery operating time	2 hours. Display shows battery status
Battery charging	In camera (AC adapter or 12V from car) or 2 bay intelligent charger
AC operation	In camera, AC adapter or 12V from car with optional 12V cable. 2 bay intelligent charger included.
Voltage	11-16VDC
Power saving	Automatic shutdown and sleep mode (user-selectable)

Environmental

Operating temperature range	-15°C to +45°C (+5°F to 113°F)
Storage temperature range	-40°C to +70°C (-40°F to 158°F)
Humidity	Operating and storage 20% to 80%, non-condensing, IEC 359
Water and dust resistant (encapsulation)	IP 54, IEC 359
Shock	25G, IEC 68-2-29
Vibration	2G, IEC 68-2-6

Physical Characteristics

Weight	< 1.5 lbs. (0.7 kg) including battery (with standard lens)
Size (L x W x H)	265mm x 80mm x 105mm (10.4"x3.2"x4.1")
Color	Titanium grey
Tripod mounting	Standard, 1/4" - 20
Cover case	Plastic and rubber

Camera includes:

IR camera, ruggedized transport case, power supply and cord, hand strap, lens cap, ThermaCAM® QuickViewTM software, USB cable, video-out cable, user manual, battery (2), 2-bay battery charger, training CD.

Interchangeable lenses (optional)

2X Telescope (12° X 9°/1.2m)

0.5X Wide angle (45° X 34°/0.1m)

Interfaces

IrDA	Two-way data transfer from laptop, PDA

A.3 HOBO WarePRO Temperature/Relative Humidity/Light/External Data Loggers

Data Storage Capacity	43.000 12-bit Samples/Readings
Sampling Rate	1 Second to 18 Hours
Measurement Range	Temperature: -20°C to 70°C (-4°C to 158°F)
	Humidity: 5% to 95% RH
	Light Intensity: 1 to 3000 foot-candles (lumens/ft2)
	External Input Channel: 0 to 2.5 Volts DC
Accuracy	Temperature: ±0.35°C from 0°C to 50°C
	Humidity: ±2.5% RH from 10% to 90% (10°C to 50°C)
	Light Intensity: Indoor Measurement of Relative Light Levels
	External Inputs: ±2 mV, ±2.5% of Absolute Reading
Resolution	Temperature: 0.03°C at 25°C (0.05°F at 77°F)
	Humidity: 0.03% RH
Drift	Temperature: 0.01°C/year (0.02°F/year)
	Humidity: <1% RH per year; RH Hystersis 1%
Response Time (airflow: 1m/s)	Temperature: 6 Minutes, typical to 90%
	Humidity: 1 Minute, typical to 90%
Time Accuracy	±1 Minute per Month at 25°C (77°F)
Operating Temperature	Logging: -20°C to 70°C (-4°F to 158°F)
	Launch/Readout: 0°C to 50°C (32°F to 122°F)
Battery Life	Typically 1 Year
Battery	3-Volt CR-2032 Lithium Battery (User Replaceable)
Standards Compliance	CE
Weight	46 g (1.6 oz)
Dimensions	58mm x 74mm x 22mm (2.3" x 2.9" x 0.9")

APPENDIX B

SATURATED WATER VAPOUR PRESSURE AT A GIVEN TEMPERATURE

Table B.1 Saturated water vapour pressures in Pa for the temperatures between 0°C and -30°C (Hens, 2007: 145)

θ (°C)	–0.0	–0.1	–0.2	–0.3	–0.4	–05	–0.6	–0.7	–0.8	–0.9
–0	611	606	601	596	591	586	581	576	572	567
–1	562	558	553	548	544	539	535	530	526	522
–2	517	513	509	504	500	496	492	488	484	479
–3	475	471	467	464	460	456	452	448	444	441
–4	437	433	430	426	422	419	415	412	408	405
–5	401	398	394	391	388	384	381	378	375	371
–6	368	365	362	359	356	353	350	347	344	341
–7	338	335	332	329	326	323	321	318	315	312
–8	310	307	304	302	299	296	294	291	289	286
–9	284	281	279	276	274	271	269	267	264	262
–10	260	257	255	253	251	248	246	244	242	240
–11	237	235	233	231	229	227	225	223	221	219
–12	217	215	213	211	209	207	206	204	202	200
–13	198	196	195	193	191	189	188	186	184	183
–14	181	179	178	176	174	173	171	170	168	167
–15	165	164	162	160	159	158	156	155	153	152
–16	150	149	148	146	145	143	142	141	139	138
–17	137	136	134	133	132	131	129	128	127	126
–18	125	123	122	121	120	119	118	116	115	114
–19	113	112	111	110	109	108	107	106	105	104
–20	103	102	101	100	99	98	97	96	95	94
–21	96	92	91	90	90	89	88	87	86	85
–22	84	84	83	82	81	80	80	79	78	77
–23	76	76	75	74	73	73	72	71	70	70
–24	69	68	68	67	66	66	65	64	64	63
–25	62	62	61	60	60	59	59	58	57	57
–26	56	56	55	55	54	53	53	52	52	51
–27	51	50	50	49	49	48	48	47	47	46
–28	46	45	45	44	44	43	43	42	42	41
–29	41	41	40	40	39	39	38	38	38	37
–30	37	36	36	36	35	35	35	34	34	33

Table B.2 Saturated water vapour pressures in Pa for the temperatures between 0°C and 40°C (Hens, 2007: 146)

θ (°C)	0.0	0.1	0.2	0.3	0.4	0.5	0.6	0.7	0.8	0.9
0	611	615	620	624	629	634	638	643	647	652
1	657	662	666	671	676	681	686	691	696	701
2	706	711	716	721	726	731	736	742	747	752
3	758	763	768	774	779	785	790	796	802	807
4	813	819	824	830	836	842	848	854	860	866
5	872	878	884	890	896	903	909	915	922	928
6	935	941	948	954	961	967	974	981	987	994
7	1001	1008	1015	1022	1029	1036	1043	1050	1057	1065
8	1072	1079	1087	1094	1101	1109	1117	1124	1132	1139
9	1147	1155	1163	1171	1178	1186	1194	1203	1211	1219
10	1227	1235	1243	1252	1260	1269	1277	1286	1294	1303
11	1312	1320	1329	1338	1347	1356	1365	1374	1383	1392
12	1401	1411	1420	1429	1439	1448	1458	1467	1477	1487
13	1497	1506	1516	1526	1536	1546	1556	1566	1577	1587
14	1597	1608	1618	1629	1639	1650	1661	1671	1682	1693
15	1704	1715	1726	1737	1748	1760	1771	1782	1794	1805
16	1817	1829	1840	1852	1864	1876	1888	1900	1912	1924
17	1936	1949	1961	1973	1986	1999	2011	2024	2037	2050
18	2063	2076	2089	2102	2115	2128	2142	2155	2169	2182
19	2196	2210	2224	2237	2251	2265	2280	2294	2308	2322
20	2337	2351	2366	2381	2395	2410	2425	2440	2455	2470
21	2486	2501	2516	2532	2547	2563	2579	2595	2611	2627
22	2643	2659	2675	2691	2708	2724	2741	2758	2774	2791
23	2808	2825	2842	2859	2877	2894	2912	2929	2947	2965
24	2983	3001	3019	3037	3055	3073	3092	3110	3129	3148
25	3166	3185	3204	3224	3243	3262	3281	3301	3321	3340
26	3360	3380	3400	3420	3440	3461	3481	3502	3522	3543
27	3564	3585	3606	3627	3649	3670	3692	3713	3735	3757
28	3779	3801	3823	3845	3868	3890	3913	3935	3958	3981
29	4004	4028	4051	4074	4098	4122	4145	4169	4193	4218
30	4242	4266	4291	4315	4340	4365	4390	4415	4440	4466
31	4491	4517	4543	4569	4595	4621	4647	4673	4700	4727
32	4753	4780	4807	4835	4862	4889	4917	4945	4973	5001
33	5029	5057	5085	5114	5143	5171	5200	5229	5259	5288
34	5318	5347	5377	5407	5437	5467	5498	5528	5559	5590
35	5621	5652	5683	5715	5746	5778	5810	5842	5874	5907
36	5939	5972	6004	6037	6071	6104	6137	6171	6205	6239
37	6273	6307	6341	6376	6410	6445	6480	6516	6551	6587
38	6622	6658	6694	6730	6767	6803	6840	6877	6914	6951
39	6989	7026	7064	7102	7140	7178	7217	7255	7294	7333
40	7372	7412	7451	7491	7531	7571	7611	7652	7692	7733

APPENDIX C

THERMO-PHYSICAL PROPERTIES OF HISTORIC MATERIALS IN THE METRIC UNITS

Table C.1 The thermo-physical properties of historic brick (HB), brick mortar (HBM), exterior plasters (HEP) and interior plasters (HIP) in metric units forming the brick dome masonry.

Layers	Samples	ρ	ϕ	c	k	α	VHC
		g cm^{-3}	%	cal g^{-1}°C^{-1}	cal s^{-1}cm^{-1}°C^{-1}	m^2 s^{-1}	cal cm^{-3} °C^{-1}
HB1	BRI.SO.M.07	1.31[(i)]	47.55[(i)]	0.21±0.01	0.0013±0.0001	4.8 10^{-7}±0.3 10^{-7}	0.28±0.01
HB2	32B	1.47[(ii)]	39.84[(ii)]	0.25±0.00	0.0013±0.0000	3.5 10^{-7}±0.1 10^{-7}	0.36±0.01
HB3	HA-A3-VB-C	1.52[(iii)]	38.90[(iii)]	0.21±0.01	0.0014±0.0001	4.5 10^{-7}±0.6 10^{-7}	0.32±0.02
HBM1	YDM1c	1.55[(iii)]	38.10[(iii)]	0.22±0.01	0.0016±0.0001	4.6 10^{-7}±0.2 10^{-7}	0.35±0.01
HBM2	YDM1d	1.52[(iii)]	38.30[(iii)]	0.22±0.00	0.0012±0.0000	3.6 10^{-7}±0.2 10^{-7}	0.33±0.01
HEP-L1	HA-R (U)	1.48[(iv)]	40.80[(iv)]	0.20±0.01	0.0022±0.0002	7.3 10^{-7}±1 10^{-7}	0.30±0.02
HEP-L2	HA-R (L)	1.39[(iv)]	43.40[(iv)]	0.24±0.00	0.0019±0.0000	5.8 10^{-7}±0.1 10^{-7}	0.34±0.00
HEP-L3	PLA.DO.HE.808A	1.70±0.08	26.23±0.21	0.22±0.02	0.0015±0.0001	4.2 10^{-7}±0.7 10^{-7}	0.37±0.03
HIP-L1	AH.I2.AP4e	1.58±0.05	45.29±3	0.23±0.02	0.0009±0.0001	2.4 10^{-7}±0.4 10^{-7}	0.37±0.03
HIP-L2	AH.I2.AP4d	1.07±0.02	53.72±4.66	0.23±0.01	0.0016±0.0001	6.4 10^{-7}±0.4 10^{-7}	0.24±0.01

NOTE.-The *ρ and ø* values of some samples were taken from the literature: [(i)]Caner-Saltik *et al*. 2005b; [(ii)]Esen *et al*., 2004; [(iii)]Caner-Saltik *et al.*, 2003a and [(iv)]Caner *et al*., 2005.

APPENDIX D

RESULTS OF PARTIAL WATER VAPOUR PRESSURE DISTRIBUTION ANALYSES OF THE DOME SECTION OF WOMEN'S HOT SPACE FOR ALL MONTHS

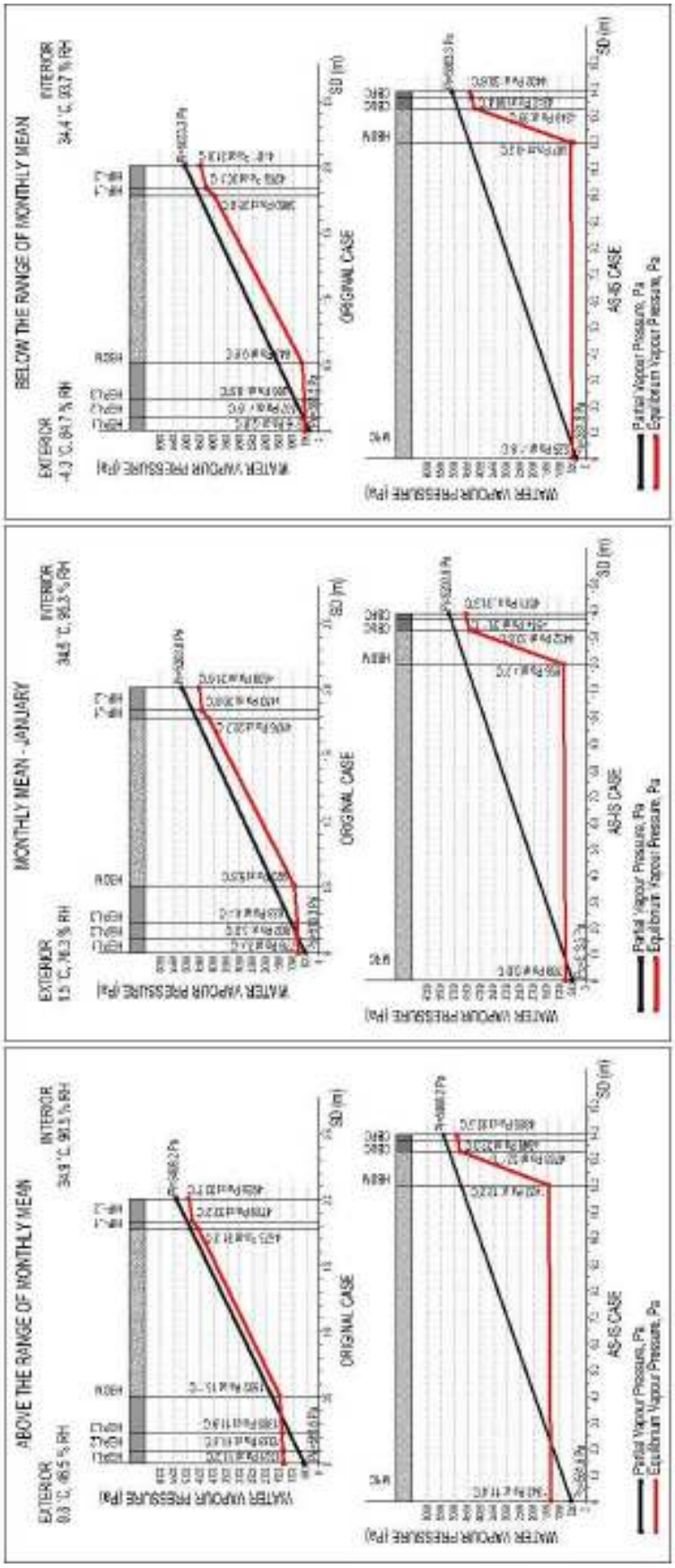

Figure D.1 The partial vapour pressure distribution analyses of the dome section of women's hot space in *ORIGINAL* (at top) and *AS-IS* (at bottom) cases for the monthly-mean temperature and RH values of January (in middle), together with those for above (at left) and below (at right) the range of monthly means.

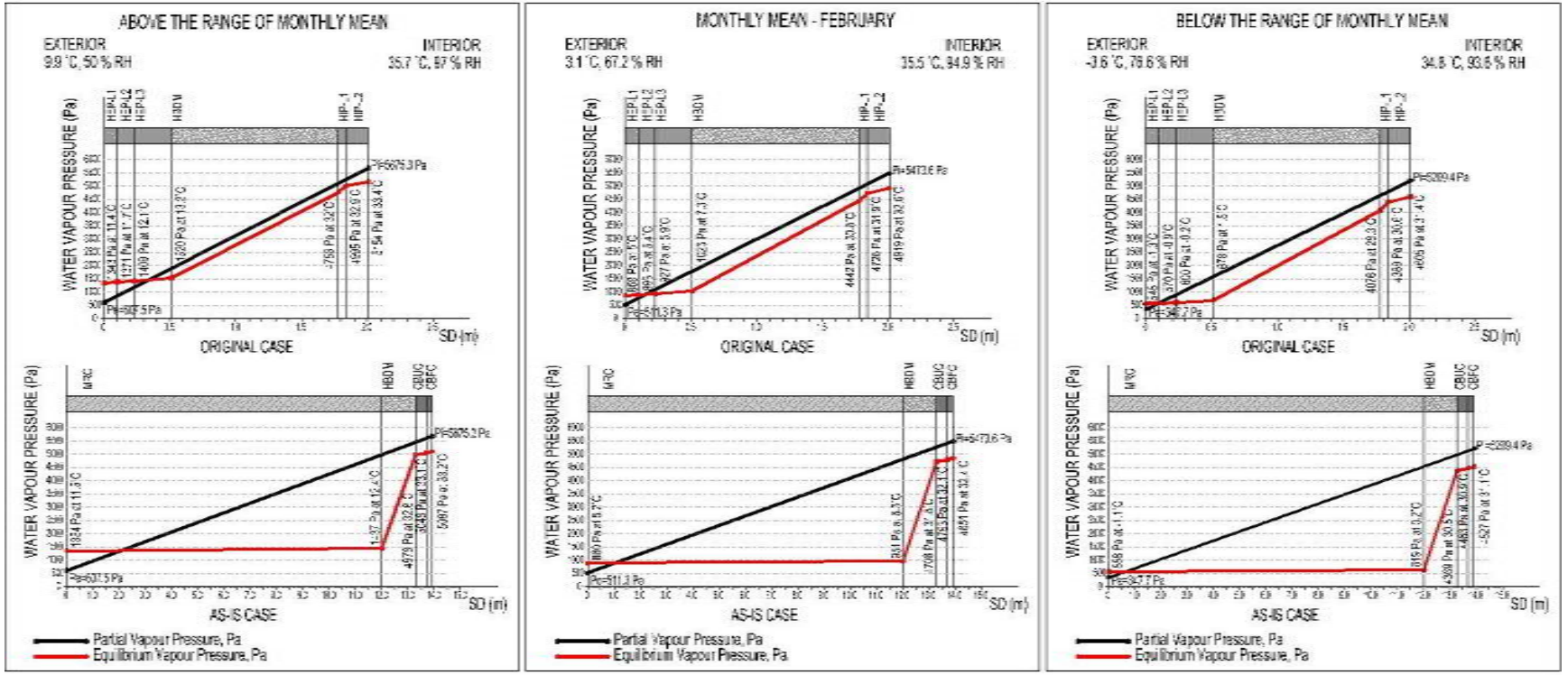

Figure D.2 The partial vapour pressure distribution analyses of the dome section of women's hot space in *ORIGINAL* (at top) and *AS-IS* (at bottom) cases for the monthly-mean temperature and RH values of February (in middle), together with those for above (at left) and below (at right) the range of monthly means.

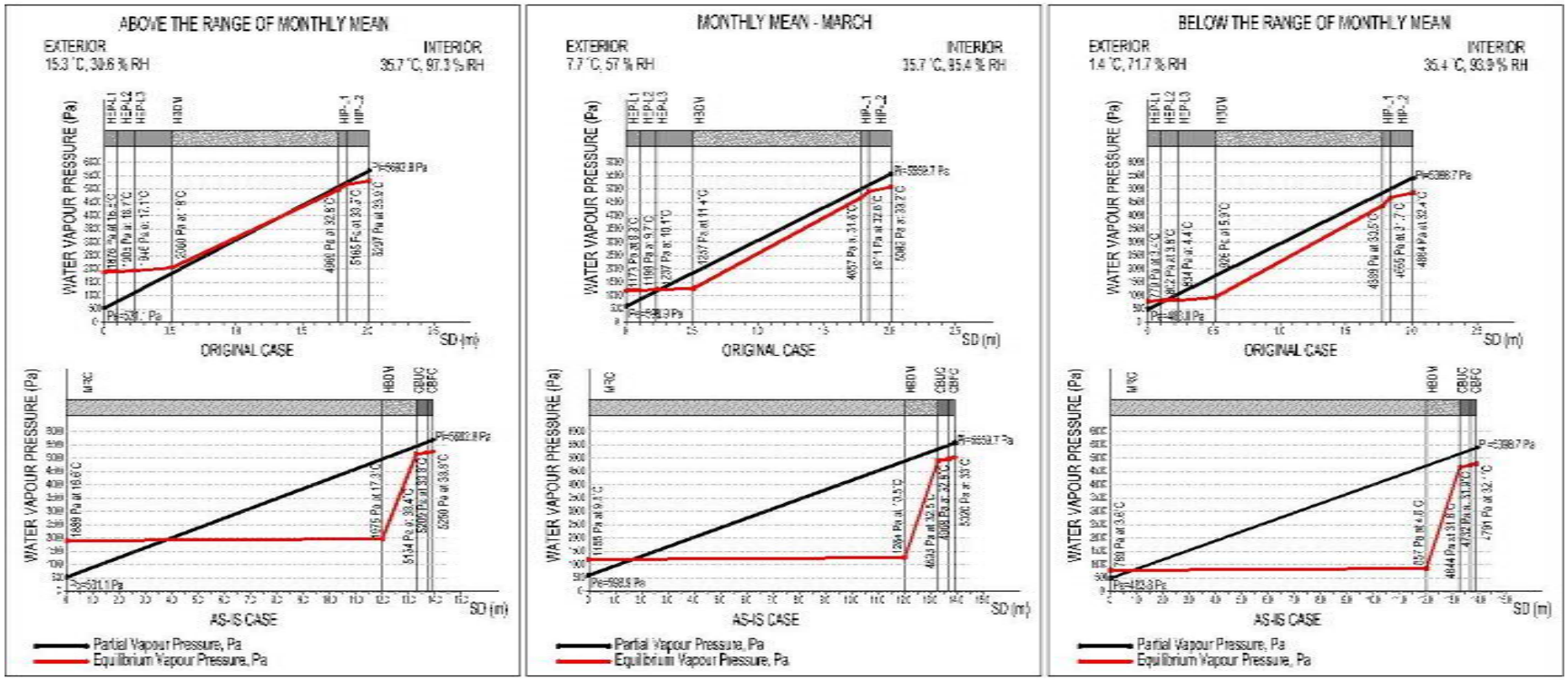

Figure D.3 The partial vapour pressure distribution analyses of the dome section of women's hot space in *ORIGINAL* (at top) and *AS-IS* (at bottom) cases for the monthly-mean temperature and RH values of March (in middle), together with those for above (at left) and below (at right) the range of monthly means.

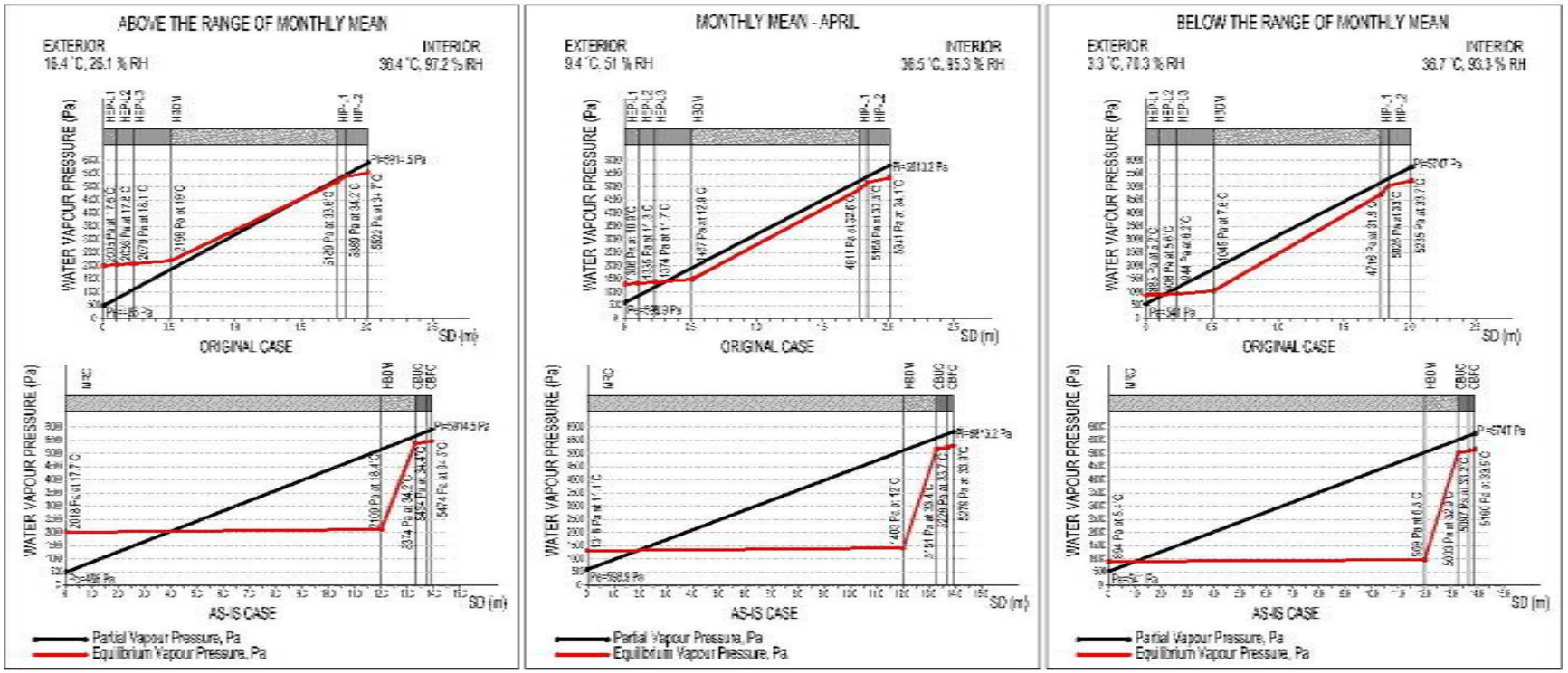

Figure D.4 The partial vapour pressure distribution analyses of the dome section of women's hot space in *ORIGINAL* (at top) and *AS-IS* (at bottom) cases for the monthly-mean temperature and RH values of April (in middle), together with those for above (at left) and below (at right) the range of monthly means.

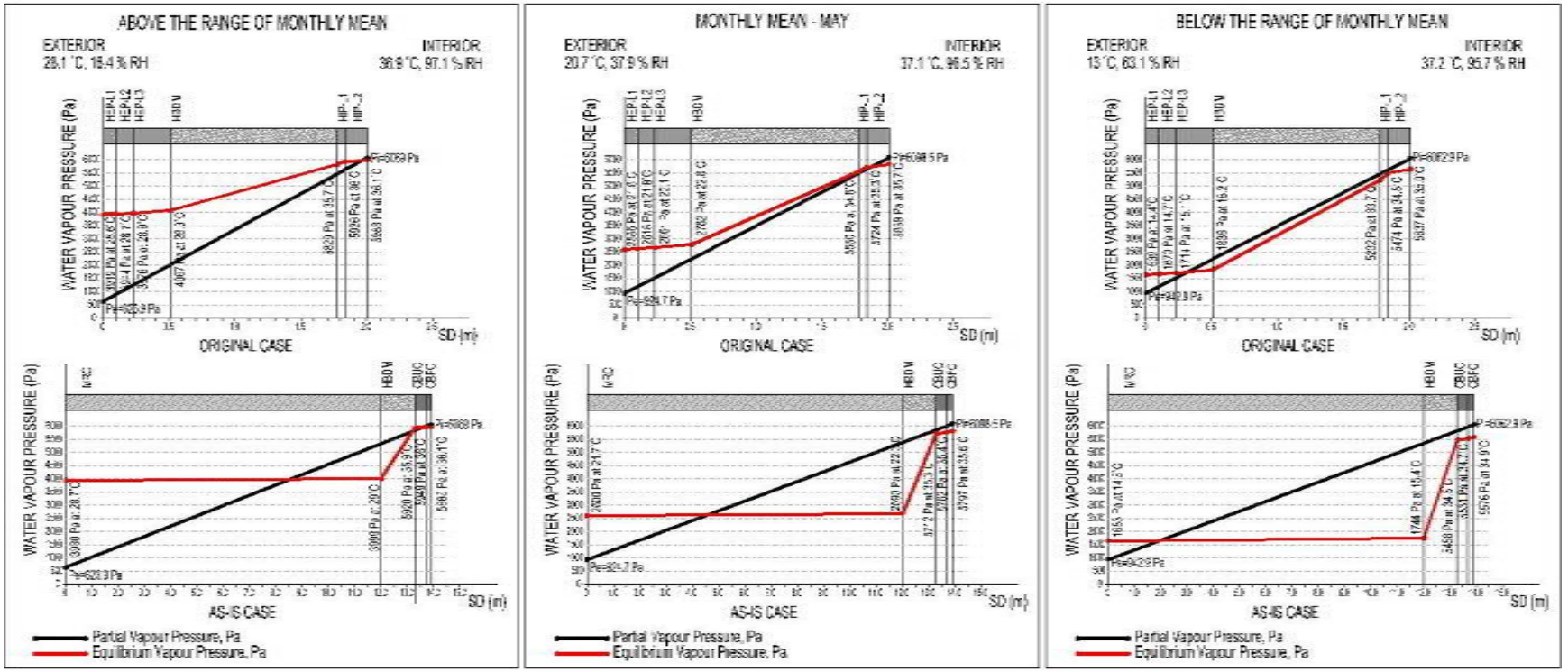

Figure D.5 The partial vapour pressure distribution analyses of the dome section of women's hot space in *ORIGINAL* (at top) and *AS-IS* (at bottom) cases for the monthly-mean temperature and RH values of May (in middle), together with those for above (at left) and below (at right) the range of monthly means.

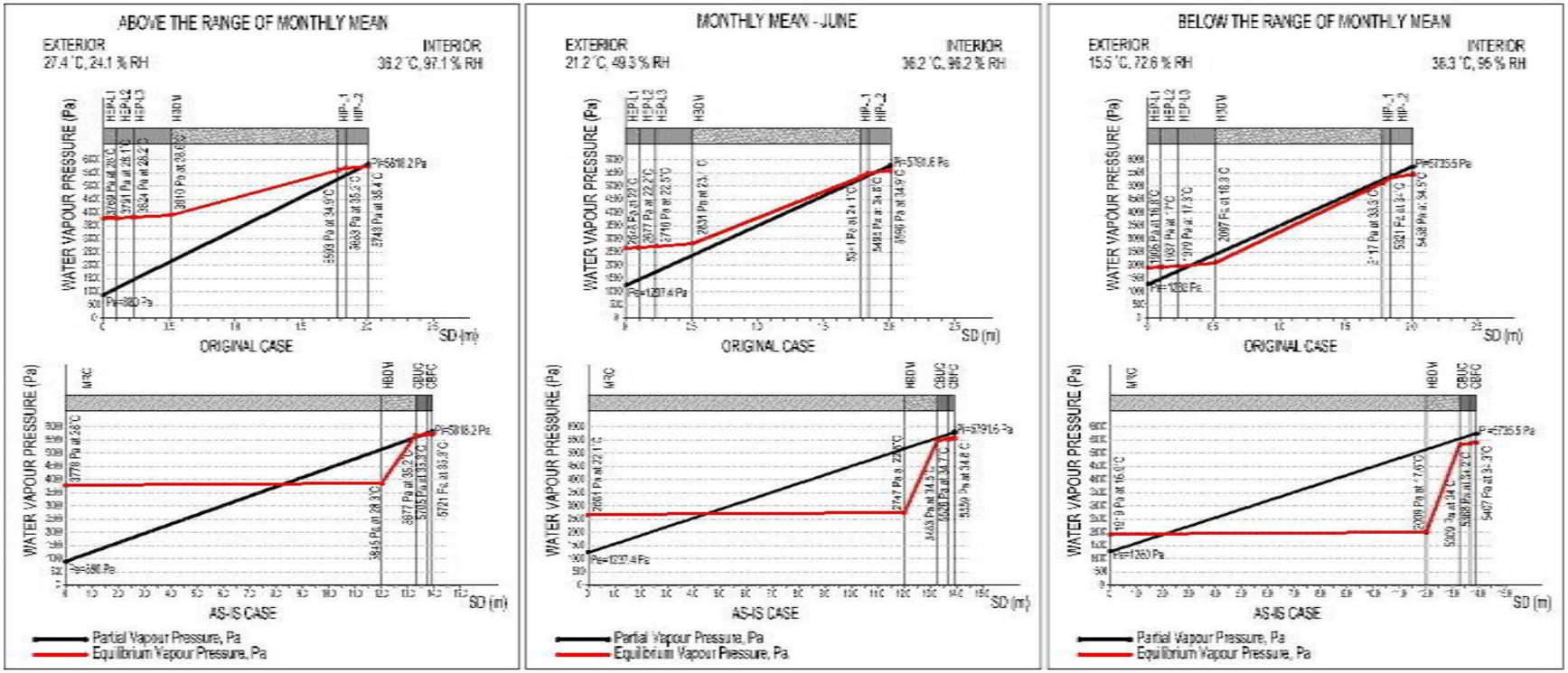

Figure D.6 The partial vapour pressure distribution analyses of the dome section of women's hot space in *ORIGINAL* (at top) and *AS-IS* (at bottom) cases for the monthly-mean temperature and RH values of June (in middle), together with those for above (at left) and below (at right) the range of monthly means.

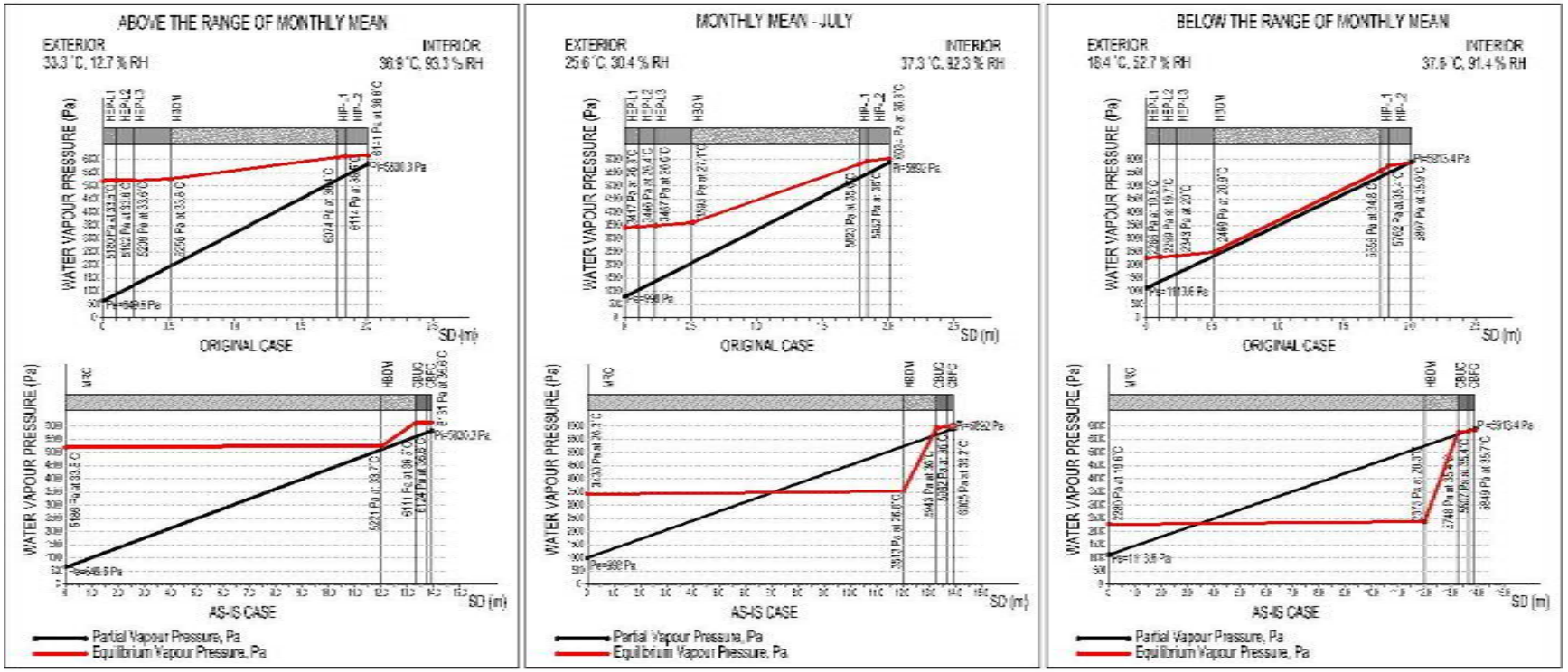

Figure D.7 The partial vapour pressure distribution analyses of the dome section of women's hot space in *ORIGINAL* (at top) and *AS-IS* (at bottom) cases for the monthly-mean temperature and RH values of July (in middle), together with those for above (at left) and below (at right) the range of monthly means.

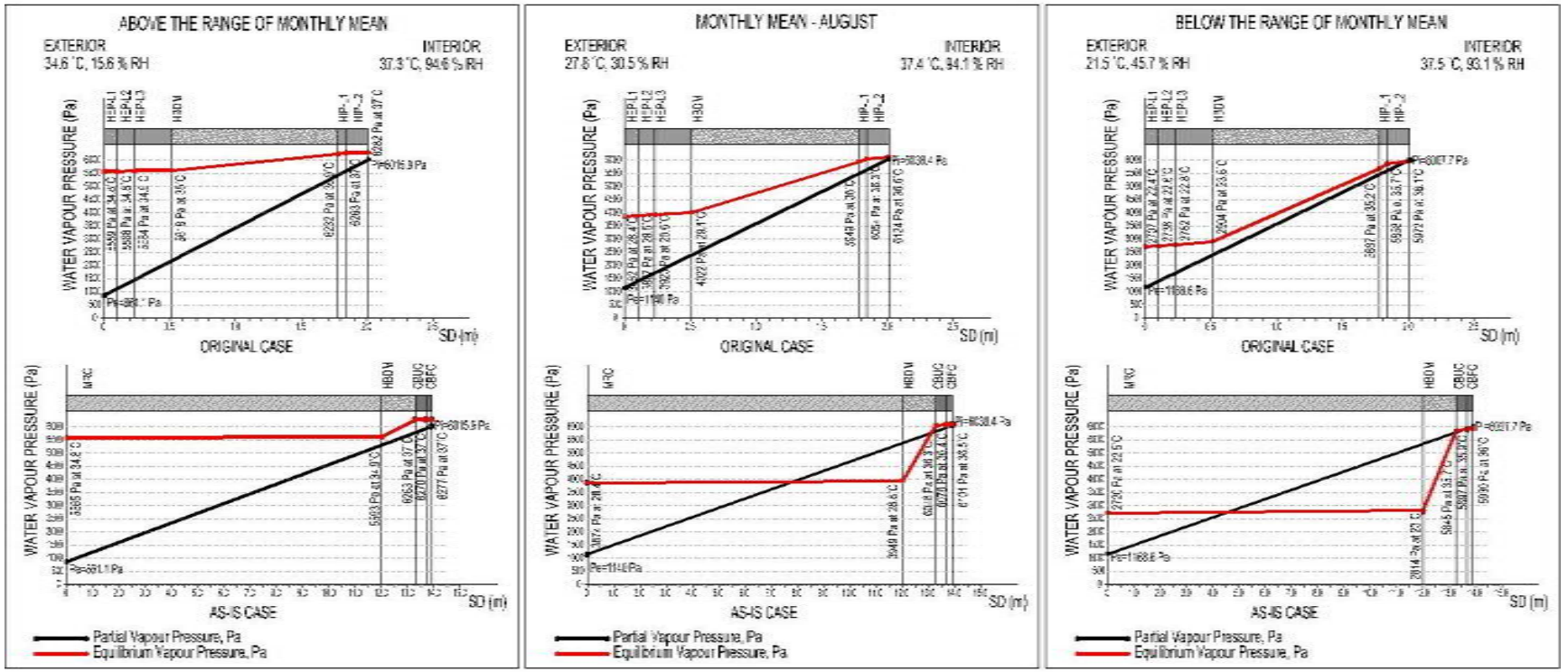

Figure D.8 The partial vapour pressure distribution analyses of the dome section of women's hot space in *ORIGINAL* (at top) and *AS-IS* (at bottom) cases for the monthly-mean temperature and RH values of August (in middle), together with those for above (at left) and below (at right) the range of monthly means.

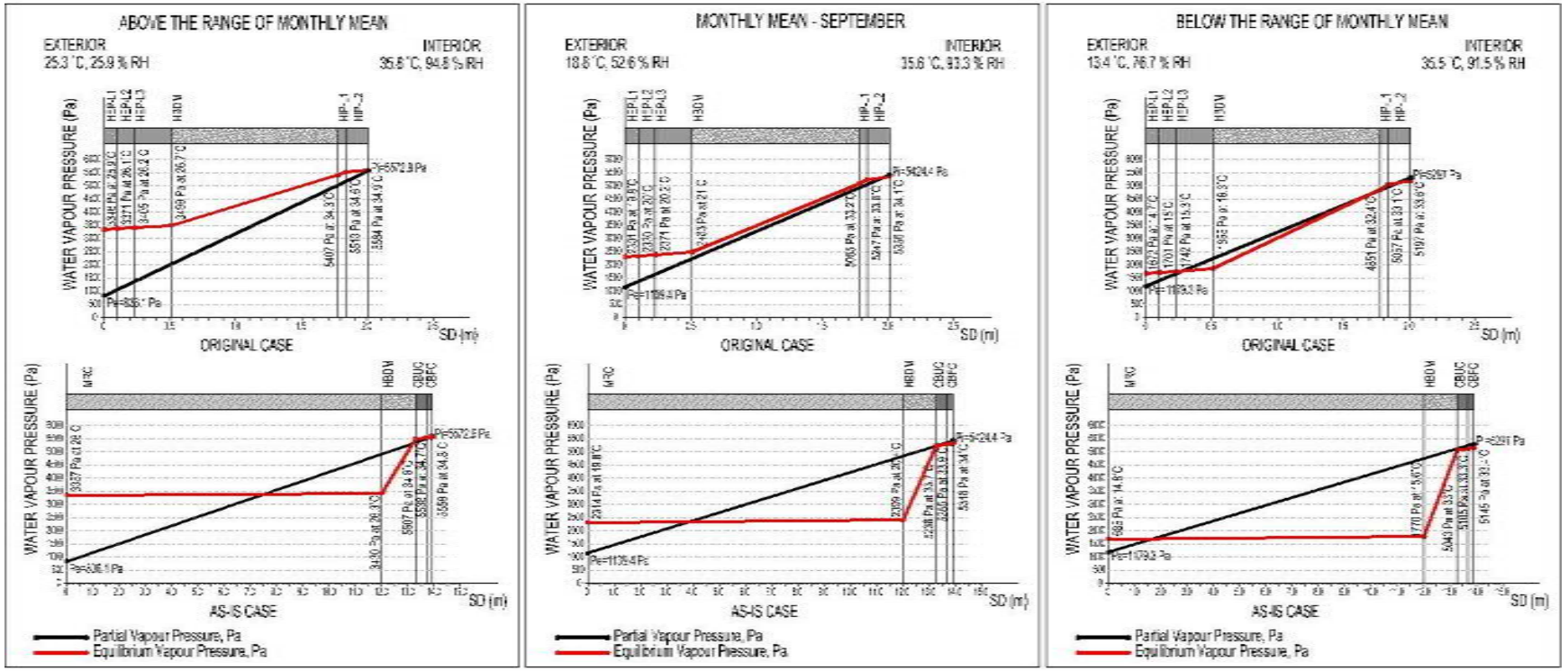

Figure D.9 The partial vapour pressure distribution analyses of the dome section of women's hot space in *ORIGINAL* (at top) and *AS-IS* (at bottom) cases for the monthly-mean temperature and RH values of September (in middle), together with those for above (at left) and below (at right) the range of monthly means.

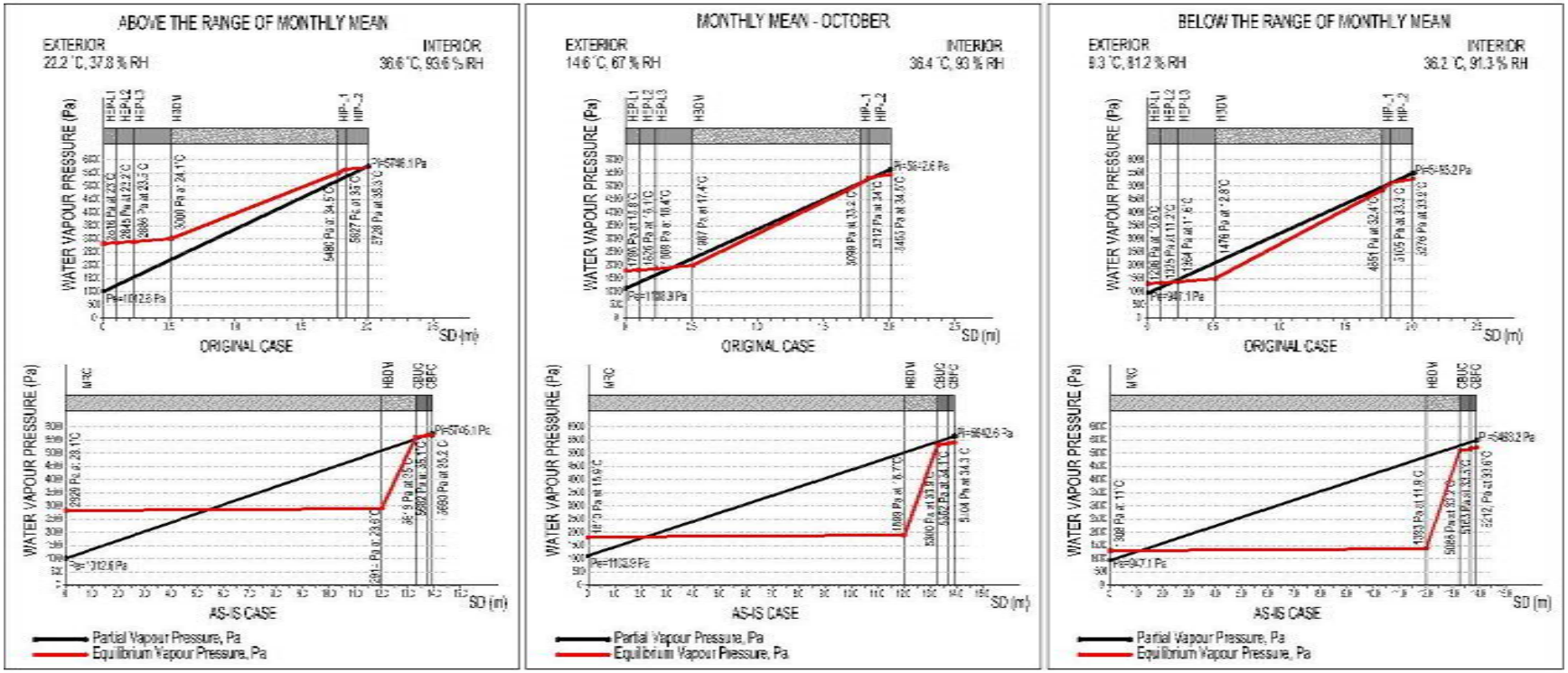

Figure D.10 The partial vapour pressure distribution analyses of the dome section of women's hot space in *ORIGINAL* (at top) and *AS-IS* (at bottom) cases for the monthly-mean temperature and RH values of October (in middle), together with those for above (at left) and below (at right) the range of monthly means.

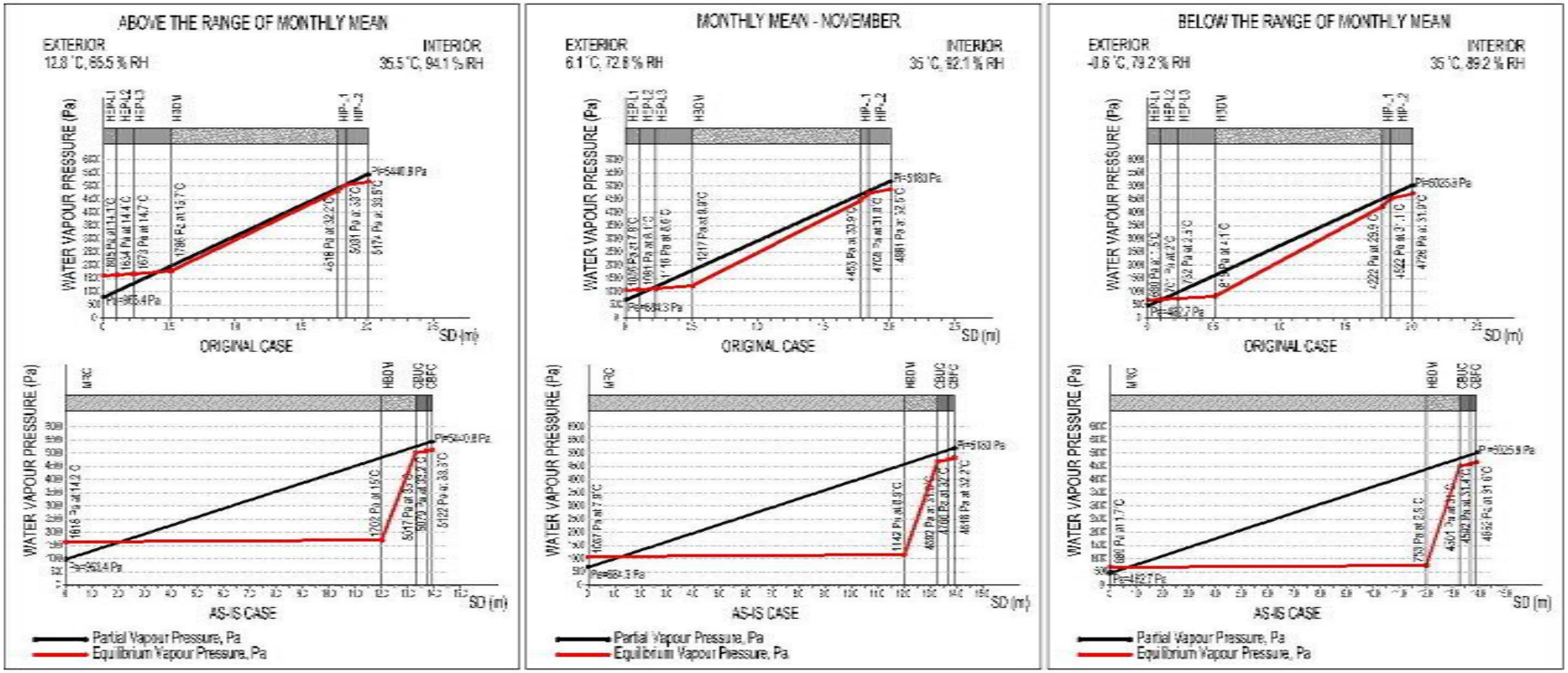

Figure D.11 The partial vapour pressure distribution analyses of the dome section of women's hot space in *ORIGINAL* (at top) and *AS-IS* (at bottom) cases for the monthly-mean temperature and RH values of November (in middle), together with those for above (at left) and below (at right) the range of monthly means.

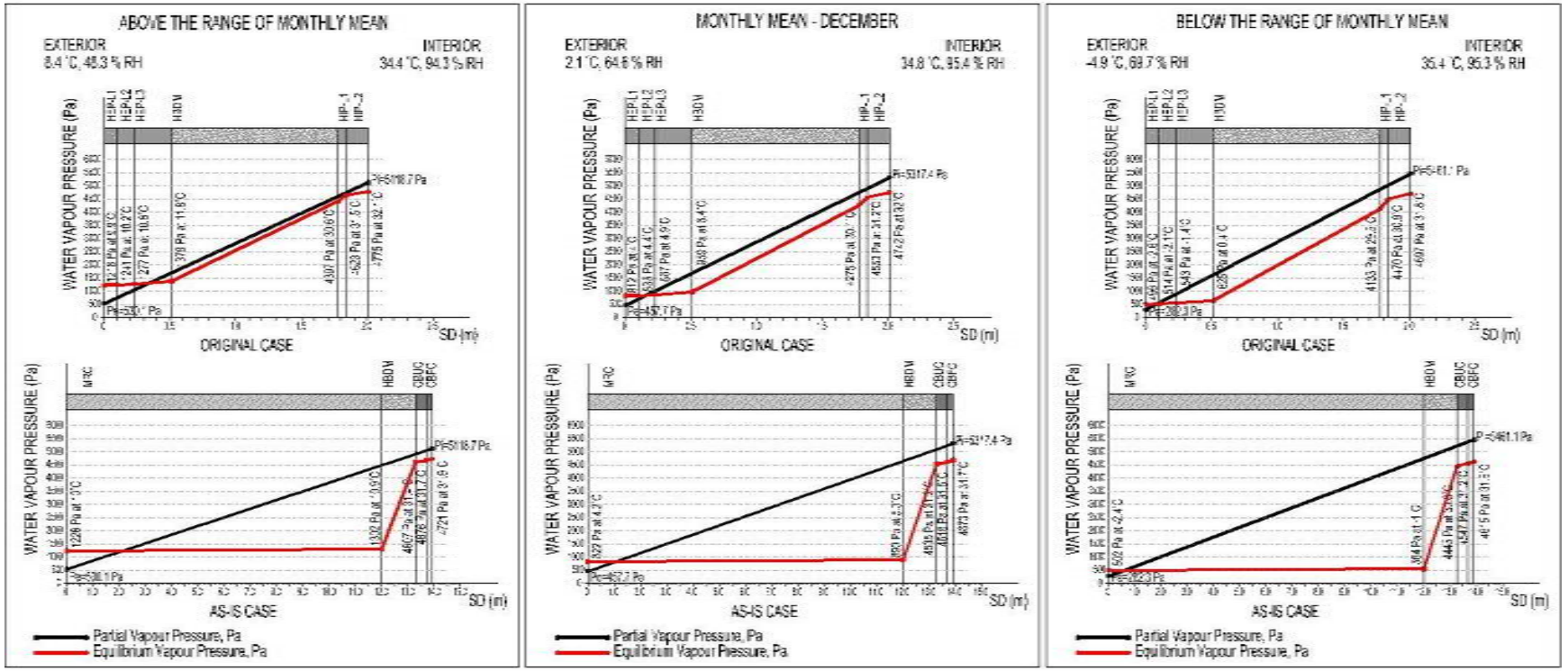

Figure D.12 The partial vapour pressure distribution analyses of the dome section of women's hot space in *ORIGINAL* (at top) and *AS-IS* (at bottom) cases for the monthly-mean temperature and RH values of December (in middle), together with those for above (at left) and below (at right) the range of monthly means.